

## Development of a new online method for compound specific measurements of organic aerosols

Thorsten Hohaus





Forschungszentrum Jülich GmbH  
Institute of Chemistry and Dynamics of the Geosphere (ICG)  
Troposphere (ICG-2)

# **Development of a new online method for compound specific measurements of organic aerosols**

Thorsten Hohaus

Schriften des Forschungszentrums Jülich  
Reihe Energie & Umwelt / Energy & Environment

Band / Volume 52

ISSN 1866-1793

ISBN 978-3-89336-596-8

Bibliographic information published by the Deutsche Nationalbibliothek.  
The Deutsche Nationalbibliothek lists this publication in the Deutsche  
Nationalbibliografie; detailed bibliographic data are available in the  
Internet at <http://dnb.d-nb.de>.

Publisher and  
Distributor: Forschungszentrum Jülich GmbH  
Zentralbibliothek, Verlag  
D-52425 Jülich  
phone:+49 2461 61-5368 · fax:+49 2461 61-6103  
e-mail: [zb-publikation@fz-juelich.de](mailto:zb-publikation@fz-juelich.de)  
Internet: <http://www.fz-juelich.de/zb>

Cover Design: Grafische Medien, Forschungszentrum Jülich GmbH

Printer: Grafische Medien, Forschungszentrum Jülich GmbH

Copyright: Forschungszentrum Jülich 2009

Schriften des Forschungszentrums Jülich  
Reihe Energie & Umwelt / Energy & Environment Band / Volume 52

D 468 (Diss., Wuppertal, Univ., 2009)

ISSN 1866-1793

ISBN: 978-3-89336-596-8

The complete volume is freely available on the Internet on the Jülicher Open Access Server (JUWEL) at  
<http://www.fz-juelich.de/zb/juwel>

Neither this book nor any part may be reproduced or transmitted in any form or by any means, electronic  
or mechanical, including photocopying, microfilming, and recording, or by any information storage and  
retrieval system, without permission in writing from the publisher.

# Zusammenfassung

Atmosphärische Aerosole spielen in vielen Umweltprozessen eine wichtige Rolle und beeinflussen dabei die menschliche Gesundheit und das Klima. In vielen Gebieten ist der organische Anteil des atmosphärischen Aerosols sehr hoch und beeinflusst dadurch die Eigenschaften der Aerosole. Auf Grund der großen Vielfalt von unterschiedlichen organischen Verbindungen, die in atmosphärischen Aerosolen enthalten sind, ist eine detailliert chemische Charakterisierung von Umgebungsaerosol entscheidend um Bildungsprozesse, Zusammensetzung und Eigenschaften der atmosphärischen Aerosole verstehen zu können. Jedoch sind derzeitige Analysemethoden noch unzureichend um eine vollständige Speziation von organischen Aerosolen zu ermöglichen und weisen zudem meistens lange Probennahmezeiten auf. Während der Probennahme und der Lagerung von Aerosolproben sind offline Probenahmemethoden Artefakteinflüssen unterworfen. In der vorliegenden Arbeit wurde eine neue Methode zur substanzspezifischen online Messung mit hoher Zeitauflösung entwickelt. Das Aerosol Collection Module (ACM) ist ein neues wissenschaftliches Messinstrument, mit welchem atmosphärische Aerosole gesammelt und transferiert werden können. Das System ist mit einer aerodynamischen Linse ausgestattet, welches Partikel in einen Strahl fokussiert. Dieser Partikelstrahl wird auf eine gekühlte Sammeloberfläche geleitet. Nach der Probennahme werden die Aerosole von der Sammeloberfläche mittels Erhitzen verdampft und in einen Detektor geleitet.

Für die Charakterisierung im Labor wurde der ACM mit einem System aus einem Gaschromatographen und einem Massenspektrometer (GC-MS) gekoppelt. Die Sammeleffizienz, die Gastransfereffizienz und die Linearität des ACM-GC-MS Systems wurden mittels im Labor erzeugten Octadecanaerosolen bestimmt. Es konnte gezeigt werden, dass das ACM-GC-MS System linear über einen Massenbereich von 2 bis 100 ng ist und dass die Wiederfindungsrate für Octadecanaerosole 100% betrug.

Der Schwerpunkt eines Experiments, welches an der Jülicher Aerosolkammer durchgeführt wurde, lag auf der Charakterisierung von sekundärem organischem Aerosol (SOA) welches durch die Oxidation von  $\beta$ -Pinen gebildet wurde. Das durch die  $\beta$ -Pinen Ozonolyse gebildete SOA wurde erfolgreich mit dem ACM-GC-MS System gemessen. Nopinon, Myrtanal, Myrtenol, 1-Hydroxynopinon, 3-Oxonopinon, 3,7-Dihydroxynopinon, und Bicyclo[3,1,1]hept-3-ene-2-one konnten als Produkte der  $\beta$ -Pinen Ozonolyse identifiziert werden. Für Nopinon, welches eines der Hauptprodukte der  $\beta$ -Pinen Oxidation ist, wurde der Verteilungskoeffizient bestimmt. Der Verteilungskoeffizient wurde im Mittel bestimmt zu  $7.75 \times 10^{-5} \pm 1.9 \times 10^{-5} \text{ m}^3 \mu\text{g}^{-1}$ , was zwischen den Erwartungswerten von  $2.4 \times 10^{-7} \text{ m}^3 \mu\text{g}^{-1}$  und  $7.6 \times 10^{-4} \text{ m}^3 \mu\text{g}^{-1}$  von Modelstudien liegt.

---

In weiterführenden Untersuchungen sollte der ACM zum Messen von Umgebungsaerosol eingesetzt werden und es sollten die weiteren analytischen Möglichkeiten des ACM durch Kopplung an verschiedene Gasphasendetektoren untersucht werden.

# Abstract

Atmospheric aerosols play an important role in many environmental processes, affecting human health and global climate. In many environments organic matter significantly contributes to the composition of atmospheric aerosols influencing its properties. Due to the huge variety of organic compounds present in atmospheric aerosol detailed chemical characterization of ambient aerosols is critical in order to understand the formation process, composition, and properties of aerosols in the atmosphere. However, current analytical methods are far from full speciation of organic aerosols and often require long sampling times. Offline methods are also subjected to artifacts during aerosol collection and storage.

In the present work a new technique for online compound specific measurements with a high time resolution was developed. The Aerosol Collection Module (ACM) is a new scientific instrument designed to sample and transfer atmospheric aerosols. The system consists of an aerodynamic lens system which focuses particles into a beam. The beam is directed to a cooled sampling surface. After collection the aerosol sample is evaporated from the collection surface through heating and transferred to a detector.

For laboratory characterization the ACM was interfaced with a Gas Chromatograph Mass Spectrometer system (GC-MS). The particle collection efficiency, gas phase transfer efficiency, and linearity of the ACM-GC-MS was determined using laboratory generated octadecane aerosols. It could be proven that the ACM-GC-MS is linear over a mass range of 2 to 100 ng and that the ACM-GC-MS had a recovery rate of 100% for octadecane aerosols.

An experiment carried out at the Jülich aerosol chamber focused on the characterization of secondary organic aerosols (SOA) formed from  $\beta$ -pinene oxidation. SOA formed by the ozone oxidation of  $\beta$ -pinene was successfully measured with the ACM-GC-MS. Nopinone, myrtanal, myrtenol, 1-hydroxynopinone, 3-oxonopinone, 3,7-dihydroxynopinone, and bicyclo[3,1,1]hept-3-ene-2-one could be identified as products of the  $\beta$ -pinene ozonolysis. For nopinone, one of the major oxidation products, the partitioning coefficient was determined. It was found to be on average  $7.75 \times 10^{-5} \pm 1.9 \times 10^{-5} \text{ m}^3 \mu\text{g}^{-1}$  which is between model estimates of  $2.4 \times 10^{-7} \text{ m}^3 \mu\text{g}^{-1}$  and  $7.6 \times 10^{-4} \text{ m}^3 \mu\text{g}^{-1}$ .

In future studies the ACM should be applied to measure ambient aerosol and to further explore the analytical potential of the ACM by coupling it to different gas phase detectors.



---

# Contents

<b>List of Figures</b>	<b>13</b>
<b>List of Tables</b>	<b>15</b>
<b>1 Introduction</b>	<b>17</b>
1.1 Organic Compounds in the Atmosphere . . . . .	17
1.2 Atmospheric Aerosols . . . . .	18
1.3 Formation of Secondary Organic Aerosols . . . . .	21
1.4 Measurement of Chemical Composition of Organic Aerosols . . . .	23
1.5 Objectives of this work . . . . .	25
<b>2 Instrument Descriptions</b>	<b>27</b>
2.1 The Aerosol Collection Module . . . . .	27
2.1.1 Overview and Measuring Principle . . . . .	27
2.1.2 Aerosol Sampling . . . . .	28
2.1.3 Aerosol Collection . . . . .	30
2.1.4 Aerosol Transfer . . . . .	31
2.2 Detectors . . . . .	34
2.2.1 Gas Chromatograph - Mass Spectrometer . . . . .	34
2.2.2 Proton Transfer Reaction Mass Spectrometer . . . . .	37
2.3 Instrument Automation and Data Acquisition . . . . .	39
2.4 Data Reduction and Compound Identification . . . . .	39
2.5 Filter measurements . . . . .	40
2.6 Aerosol Mass Spectrometry . . . . .	41
2.7 Particle Size Distribution . . . . .	43
2.8 Particle Density . . . . .	44
<b>3 Instrument Characterization</b>	<b>47</b>

## CONTENTS

---

3.1	GC-MS Characterization . . . . .	47
3.1.1	Experimental Setup . . . . .	48
3.1.2	GC-MS Detector Calibration . . . . .	49
3.2	ACM Characterization . . . . .	55
3.2.1	Choice of the Test Compound . . . . .	55
3.2.2	ACM Gas Phase Transfer Efficiency . . . . .	56
3.2.3	ACM Particle Collection, Desorption and Transfer Efficiency . . . . .	59
<b>4</b>	<b>Secondary Organic Aerosol Formation from <math>\beta</math>-pinene Ozonolysis</b>	<b>65</b>
4.1	Aerosol Chamber of the FZJ and Experimental Set Up . . . . .	65
4.1.1	Description of the Aerosol Chamber of the FZJ . . . . .	65
4.1.2	Instrumentation for the Aerosol Chamber Experiment . . . . .	67
4.1.3	Experimental Conditions and Procedure . . . . .	68
4.2	Results of the Gas Phase and Particle Phase Measurements . . . . .	71
4.2.1	Results of the PTR-TOF-MS Measurements . . . . .	71
4.2.2	Results of the CPC and SMPS Measurements . . . . .	72
4.2.3	Results of the ACM-GC-MS Measurements . . . . .	75
4.2.4	Results of the Filter Sample Measurements . . . . .	78
4.3	Identification and Temporal Evolution of $\beta$ -pinene ozonolysis products in the SOA . . . . .	79
4.3.1	Identification of $\beta$ -pinene ozonolysis products . . . . .	79
4.3.2	Source of Acetone in the SOA . . . . .	84
4.3.3	Time Series of Aerosol Composition . . . . .	85
4.4	Intercomparison of ACM-GC-MS and SMPS . . . . .	87
4.4.1	Total Mass measured by ACM-GC-MS . . . . .	87
4.4.2	Temporal evolution of the mass fractional abundances of SOA compounds . . . . .	89
4.5	Intercomparison of ACM-GC-MS and Filter Samples . . . . .	93
4.6	SOA Yield and Nopinone Partitioning . . . . .	95
4.6.1	SOA Yield of the $\beta$ -pinene ozonolysis . . . . .	95
4.6.2	Nopinone partitioning . . . . .	96
4.7	Time evolution of the SOA composition and corresponding ACM marker compounds . . . . .	102
4.7.1	Time evolution of PMF factors and O/C ratios . . . . .	102
4.7.2	AMS PMF factors and ACM Marker Compounds . . . . .	106
4.8	Scientific findings of the $\beta$ -pinene ozonolysis experiment . . . . .	110

5	Summary & Outlook	113
A	Fit Coefficients for the Characterization Measurements	125
B	ACM-GC-MS Chromatograms of the aerosol chamber experiment	127
C	Mass Spectra of the identified $\beta$ -pinene ozonolysis products	139
D	Retention Index Method for GC-MS Peak Identification	145
E	Temporal evolution of the mass fractional abundances of all unidentified SOA compounds	147
F	Positive Matrix Factorization (PMF) Analysis	151
	Abbreviations	153

## CONTENTS

---

# List of Figures

1.1	Aerosol size distribution . . . . .	19
1.2	Composition of PM1 aerosol . . . . .	20
1.3	Speciation results for organic aerosol in Southern California . . . .	21
1.4	Schematic of SOA formation from VOC oxidation . . . . .	22
2.1	Schematic of the ACM instrument . . . . .	28
2.2	Schematic of ACM collector . . . . .	30
2.3	ACM valve system . . . . .	33
2.4	Schematic of the GC-MS detector . . . . .	35
2.5	ACM - PTR-MS coupling . . . . .	38
2.6	Schematic of the AMS . . . . .	42
3.1	General instrumental setup for the characterization experiments .	48
3.2	GC-MS detector schematic with liquid injection . . . . .	49
3.3	Chromatograms of the direct injection into the GC-MS . . . . .	51
3.4	Calibration curves for standards compounds obtained by direct injections into the GC-MS . . . . .	52
3.5	Comparison of mass spectra with mass spectra from the NIST database . . . . .	54
3.6	Schematic of the modified ACM valve array for diffusion source measurements . . . . .	56
3.7	Example chromatogram of the diffusion source measurement . . .	58
3.8	Comparison of the diffusion source measurements with the direct injection of octadecane in the GC-MS system . . . . .	59
3.9	Experimental setup for the Octadecane Aerosol Measurement . . .	60
3.10	Octadecane size distribution . . . . .	62
3.11	Calculated total volume concentration of octadecane particles . .	63
3.12	Measurement of Octadecane aerosols with the ACM . . . . .	64

## LIST OF FIGURES

---

4.1	Schematic of the FZJ aerosol chamber . . . . .	66
4.2	Gas phase measurements of the $\beta$ -pinene ozonolysis experiment .	71
4.3	Particle concentration and total volume concentration during the aerosol chamber experiment . . . . .	73
4.4	Time series of the mean particle diameter and upper detection limit for measuring the particle volume distribution of the SOA in the aerosol chamber . . . . .	74
4.5	ACM-GC-MS FID chromatogram of the empty aerosol chamber .	76
4.6	Comparison of ACM-GC-MS FID chromatograms measured over the course of the $\beta$ -pinene experiment . . . . .	77
4.7	Total amount of nopinone of the filter samples . . . . .	79
4.8	ACM-GC-MS FID chromatogram with retention times of the homologous alkane series . . . . .	82
4.9	Time series of the total SOA mass measured by the ACM-GC-MS system . . . . .	85
4.10	Time series of the nopinone and acetone mass determined from the ACM-GC-MS FID chromatograms . . . . .	86
4.11	Time series of the identified peaks determined from the ACM-GC-MS FID chromatograms . . . . .	87
4.12	Comparison of the ACM collector mass loading and the total mass measured with the ACM-GC-MS . . . . .	88
4.13	Fractional abundances of identified compounds in the SOA . . . .	90
4.14	Fractional abundance of the unidentified peaks in the SOA . . . .	92
4.15	Comparison of total nopinone mass sample with filters and the ACM-GC-MS. . . . .	93
4.16	Examples for different AMS $m/z$ temporal evolution . . . . .	103
4.17	Factors derived from the PMF analysis . . . . .	104
4.18	Mass spectral profiles of the PMF factors . . . . .	105
4.19	Fraction of total mass and oxygen to carbon ratio of the PMF factors	106
4.20	Comparison of the temporal evolutions of the PMF and ACM factors	107
4.21	Comparison of the PMF factors with the total fractional abundances of the ACM factors . . . . .	108
B.1	ACM-GC-MS FID Chromatogram of sample S1 . . . . .	127
B.2	ACM-GC-MS FID Chromatogram of sample S2 . . . . .	128
B.3	ACM-GC-MS FID Chromatogram of blank B1 . . . . .	128
B.4	ACM-GC-MS FID Chromatogram of sample S3 . . . . .	129
B.5	ACM-GC-MS FID Chromatogram of blank B2 . . . . .	129

B.6	ACM-GC-MS FID Chromatogram of sample S4 . . . . .	130
B.7	ACM-GC-MS FID Chromatogram of blank B3 . . . . .	130
B.8	ACM-GC-MS FID Chromatogram of sample S5 . . . . .	131
B.9	ACM-GC-MS FID Chromatogram of blank B4 . . . . .	131
B.10	ACM-GC-MS FID Chromatogram of sample S6 . . . . .	132
B.11	ACM-GC-MS FID Chromatogram of sample S7 . . . . .	132
B.12	ACM-GC-MS FID Chromatogram of sample S8 . . . . .	133
B.13	ACM-GC-MS FID Chromatogram of sample S9 . . . . .	133
B.14	ACM-GC-MS FID Chromatogram of sample S10 . . . . .	134
B.15	ACM-GC-MS FID Chromatogram of blank B5 . . . . .	134
B.16	ACM-GC-MS FID Chromatogram of sample S11 . . . . .	135
B.17	ACM-GC-MS FID Chromatogram of blank B6 . . . . .	135
B.18	ACM-GC-MS FID Chromatogram of sample S12 . . . . .	136
B.19	ACM-GC-MS FID Chromatogram of sample S13 . . . . .	136
B.20	ACM-GC-MS FID Chromatogram of sample S14 . . . . .	137
B.21	ACM-GC-MS FID Chromatogram of sample S15 . . . . .	137
B.22	ACM-GC-MS FID Chromatogram of sample S16 . . . . .	138
B.23	ACM-GC-MS FID Chromatogram of blank B7 . . . . .	138
C.1	Mass spectrum of acetone . . . . .	139
C.2	Mass spectrum of bicyclo[3,1,1]hept-3-ene-2-one . . . . .	140
C.3	Mass spectrum of nopinone . . . . .	140
C.4	Mass spectrum of myrtanal . . . . .	141
C.5	Mass spectrum of myrtenol . . . . .	141
C.6	Mass spectrum of 1-hydroxinopinone . . . . .	142
C.7	Mass spectrum of 3-oxonopinone . . . . .	142
C.8	Mass spectrum of 3,7-dihydroxynopinone . . . . .	143
E.1	Unidentified compounds in the SOA assigned to group 1 . . . . .	147
E.2	Unidentified compounds in the SOA assigned to group 2 . . . . .	148
E.3	Unidentified compounds in the SOA assigned to group 3 . . . . .	148
E.4	Unidentified compounds in the SOA which cloud not be clearly assigned to group 1, 2 or 3 . . . . .	149



## LIST OF FIGURES

---

# List of Tables

3.1	Chemicals used for the calibration measurements. . . . .	50
4.1	Overview of the course of the $\beta$ -pinene experiment . . . . .	70
4.2	Identified products in the $\beta$ -pinene ozonolysis experiment . . . . .	81
4.3	Comparison of determined linear retention indices of the identified products with literature values . . . . .	83
4.4	SOA yield of the $\beta$ -pinene ozonolysis experiment . . . . .	96
4.5	Partitioning coefficient and vapor pressure of nopinone . . . . .	99
4.6	Comparison of the O/C ratio of the PMF factors with the identified compounds . . . . .	105
A.1	Fit coefficients of the GC-MS calibration and the diffusion source measurements . . . . .	126

## LIST OF TABLES

---

# 1. Introduction

## 1.1 Organic Compounds in the Atmosphere

Organic compounds enter the atmosphere through a variety of processes such as combustion processes, biomass burning and the use of fossil fuel. Also biogenic sources, mainly vegetation in marine and terrestrial environments, emit large quantities of non-methane organic compounds into the atmosphere. These biologically emitted volatile organic compounds (VOC) include isoprene ( $C_5H_8$ ), monoterpenes ( $C_{10}H_{16}$ ) (e.g.  $\alpha$ -pinene,  $\beta$ -pinene, limonene, *cis*-ocimene, 3-carene), sesquiterpenes (e.g.  $\beta$ -caryophyllene, longifolene,  $\alpha$ -humulene), oxygenated VOC (e.g. acetone, camphor, linalool), reactive VOC and other VOC (Guenther et al., 1995). The global emission of biogenic non-methane VOC is estimated to be 1150 Tg C/yr (Guenther et al., 1995) which is an order of magnitude larger than the estimated emission of anthropogenic VOC of 109 Tg C/yr (Penner et al., 2001). However large uncertainties exist for these estimates.

The number of organic compounds actually present in the atmosphere is unknown. Goldstein and Galbally (2007) estimated that  $1 \times 10^4$  to  $1 \times 10^5$  different organic compounds have been measured until now in the atmosphere. They also estimated for alkanes with 10 carbon atoms that there are over 100 possible isomers increasing the C10 organic species to over  $1 \times 10^6$  individual organic compounds which can occur in the atmosphere covering a wide range of polarities, volatilities and masses.

Biogenic VOC are important for the tropospheric chemistry due to their high reactivity with atmospheric oxidants such as ozone ( $O_3$ ), hydroxyl (OH) and nitrate ( $NO_3$ ) radicals. Their oxidation lead to a variety of oxidation products of different volatilities and reactivities. In the presence of NO oxidation of VOC can also lead to formation of ozone (Atkinson and Arey, 2003). Due to a typically high vapor pressures most organic compounds emitted to the atmosphere are gaseous. As oxidation proceeds the vapor pressure of the oxidation products decreases with increasing polarity. The oxidation products can condense on existing atmospheric aerosols or lead to the formation of new particles. Partitioning between

the gas phase and the aerosol phases in the atmosphere depends on the liquid- or solid-phase vapor pressure of the compounds. In general, compounds with a vapor pressure of  $> 0.1$  hPa at ambient temperature are in the gas phase. If their vapor pressure is between 0.1 hPa and  $1 \times 10^{-7}$  hPa they will be semivolatile and for vapor pressures below this liquid or solid particles (Goldstein and Galbally, 2007).

## 1.2 Atmospheric Aerosols

Aerosols are defined as a suspension of solid or liquid particles suspended in a gas. Therefore the term aerosol or aerosol component usually refers to both the aerosol particles phase and the aerosol gas phase. However in atmospheric research the term aerosol is often used in describing the particulate phase (the condensed phase) only. On this note the terms aerosol and particle are interchangeable. Only when gas-particle interactions are considered it is explicitly distinguished between the particle components and the gas phase components. In this work both terms aerosol and particle will be used referring to the particulate phase when gas-particle phase interactions are not considered.

Aerosol sizes typically range from  $10^{-9}$  m to  $10^{-4}$  m. The formation of aerosols is a complex process. It includes direct emission of primary particles and the formation of secondary particles from gas phase oxidation of aerosol precursors and gas-particle partitioning. Primary aerosols are directly emitted into the atmosphere by combustion processes such as biomass burning, and vehicle emissions or by wind-driven processes such as the resuspension of dust and sea salt. Secondary aerosols are formed from oxidation products of gas phase compounds that are directly emitted into the atmosphere. The resulting oxidized compounds, which are less volatile, can form new particles or condense on existing particle surfaces. A common example is the oxidation of gas phase organic compounds resulting in less volatile organic products which can form the so called secondary organic aerosols (SOA) (Seinfeld and Pandis, 1998).

Atmospheric aerosols are subjected to a variety of chemical and physical processes. They are normally separated into different classes according to their size related to their formation process. Ambient particles normally occupy one of four modes. Figure 1.1 shows the relevant processes affecting atmospheric aerosols including the main loss processes for aerosols. Aerosols in the coarse mode ( $> 2 \mu\text{m}$ ) are usually produced by mechanical processes such as grinding, sea spray, dust and eroded material suspended in the air by wind. As these particles are large sedimentation is the main loss process. The accumulation mode includes particles

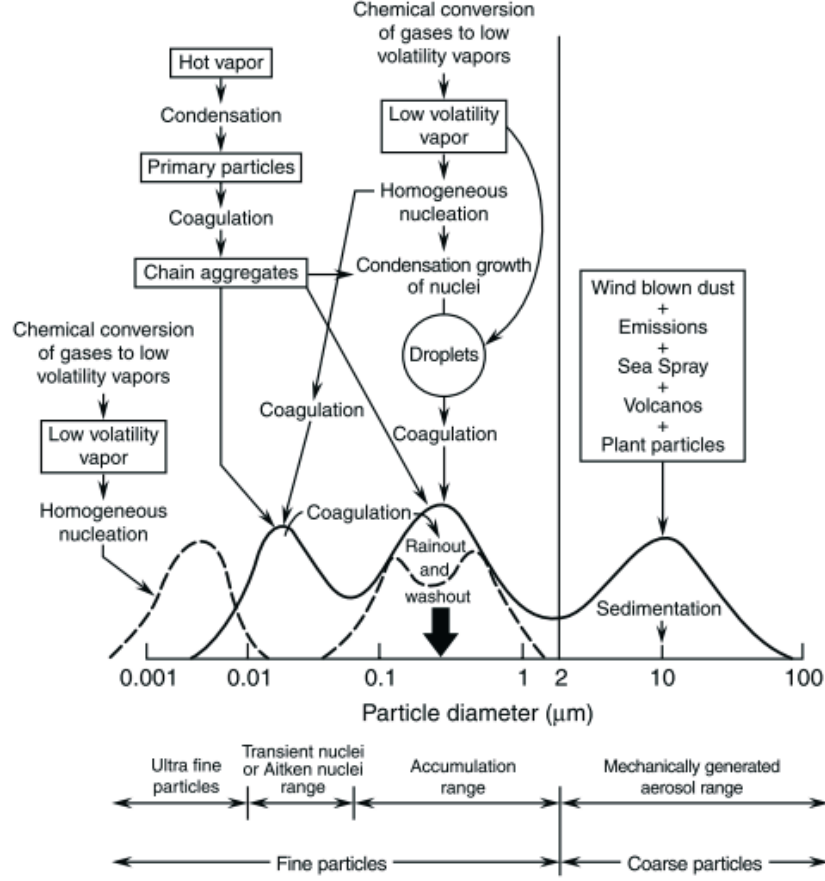


Figure 1.1: *Aerosol size distribution.* Taken from Finlayson-Pitts and Pitts (2000). Shown is the typical four mode size distribution with the formation and loss processes for each mode. The solid lines represents the original hypothesis of Whitby and Sverdrup (1980). The dashed lines include the ultra fine particle mode in the aerosol size distribution.

of diameters between 0.1 and 1  $\mu\text{m}$ . These particles are mainly from condensation of vapors with low volatility and from coagulation of smaller particles. The Aitken mode includes particles of diameters between 0.01 and 0.1  $\mu\text{m}$ . These particles arise from the growth or coagulation of smaller particles and are also produced in combustion sources such as vehicle exhausts. Particles smaller than 0.01  $\mu\text{m}$  are known as ultrafine particles. These are formed through nucleation processes directly from gas phase species such as sulphuric acid (Kulmala et al., 2004). Loss processes for all aerosols are the dry and wet deposition. Dry deposition occurs after transport of the aerosols due to impaction or diffusion of the aerosols onto surfaces. Wet deposition describes the process of the aerosol loss

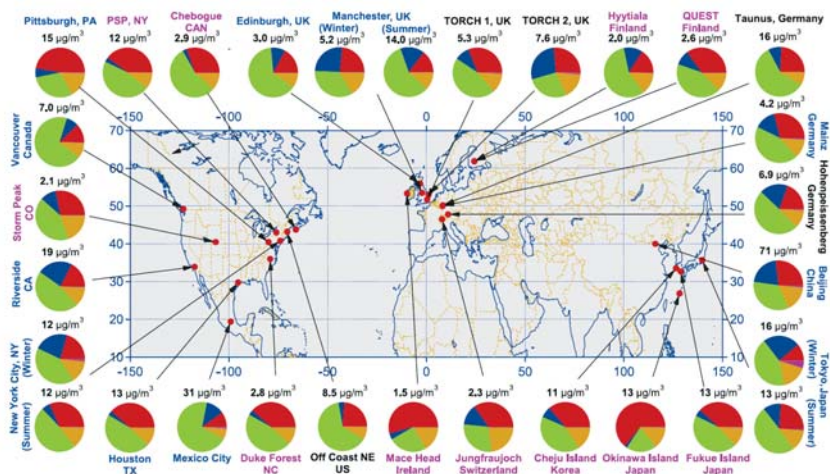


Figure 1.2: *Composition of PM<sub>1</sub> aerosol determined from AMS measurements. Type of sampling location is indicated as following: urban areas (blue), <100 miles downwind of major cities (black), rural/remote areas >100 miles downwind (pink). Pie charts show the average mass concentration and chemical composition: organics (green), sulfate (red), nitrate (blue), ammonium (orange), chloride (purple). Taken from Zhang et al. (2007).*

through rain or other forms of precipitation.

The chemical composition of atmospheric aerosols significantly varies depending on their sources. In Figure 1.2 composition of non-refractory submicron particle (PM<sub>1</sub>) mass measured with the Aerosol Mass Spectrometer (AMS) is shown (Zhang et al., 2007). Organic matter is a major constituent of atmospheric aerosols, comprising 18-70% of the PM<sub>1</sub>. The rest of the organic aerosols consists of sulfate (10-67%), nitrate (1.2-28%), ammonium (6.9-19%), and chloride (<detection limit-4.8%). This shows that most of the atmospheric aerosols are a mixture of organic compounds and sulfate. However the actual chemical composition of the organic fraction in aerosols is complex, and largely unknown. In Figure 1.3 chemical speciation of organic aerosol in California by Rogge et al. (1993) is shown. Only about 15% of the organic fraction could be identified in this study. However the knowledge of the chemical composition in organic aerosols is important. Both the size of the aerosols and also the chemical composition of the aerosols determines its properties and impact regarding global climate, aerosol chemistry and human health.

Aerosols in the atmosphere can directly influence the climate by scattering and absorbing solar and terrestrial radiation, the so called aerosol direct radiative forcing. In the current IPCC report the total direct climate forcing from aerosol

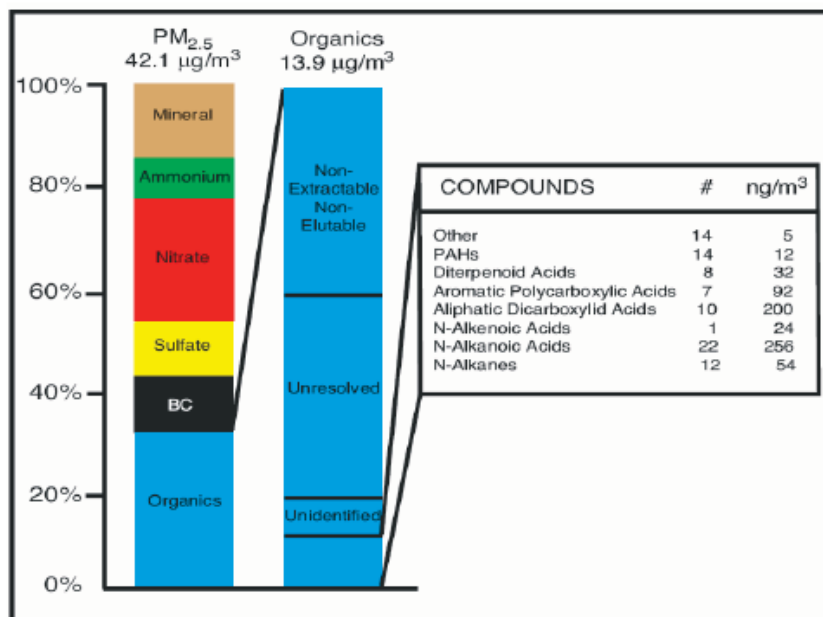


Figure 1.3: *Speciation results for organic aerosol in Southern California. Taken from NARSTO Assessment report 2003, originally by Rogge et al. (1993).*

is estimated to be  $0.50 \pm 0.40 \text{ Wm}^2$  (Forster et al., 2007).

Aerosols also indirectly effect earths radiative energy budget by acting as cloud condensation nuclei (CCN) and/or ice nulei (IC). Their chemical composition, size, and mixing state have an impact on formation, lifetime and optical properties (albedo) of the clouds. The cloud albedo radiative forcing estimate lies in the range of  $0.3$  to  $1.8 \text{ Wm}^2$  (Forster et al., 2007).

Aerosol particulate matter, especially the fine particulate matter smaller than  $100 \text{ nm}$ , can deposit in the human respiratory system and directly enter the blood stream. Fine particulate matter has been implicated in heart and lung diseases, allergies, and increased mortality (Pöschl, 2005; Pope, 2007). The health effects are dependent on both exposure concentrations and length of exposure (Pope, 2007).

### 1.3 Formation of Secondary Organic Aerosols

Recent studies indicated that SOA is a major fraction of total organic aerosol in the atmosphere. SOA can be more than 50% of the total organic aerosol and regionally up to 90% (Kanakidou et al., 2005). However current model under-



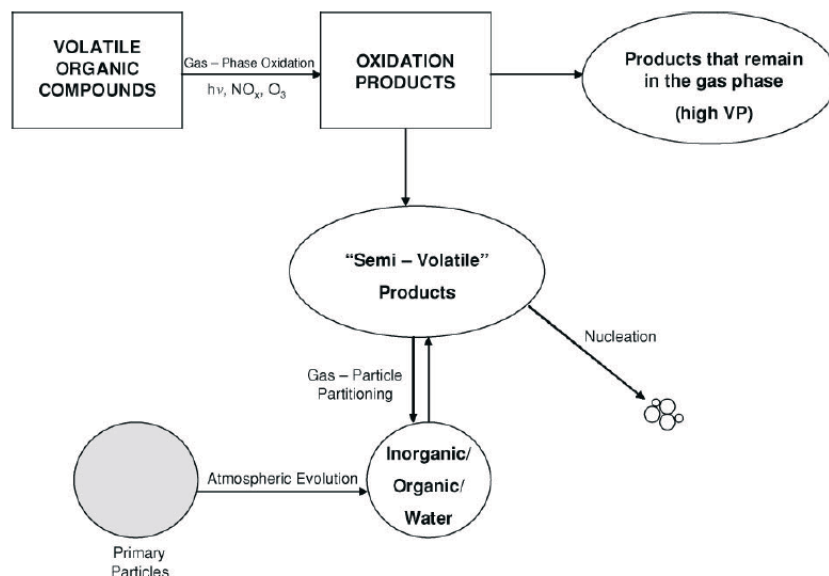


Figure 1.4: Schematic of SOA formation from VOC oxidation. Taken from Seinfeld and Pankow (2003).

estimate the abundance of organic aerosols by factor of 10 to 100 in the free troposphere (Heald et al., 2005; Volkamer et al., 2006; Goldstein and Galbally, 2007). Goldstein and Galbally (2007) suggested that this deviations are either due to higher SOA yields than expected from previous studies or due to unmeasured precursors which are more important for the SOA formation than the measured compounds. This indicates that the chemistry of atmospheric SOA formation is incompletely understood till now.

SOA is formed by the oxidation of both anthropogenic and biogenic volatile organic compounds (VOC) through ozone, hydroxyl radicals, or nitrate radicals. The relevant processes for SOA formation are schematically shown in Figure 1.4. The oxidation products formed have a lower volatility than the precursor compound due to the addition of oxygen and/or nitrogen to the organic molecules (Odum et al., 1996; Seinfeld and Pankow, 2003). Condensation will occur when the gas phase pressure of the compound exceeds its vapor saturation pressure. The condensation yield of this compound increases proportional to further increase in its production. The compound concentration in the gas phase will be constant and is equal to its saturation vapor pressure. The total concentration of a the product  $i$  can be calculated considering the precursor concentration as

follows (Seinfeld and Pandis, 1998):

$$c_{t,i} = a_i \frac{M_i}{M_{ROG}} \Delta ROG \quad (1.1)$$

$c_{t,i}$	= total concentration of product $i$	$[\mu g m^{-3}]$
$a_i$	= molar yield of product $i$	[1]
$M_i$	= molecular weight of product $i$	$[g mol^{-1}]$
$M_{ROG}$	= molecular weight of parent compound	$[g mol^{-1}]$
$\Delta ROG$	= reacted precursor concentration	$[\mu g m^{-3}]$

This calculation is valid if this system describes only one compound/product and if no pre existing organic aerosols are present because most particles can adsorb vapor molecules on their surfaces. The partitioning of a compound between the gas and the aerosol phase is described by a partitioning coefficient (Pankow, 1994a):

$$K_{p,i} = \frac{F_i}{A_i TSP} \quad (1.2)$$

$K_{p,i}$	= equilibrium partitioning coefficient	$[\frac{m^3}{\mu g}]$
$F_i$	= concentration in the aerosol phase	$[\mu g m^{-3}]$
$A_i$	= concentration in the gas phase of species $i$	$[\mu g m^{-3}]$
$TSP$	= total suspended particulate matter concentration	$[\mu g m^{-3}]$

This equation shows that the amount of the compound adsorbed onto the particle (or absorbed into the particle) depends on the total amount of particulate matter present. If the total aerosol mass increase more of the organic compound will be in the particulate phase due to the fact that a greater surface and volume of the particulate matter is available.

## 1.4 Measurement of Chemical Composition of Organic Aerosols

Numerous techniques for the analysis of the chemical composition of organic aerosols (OA) exist. The complexity of OA and SOA due to the sheer number of individual compounds present (Goldstein and Galbally, 2007) is a major obstacle in the complete speciation of OA. The following chapter will give a brief overview over the most common analytical techniques for OA speciation. For a

complete overview it is referred to a number of reviews published in the last years (McMurry, 2000; Rudich et al., 2007)

The most common methods of chemical speciation are filter-based techniques where particles are collected on quartz fiber filters or teflon filter. After sampling the filter content is analyzed in the laboratory using standard analytical procedures. This includes solvent extraction, supercritical fluid extraction or thermal desorption of the filter samples. Pre-treatment of the filters, such as derivatization, can be used to increase the range of measurable compounds. Subsequent analysis with analytical techniques, such as gas chromatography coupled to mass spectrometry (GC-MS, most widely used) and liquid chromatography coupled to MS (LC-MS) (especially for polar compounds) will lead to the molecular characterization of the OA. Recent studies showed improvements of the resolution of such techniques by using two-dimensional GC coupled to time-of-flight (TOF) MS (Hamilton et al., 2004). The high quantities needed for laboratory analysis of filter samples often require sampling for several hours or days. In a recent study an improved system with 1 h time resolution with subsequent GC-MS analysis has been presented by Williams et al. (2006).

Off-line time integrating bulk measurements are often subjected to positive and negative sampling artifacts, such as loss of compounds due to volatilization, gas phase adsorption and reactions during collection that can alter the sample (Turpin et al., 2000). Thus, uncertainties exist as to how representative these samples are for the atmospheric aerosol composition.

The type of sampling described before have limitations regarding the spatial and temporal sampling densities. Therefore an important focus lies today on the on-line measurements of aerosol chemistry in real time with a high time resolution. Two main types of online techniques are used, the aerosol mass spectrometry (AMS) and the particle-into-liquid sampling (PILS). Aerosol particles which are introduced into the PILS instrument are grown to large sizes in a supersaturated environment. They impact onto a surface which is continuously flooded with water. The water is then periodically analyzed using Ion Chromatography with a time resolution of several minutes. The general principle of the AMS involves that airborne aerosols are introduced into the instrument with subsequently vaporization and ionization of the aerosol components followed by MS detection. The AMS technique has proven to be most useful in the investigation of organic aerosol in real time. Further details on the AMS will be presented in chapter 2.6.

## 1.5 Objectives of this work

Within the present work a new technique for online compound specific measurements with a high time resolution was developed: the Aerosol Collection Module (ACM). The ACM is designed to sample and transfer atmospheric aerosol to a gas phase detector through thermal desorption. This technique was applied during an aerosol chamber simulation experiment which focused on studying the formation of SOA from the  $\beta$ -pinene ozonolysis.

The first part of this work comprises the technical description and the laboratory characterization of the ACM. The aim was to determine the particle collection efficiency, gas phase transfer efficiency, and linearity of the ACM interfaces with a GC-MS system. This characterization requires the simultaneous measurement of the test aerosol with an independent measurement which was realized using a Scanning Mobility Particle Sizer (SMPS).

The second part of this work comprises the analysis of SOA from the ozone oxidation of  $\beta$ -pinene. The focus of this study was on the analysis of the aerosol phase and the partitioning of nopinone between the gas and particulate phase using the new technique of the ACM-GC-MS and additional measurements of PTR-ToF-MS, AMS and SMPS and filter samples. The ACM-GC-MS measurements of nopinone were compared to the results of the filter measurements thereby comparing the new online technique with the common offline technique. The further analysis of the aerosol phase included the identification of  $\beta$ -pinene ozonolysis products and their temporal evolution during the experiment.



## 2. Instrument Descriptions

This chapter contains the technical description of the Aerosol Collection Module set up (ACM), and of the detectors coupled to the ACM. In the first part the measuring principle and the overall setup of the ACM will be presented. Each part of the ACM will be described in detail. In the second part two types of detectors for gas phase VOC will be briefly described and the coupling with the ACM is presented. In the last part of this chapter filter sampling, the aerosol mass spectrometer (AMS) and the scanning mobility particle sizer (SMPS) are presented. These instruments measure particles with different approaches and were used for simultaneous measurement of organic aerosol in the aerosol chamber experiment in parallel with the ACM.

### 2.1 The Aerosol Collection Module

#### 2.1.1 Overview and Measuring Principle

The ACM is designed to sample atmospheric aerosol and transfer the preconcentrated aerosol to a detector. In practice, sampling is achieved in an evacuated environment on a small collection surface. Aerosols are thermally desorbed by heating the surface. The evaporated aerosols are transferred by a carrier gas through a transfer section and injected into a gas phase detector. A schematic of the ACM is shown in Figure 2.1.

The ACM consists of three main sections: an aerosol focusing and sampling section, a particle collection section and a transfer section. In the first section an atmospheric air sample is drawn into the ACM through the particle inlet. The aerosol particles are focused into a narrow beam inside the aerodynamic lens and pass through the vacuum chamber. The particle beam is directed to the cooled collector where the aerosols impact onto a small sampling surface. After the sampling is completed the sampling valve closes and the collector is heated. The aerosols are desorbed from the collection surface. At the same time the carrier gas

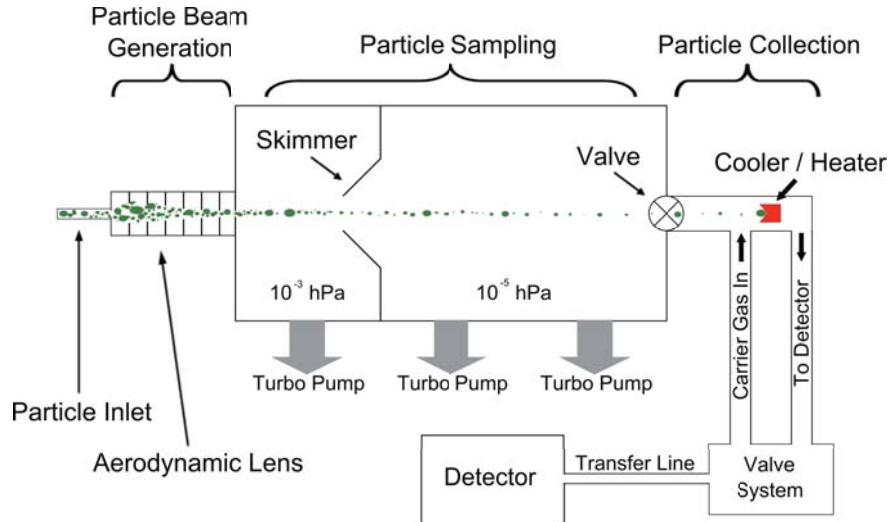


Figure 2.1: Schematic of the ACM instrument. The ACM is composed of three main sections: the aerosol sampling section consisting of the aerodynamic lens and the vacuum system, the aerosol collection section including the collector and the cooling/heating system and the aerosol transfer section which contains the valve system and the transfer line.

is introduced into the collector flushing the evaporated aerosols into the transfer section. The sample passes through the adjacent valve system and the transfer line. A gas phase detector for analysis of the vapors is connected to the transfer line. A detailed description of each of the sections is presented in the following.

### 2.1.2 Aerosol Sampling

The aerosol sampling section consists of two parts, an aerodynamic lens system (Liu et al., 1995a,b) which is coupled to the vacuum system. A particle beam is produced by the expansion of aerosol through a nozzle at the exit of the aerodynamic lens into the vacuum system. The aerosols are accelerated by this expansion. Behind the nozzle the gas phase of the aerosol expands rapidly while the particles continue in their motion due to their inertia. Thus the gas phase can be pumped off and the particles are concentrated relative to the gas phase by a factor of  $\sim 10^7$ .

### **Aerodynamic lens**

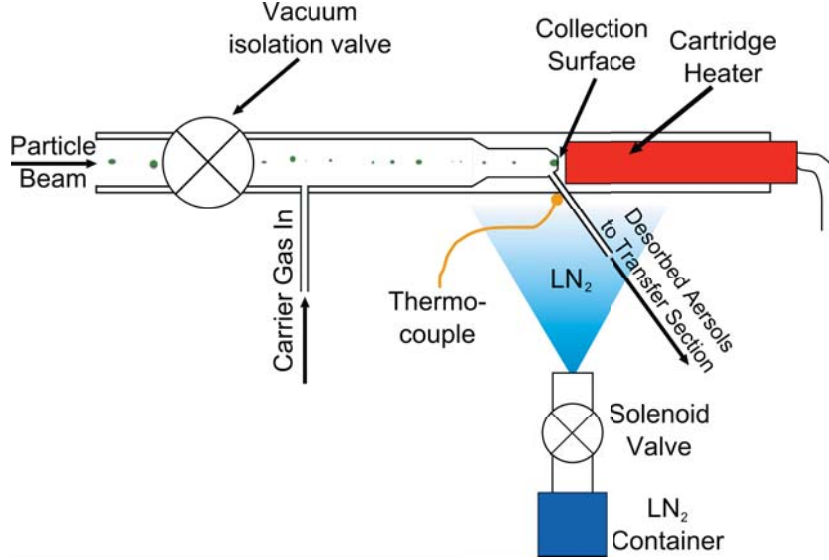
The aerodynamic lens system consists of six orifice lenses ranging from 5 mm diameter at the entrance of the lens to 3 mm diameter at the exit (Jayne et al., 2000). The lenses are mounted inside a stainless steel tubing of 12.7 mm outer diameter and a length of 178 mm. The pressure inside the lens is approximately 2.6 hPa. When the particle laden gas passes through one of these lenses the particle trajectories are forced closer to the centerline. After passing all lenses the particles are confined very close to the axis at the entrance of the nozzle. Particles close to the axis experience small radial drag forces and stay close to the centerline after passing the nozzle. A narrow particle beam is formed which passes through the vacuum system. However due to the Brownian motion of the particles the narrowness of the beam is limited. Additionally non-spherical particles can experience lateral forces after the nozzle expansion. The lens focuses the particle into a narrow beam which is smaller than 1 mm in diameter.

The pressure is held constant by the use of a critical orifice with a diameter of 100  $\mu\text{m}$  at the entrance to the aerodynamic lens inlet. Due to the orifice the sampling flow is kept constant at 80 ml/min. The particle transmission efficiency for particles in the size range between 70 and 500 nm in diameter is 100% (Liu et al., 2007).

### **Vacuum system**

The vacuum system consists of two differentially pumped vacuum chambers which are separated by a skimmer. A turbomolecular pump (Varian Turbo-V 301 Navigator Pump) with a pumping speed of 250 l/min is used to evacuate the first vacuum chamber. The pressure in this chamber is maintained below  $10^{-3}$  hPa which ensures a constant flow through the aerodynamic lens. The second vacuum chamber is pumped with two Varian Turbo-V 81 Pumps with a pumping speed of 50 l/min. The chamber is maintained at a pressure below  $10^{-5}$  hPa. In a differentially pumped vacuum system an additional orifice, known as the skimmer cone, is necessary. Use of this additional orifice between the vacuum chambers allows the particle beam to be free from boundary layer or shock wave interferences. The skimmer cone has a diameter of 2 mm. The turbo pumps of the vacuum system are backed by a 60 l/min diaphragm pump. It is connected to the particle inlet and the vacuum chambers and operates such that the particle inlet pressure is approximately 1.6 hPa. The vacuum system can be separated from the collector with an automated controlled vacuum isolation valve.



Figure 2.2: *Schematic of ACM collector.*

### 2.1.3 Aerosol Collection

The aerosol collection system of the ACM consists of a collector and a cooling/heating system. A schematic of the collector is shown in Figure 2.2. The collector is a 316 stainless steel tubing with an inner diameter of 5.3 mm and a length of 80.8 mm. The tubing is separated into two parts, the collection section and the heating section, which are completely separated from each other. The collection section is connected to the vacuum isolation valve and is 50 mm long. After 43 mm the tubing tapers for 7 mm and ends at the collection surface which is approximately 3.4 mm in diameter. The aerosol sampling system is aligned in such a way that the focused particle beam passing the vacuum isolation valve is directed to the center of the sampling surface. The collector is chemically passivated with an Inertium<sup>®</sup> coating (Advanced Materials Components Express, Lemont, PA). Two additional 1/16" tubings are connected to the collection section. Both tubings have an outer diameter of 1.6 mm and an inner diameter of 1 mm and are chemically passivated with Silcosteel<sup>®</sup> (SilcoTek, Bellefonte, PA). The first tube is located between the vacuum isolation valve and the collection surface. It introduces a carrier gas into the collector. The second tube is located directly below the sampling surface and connects the collector with the transfer section. This connection is additionally heated using a heat tape which is wrapped around the tubing. The temperature of the heat tape is controlled through a electrical power controller and measured with a thermocouple

connected outside of the tubing.

During sampling the collector can be cooled with liquid nitrogen. A liquid nitrogen container is connected to the stainless steel tubing which ends closely under the collector. The amount of liquid nitrogen which is sprayed towards the collector is controlled through automated opening and closing of a solenoid valve. The temperature achieved by this cooling mechanism is approximately -60 °C.

On the back of the collector is a bore hole which can hold a cartridge heater. The bore hole has an inner diameter of 5.3 mm. The cartridge heater can be completely inserted into the hole so that the tip of the heater is centered 6.6 mm behind the collection surface. It can heat the collector to a preset temperature, and due to its position rapid heating of the collected sample is assured. To control the cooling and heating procedure a thermocouple is connected outside the collector at the junction of the collector with the tubing which leads to the transfer section. The thermocouple readout is used by the ACM controller board to operate the cartridge heater voltage and the opening and closing of the solenoid valve during the sampling and transfer process. The complete measurement cycle of the collector and transfer system is presented in chapter 2.1.4.

#### **2.1.4 Aerosol Transfer**

In this section the transfer of the desorbed particles through the valve array and the transfer line is described. Also the different stages of the measurement cycle regarding the sequence of the valve switching and the temperatures applied to the system is presented.

##### **Valve system & Transfer Line**

The valve system consist of two 4 port valves with 1/16" fittings and 0.75 mm ports (Valco Instruments Company Inc., Houston, TX) which are controlled by an microelectric actuator. The valves are connected with the collector and among each other with 1/16" stainless steel tubings. The length of the tubings for the different connections vary between 3 cm to 20 cm. The transfer line is also a 60 cm 1/16" tubing which is connected to the valve system at port 4 of valve 2. The valve system is installed inside a thermally isolated box which can be heated. The temperature of the valve box is controlled via a thermocouple. The transfer line is constantly heated through a heat tape wrapped around the tubing. The temperatur of the heat tape is controlled through the ACM controller. Both valves and the transfer line are chemically passivated with an Inertium® coating.

The 1/16" tubings are passivated with Silcosteel®. A schematic of the valve system is shown in Figure 2.3.

The valves have two possible settings: *load* and *inject*. When the valves are set to *load* port 1 is connected to port 4 and port 2 is connected to port 3. When the valves switch to *inject* the connections are between port 1 & 2 and 3 & 4, respectively. The carrier gas flow through the collector and to the detector is controlled by the different *load/inject* status of the valves. In every experiment and set up presented here the carrier gas is helium 6.0. The helium flow is pressure regulated at the entrance to the ACM and held constant at 2400 hPa.

### Measurement Cycle

The measurement cycle of the ACM consists of three parts: the standby/backflush mode, the sampling mode, and the desorption/inject mode.

The valve settings for standby/backflush mode are shown in Figure 2.3(a). The carrier gas enters the ACM and is splitted into two streams. In standby mode stream one flows through valve 1 to the detector. Independent of the valve settings it is ensured that the detector will be constantly provided with helium which is a necessity for certain analytic gas detectors such as a gas chromatograph. The second stream flows through valve 2 into the collector, flushes over the collection surface, leaves the collector, passes through the two valves and is lead out a vent. In standby the collector is not actively heated. Due to the surrounding heating of the valve box and the connection of the collector to the valve system the temperature of the collector in standby mode is approximately 80 °C.

A measurement cycle is started by opening of the solenoid valve until the collector is cooled down by the liquid nitrogen to the desired temperature. As soon as the collector reaches the programmed temperature valve 2 is switched to the *inject* mode. Thereby the collector is separated from the carrier gas. The entrance and the exit of the 1/16" tubing of the collector are now connected into a loop (Figure 2.3(b)). The vacuum isolation valve opens and the collector and the loop are evacuated. The particle beam is directed to the collection surface where the aerosol impact upon. The solenoid valve opens and closes as necessary to ensure a constant cooling of the collector with liquid nitrogen and to maintain the collection temperature. The transfer valve system and the transfer line are heated during the whole measurement cycle.

After the sampling is completed the vacuum isolation valve closes and valve 1 is switched to *inject*. The carrier gas is introduced again into the collector. A voltage is applied to the cartridge heater and the collector starts to heat up. The aerosol sample is desorbed from the collection surface. The carrier gas flushes the

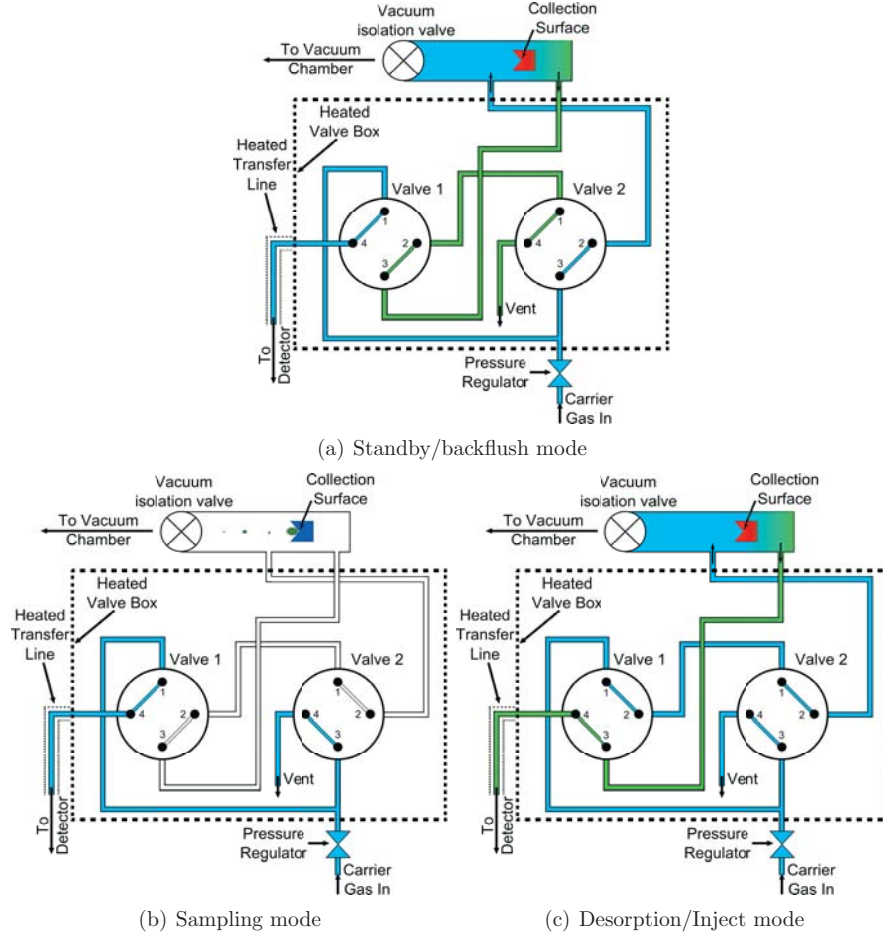


Figure 2.3: Schematic of the transfer valve system. (a) In standby/backflush mode valve 1 and 2 are set to load and the collector and detector are supplied with the carrier gas. For cleaning purpose the collector can be heated (backflush mode). (b) With valve 1 set to load and valve 2 to inject, the ACM is in sampling mode. The collector is separated from the carrier gas supply and the particle beam is directed to the collection surface where the aerosol sample is accumulated. During sampling the collector is cooled with liquid nitrogen. (c) For the desorption/inject mode both valves are set to inject. The vacuum isolation valve is closed and the collector heated. The aerosol sample is desorbed from the collection surface and transferred with the carrier gas stream to the detector.

evaporated aerosols through valve 1 into the transfer line and to the detector. It is ensured that the path of the desorbed sample through the valve system is as short as possible to minimize losses during the transfer process. The desorption mode period lasts at least several minutes to insure that the aerosol sample is completely transferred to the detector. Test measurements with the ACM cou-

pled to a PTR-MS showed that a test aerosol (heptadecanone) was desorbed at 250 °C from the collector and transferred to the detector in approximately 2 minutes.

After the desorption is completed valve 1 and 2 are switched back to *load*. The ACM enters the cleaning mode called backflush mode. The cartridge heater remains active and as a general rule is set in this stage to a higher temperature than the desorption temperature previously applied. Due to the higher temperature of the collector and therefore of the collection surface any residuals of the sampling are now desorbed and flushed out of the system through the vent passing both valves. This cleaning of the collector is always performed after each measurement. The duration of the backflush mode can be set to meet the actual requirements regarding possible remaining contaminations. After the cleaning is completed the cartridge heater is powered down and the ACM is again in standby and ready for the next cycle.

## 2.2 Detectors

The ACM is coupled to a detector where a direct online analysis of the collected aerosol samples can be conducted. It is possible to couple the ACM with different types of analytic gas detectors and thereby address different scientific questions without changing the type of sampling and further on using the advantage of online and in-situ analysis of the sample. The type of detector can be chosen in regard to the specific analytical abilities of the detectors, for example the chemical speciation of a sample using a gas chromatograph (GC) couple with a mass spectrometer (MS) or the high time resolution of a proton transfer reaction mass spectrometer (PTR-MS). The first prerequisites is that the detector is capable of establishing a leak free connection with the ACM transfer line. The second prerequisites is that the detector depends on the carrier gas feed or at least is undisturbed in its analytical performance by the carrier gas with which the sample is introduced into the detector.

### 2.2.1 Gas Chromatograph - Mass Spectrometer

At first the coupling of the ACM with a combination of a gas chromatograph (Fisons GC8060) and a quadrupole mass spectrometer (Fisons MD800) (from now on abbreviated as GC-MS) is presented.

Gas chromatographs are used to separate compounds of mixtures, in this case the compounds of the vaporized aerosol sample. In general a GC system consist

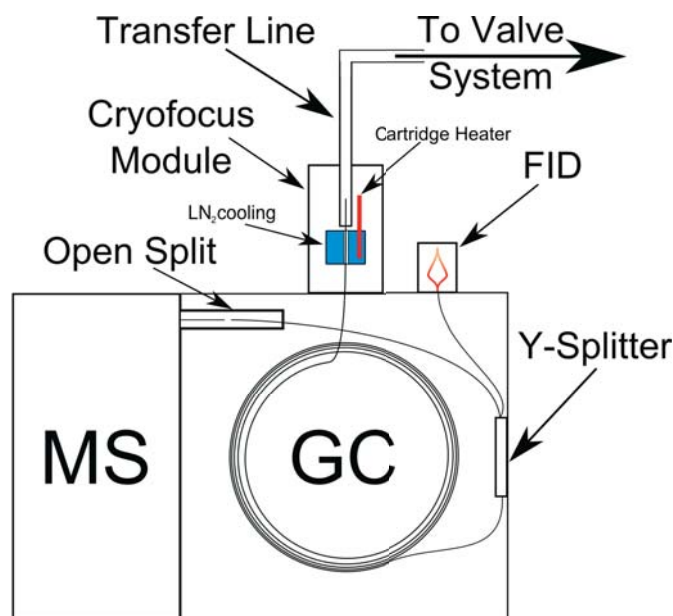


Figure 2.4: *Schematic of the GC-MS detector. The GC-MS system consists of a cryo-focusing module and an additional flame ionization detector.*

of an injector, a gas chromatographic column which is installed inside a oven, and a detector. The sample is injected for example by means of a syringe or a sample loop into a heated injection port where the sample is vaporized into a flowing gas stream. The inert carrier gas, called the mobile phase, transports the sample through the column. In case of a capillary column, the column is a tubing made of fused silica coated with a thin film of liquid, called the stationary phase, onto the inside of the tubing wall. Separation of the injected mixture occurs by partitioning between the gas stream and the stationary phase. The chemical properties of the sample molecules of importance now is their difference in ability to dissolve in the stationary phase, i.e. their difference in partition between the mobile and the stationary phase. Those compounds which are more soluble in the stationary phase are retained the longest. Therefore, a mixture of compounds can be separated due to differences in the partitioning of each compound between the two phases. The gas stream which contains the separated compounds is then passed through a detector. The detector signal is monitored continuously and measures subsequently the compounds which are eluted from the column.

A schematic of the GC-MS set up used for the experiments described in this work is shown in Figure 2.4. The GC-MS system consists of a cryofocusing module (Tekmar 3000) and an additional flame ionization detector (FID). An Agilent J&W DB-5ms capillary column with 0.25 mm inner diameter, a film thickness of

0.25  $\mu\text{m}$  and a length of 60 m is installed in the gas chromatograph.

The coupling of the GC to the transfer line of the ACM was accomplished using a 1/16" Swagelok connector. The transfer line was connected with a stainless steel ferrule on one side of the connector. On the other side the DB-5ms column was connected to the connector using a graphite ferrule.

The column was pushed through the connector and approximately 5 mm further into the transfer line. The introduction of the column into the transfer line ensures that the possibility of a dead volume between the transfer line and the GC column is reduced to a minimum.

The connection between the transfer line and the GC column is installed inside the cryofocusing module (CFM). The cool down of the module is started and reaches its final temperature during the ACM sampling. The aerosols samples desorbed from the ACM is refocused at the beginning of the GC column. One minute after the desorption is completed the CFM is rapidly heated and the sample is injected into the GC for chromatographic separation.

The electronic signal which starts the injection of the sample into the GC also starts the data acquisition of the GC-MS system. Compounds eluted from the column are splitted with a Y-splitter with a constant split ratio of 1:1 to be detected simultaneously with a Flame Ionization Detector (FID) and a mass selective detector (MS). Thus, a quantitative analysis with FID and an identification with the MS can be provided for each compound detected with the GC-MS system. The columns after the split are 30 cm of passivated fused silica columns without a stationary phase which have no chromatographic separation capabilities. One split-column is installed into the FID. The FID is a gas chromatographic detector for volatile hydrocarbons and many carbon containing compounds with a limit of detection in the picogram range. The FID is used for quantification due to its wide linear dynamic range that extends over 6 to 7 orders of magnitude (e.g., Jorgensen et al., 1990; Goldstein et al., 1995).

The other split-column and the mass spectrometer are connected with a open split. The open split assures that the two exits of the split-columns are kept at ambient pressure. Thus the split ratio is constant at 1:1. It also has the benefit that the retention time of the eluted compounds measured with the FID matches with the retention time detected in the MS. The quadrupole mass selective detector (MS) is equipped with a 70 eV electron impact (EI) ion source. The MS is operated in total ion scan mode in the range of 10 to 260  $m/z$  with a scan time of 1 second for one complete spectrum. The collected full mass spectra are used for compound identification.

The head pressure of the GC-MS system is predetermined by the constant head pressure of the ACM which is kept at 2400 hPa (see chapter 2.1.4). The head

pressure was adjusted with regard to the GC column dimensions and type of carrier gas. With this adjustment the average linear velocity of the carrier in the column is  $\bar{u} = 34.3 \frac{\text{cm}}{\text{s}}$  allowing good compound separation conditions. The FID detector gas flows are 30 mL/min for hydrogen and 300 mL/min for synthetic air. The open split has a separate gas flow of 2 mL/min of helium.

### 2.2.2 Proton Transfer Reaction Mass Spectrometer

The ACM can also be coupled to a proton transfer reaction mass spectrometer (PTR-MS). PTR-MS allows the simultaneous real-time monitoring of volatile organic compounds (VOC) (Lindinger et al., 1998; de Gouw and Warneke, 2007). The instrument is divided into three mayor parts: the ion source, the drift tube and the detector. In the ion source protonated water ( $H_3O^+$ ) is generated from vapor of distilled water through an electrical discharge. Afterwards the protonated water is injected into the drift tube. Trace gases which enter through the sample inlet of the drift tube interact with the protonated water. During this interaction a proton transfers from the hydronium to the trace gas molecule, which leads to a protonated and therefore ionized molecule and a neutral water molecule. However, only compounds with a proton affinity that is larger than the proton affinity of water can be measured with a PTR-MS. Since proton transfer is a soft ionization method, the fragmentation rates can be kept very low compared to electron impact ionization. The ionized trace gas components are then detected with a quadrupole mass spectrometer. The PTR-MS is calibrated using temperature controlled diffusion sources with standard reference compounds.

The coupling of the ACM to the PTR-MS deviates from the GC-MS coupling due to its special prerequisite for the condition of the the drift tube. The PTR-MS drift tube requires that inside the drift tube a pressure of 2 to 2.5 hPa is kept constant. Changes in pressure during the measurement can complicate the interpretation of the PTR-MS data later on. Additionally at high pressure (larger than 2.5 hPa) the fragmentation rate increases (Tani et al., 2004). Increasing the pressure in the drift tube significantly in comparison to the optimal operation conditions can lead to conditions which prevent ionization of the trace gases. Since we need a high head pressure for the ACM (2400 hPa) to ensure a sufficient and rapid transfer of the evaporated sample to the detector we need to have a coupling which reduces the pressure at the entrance of the inlet of the PTR-MS. This pressure reduction should be as constant as possible.

Under normal operating conditions the drift tube is under the influence of an electric field (typically  $62.5 \text{ V cm}^{-1}$ ). Therefore it is necessary that the coupling



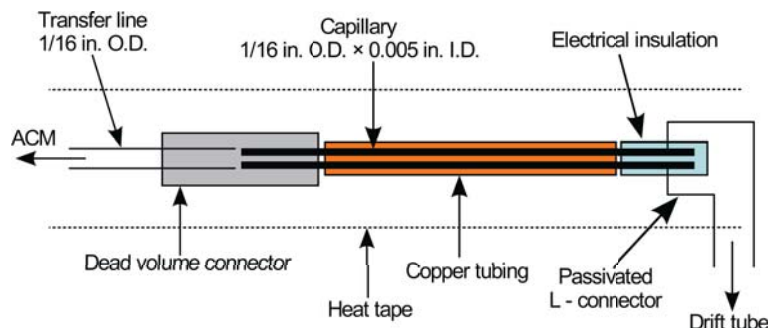


Figure 2.5: Schematic of the ACM - PTR-MS coupling.

is electrically insulated from the drift tube.

Also the drift tube can not exceed a certain temperature range. In general the heated drift tube of the PTR-MS is operated at a maximum temperature of 60 °C however the temperature of the transfer line is about 200 °C. One has to make sure that the temperature drop from the transfer line to the drift tube is large enough not to overheat the drift tube. On the other hand too large temperature gradients need to be avoided since they could lead to condensational loss of semivolatile compounds.

A schematic of the ACM-PTR-MS coupling is shown in Figure 2.5. In contrast to the ACM-GC-MS coupling, the ACM transfer line can not be linked directly to the PTR-MS. Due to the limited pressure allowed in the drift tube a stainless steel capillary with an outer diameter of 1/16" and an inner diameter of 0.005" was used to couple the transfer line of the ACM with the drift tube inlet. The transfer line is connected with the capillary through a free dead volume connector. The other side of the capillary is introduced directly into the L-connector of the drift tube inlet. A 3 cm long electrically isolating teflon tubing is slipped over the end of the capillary to separate the electrical potential of the drift tube from the rest of the system. The length of the capillary (18 cm) was adjusted such that the pressure in the drift tube is approximately 2 hPa. Fine tuning of the pressure in the drift tube could be done by changing the ACM carrier gas head pressure. This will not significantly change the condition for the transfer of the sample through the ACM. The capillary is encased with an additional copper tubing to increase the heat conductance. The transfer line and the capillary are heated by heat tapes and the temperatures are controlled with thermocouples. The L-connector and the drift tube are heated through a heating system controlled by the PTR-MS system. 2 cm of non heated space between the capillary and the L-connector is sufficient to achieve a drop in temperature over the length of the L-connector to ensure not to overheat the drift tube. The temperatures of

the L-connector and the drift tube are also controlled with thermocouples.

## 2.3 Instrument Automation and Data Acquisition

The ACM is a semi-automated system described in the following. The data acquisition and the data reduction presented are for the GC-MS system. The characterization and aerosol chamber experiments presented in this work have all been conducted with the ACM coupled to the GC-MS system.

The measurement cycle of the ACM is completely automated regarding the collection and transfer sections. However, some of the temperatures settings and the start signal for the cryofocusing module have to be applied manually. The ACM consists of two control units. The pump controller regulates the speed of turbo molecular pumps (see details of the vacuum system in chapter 2.1.2). The ACM controller regulates the temperatures which are applied to the collector (chapter 2.1.3). It also controls the vacuum isolation valve, the solenoid valve and the different valve positions of the transfer section. The length of the time intervals for each step of the measurement cycle can be set via the ACM controller. The temperatures of the valve box and the transfer line (chapter 2.1.4) are controlled through separated controllers.

The cryofocusing module status is regulated by the Tekmar 6000 control unit. The cooling of the module and subsequent injection of the sample onto the column can only be initiated manually. Note that with the start signal for the injection of the sample into the GC-MS the detectors data acquisitions are started automatically. This guarantees that each run of the GC-MS is comparable to each other regarding the retention times. The data of the flame ionization detector is recorded with the APEX data acquisition software and the MS spectra with MassLab (version 1.4).

## 2.4 Data Reduction and Compound Identification

All chromatograms were baseline corrected. Retention windows were set to regions in the chromatograms which does not contain a chromatographically separated peak. Afterwards, a polynomial function was fitted to the baseline of the

chromatogram:

$$f(x) = K_0 + K_1x + K_2x^2 \quad (2.1)$$

The fit for the baseline was then subtracted from the chromatogram.

The integration of the chromatograms was done using WaveMetrics Igor Pro (Version 6.0.2.4). The peaks in the chromatograms were fitted with a exponentially modified gaussian function. This function is a convolution of a gaussian peak with an exponential decay and often used for the deconvolution or smoothing of chromatographic peaks (Li, 2002). The analytical expression of the function is:

$$f(c, \sigma, t) = c \cdot \exp(-ct + \frac{\sigma^2 c^2}{2}) \cdot g(\frac{t}{\sigma} - \sigma c) \quad (2.2)$$

$$g(t) = \Gamma(0.5, 0.5t^2)$$

$c$  = exponential decay constant

$\sigma$  = standard deviation

$t$  = Retention time

It is possible to deconvolute chromatographic peaks which are not baseline separated. The Igor procedure applies a separate fit function to each peak. The parameters of each fit function are adjusted such that the combination of the calculated fit functions represents the measured data points. Residuals of the fit results can be plotted to verify the quality of the fitting procedure and the area under the fit for each chromatographic peak is calculated.

The identification of compounds with the MS was done by matching the mass spectra of resolved peaks with the content of the NIST (National Institute of Standards and Technology) Mass Spectral Library and with mass spectra obtained from direct injection of single compounds into the GC-MS system. In the MassLab program retention time windows can be set for the chromatographically separated peaks. The mass spectra in the retention time windows are averaged. These mass spectra are then corrected by subtracting the averaged background which is adjacent to the retention time windows. These mass spectra are then used for the comparison to the standard mass spectra mentioned earlier.

## 2.5 Filter measurements

Filter measurements is a off-line method to sample and analyze aerosol. In this work filter samples were taken during the aerosol chamber experiment (see chapter 4). Filter samples were always taken with two filter holders connected in

series, the so called front filter holder and back filter holder. During sampling both filter holders were equipped with the same type of quartz fiber filters. The front filter essentially collects 100% of the aerosols while the back filter is only exposed to the gas phase compounds some of which adsorb onto the back filter (Turpin et al., 2000). The measurements of the back filter was afterwards used to correct the amount measured on the front filter for each compound.

For compound specific measurements of the aerosol samples collected on the filters a gas chromatograph coupled to a isotope ratio mass spectrometer (GC-IRMS) was used. The instrumentation used in this work was an Agilent 6890 (1530A) GC coupled to an Isoprime IRMS (GV Instruments, Manchester). The GC was equipped with two fused silica columns, a Rtx-1 (Restek Corporation, Bad Homburg) and a BP624 (SGE Scientific, Griesheim) and with a Flame Ionization Detector (FID). Only the first column in the GC, the Rtx-1 (105 m x 0.32 mm ID, 100% dimethyl polysiloxane, film thickness 3.0  $\mu\text{m}$ ) was used in this work for separation of compounds. The GC was also connected to a custom build cryosampling thermal desorption system (Gerstel GmbH, Mühlheim) with which the aerosols were desorbed from the filters, preconcentrated and refocused before they were injected into the GC. The setup is described in detail by Iannone et al. (2007). For the aerosol sample measurements a circular filter piece (3 mm  $\pm$  10% in diameter) was cut out from the whole filter and placed inside a quartz tube which could be inserted into the cryosampling thermal desorption system. The aerosols were evaporated heating the quartz tube and the sample was flushed into the preconcentration and focusing system using helium as a carrier gas. The focused sample was then flash injected into the GC. Only the FID detector was used to measure the chromatographically separated compounds. Compound identification and quantization was done by calibrating the GC-IRMS using diffusion sources measurements with standard reference compounds.

## 2.6 Aerosol Mass Spectrometry

The Aerosol Mass Spectrometer (AMS) (Aerodyne Research Inc, Massachusetts) is an instrument for the real-time quantitative measurement of size-resolved aerosol chemical composition (Jayne et al., 2000). A schematic of the AMS is shown in Figure 2.6. The AMS consists of three main parts: an aerosol inlet, a particle sizing chamber, and a particle composition detection section. The AMS aerosol inlet is identical to the ACM aerosol inlet. The AMS aerosol inlet also consist of a critical orifice and an aerodynamic lens system as previously describe in chapter 2.1.2. The particles are focused into a narrow particle beam which enters

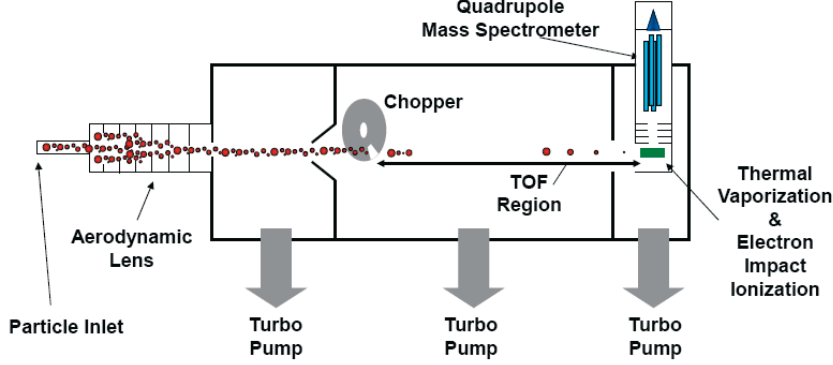


Figure 2.6: Schematic of the AMS according to Jayne et al. (2000) (courtesy A. Kiendler-Scharr).

the particle sizing chamber. The AMS particle sizing chamber is a high vacuum chamber similar to the ACM vacuum chamber (2.1.2). Additionally particle sizes can be determined through a particle time-of-flight measurement. Due to the super sonic expansion of the particles which enters the high vacuum chamber the particles consist of size dependent velocities. The focused beam is modulated by a rotating wheel chopper. When the chopper cuts the particle beam the start signal for the time-of-flight measurement is initiated. The flight time of the particles after a known flight distance from the chopper to the detection section gives the particle velocities from which the particle vacuum aerodynamic diameters  $d_{va}$  are determined. The particles are then directed onto a heated surface (approximately 600 °C). Upon impaction the volatile and semi-volatile constituents of the particles are vaporized. afterwards the evaporated constituents are ionized by an electron impact ionizer at 70 eV and transferred to a quadrupole mass spectrometer where the molecular fragments are measured.

The chemical composition of the particles is determined by separation of the raw data into partial mass spectra for distinct chemical compounds. This is achieved by using a user-definable fragmentation table for each chemical compound or group of compounds.

The mass concentration of compound  $s$  in the aerosol can be calculated by the following equation (Jimenez et al., 2003; Allan et al., 2004):

$$C_s = \frac{10^{12} \cdot MW_{NO_3}}{RIE_s \cdot IE_{NO_3} Q N_A} \sum I_{s,i} \quad (2.3)$$

$$\begin{aligned} C_s &= \text{mass concentration of compound } s & [\frac{\mu g}{m^3}] \\ MW_{NO_3} &= \text{molecular weight of } NO_3 & [\frac{g}{mol}] \end{aligned}$$

$RIE_s$	= relative ionization efficiency of compound s	[1]
$IE_{NO_3}$	= ionization efficiency of $NO_3$	[1]
$N_A$	= Avagadro's number	$[\frac{1}{mol}]$
$Q$	= volumetric sample flow	$[\frac{cm^3}{s}]$
$\sum I_{s,i}$	= sum of the ion rate of the partial mass spectrum due to compound s	[Hz]

Values for the relative ionization efficiencies for different compounds can be taken from the literature. The ionization efficiency of  $NO_3$  is measured regularly. For the calibration a solution of  $NH_4NO_3$  is sprayed with an aerosol generator and one particle size is selected with a Differential Mobility Analyzer (DMA) before the particles are introduced into the AMS. The ratio between the intensity of the  $NH_4NO_3$  signal measured by the AMS to the amount of  $NH_4NO_3$  molecules which are introduced into the AMS determines the ionization efficiency  $IE_{NO_3}$ . The calibration of the particle sizing of the AMS is done using a suspension of polystyrene latex particles (PSL) with known sizes. The solution is sprayed with an aerosol generator and the flight times of the PSL particle are measured in the time-of-flight measuring mode of the AMS. The comparison of the known PSL particle sizes with the determined aerodynamic particle sizes gives the calibration parameter.

## 2.7 Particle Size Distribution

To measure the particle size distribution a Electrostatic Classifier (EC) is coupled to a Condensation Particle Counter (CPC). The combination of these two instruments is called a Scanning Mobility Particle Sizer (SMPS). For the experiments in this work a commercially available SMPS system (TSI, model 3934) is used. A polydispersed aerosol flow enters the Electrostatic Classifier and is introduced into a neutralizer containing a Kr-85 source. The aerosols are exposed to high concentration of bipolar ions. Through interaction between the ions and the aerosols the particles reach a Boltzmann equilibrium with a known size dependent charge distribution. Then the particles are directed to a Differential Mobility Analyzer (DMA). The DMA consist of a metal cylinder and a cylindrical collector rod. The collector rod is centered inside the metal cylinder. The aerosols and an additional particle free sheath air are introduced at the top of the DMA and flow laminary down the annular space between the collector rod and the metal cylinder. The outer cylinder is electrically grounded and the inner rod is maintained at a neg-

ative voltage. An electrical field is produced between the rod and the cylinder. Due to the electrical field positive charged particles are attracted through the sheath air to the collector rod. The location on the collector where the positively charged particles impact depends on their electrical mobility. Depending on the voltage applied to the rod a narrow range of electrical mobilities exists that can exit the DMA through a small slit at the bottom of the collector rod. These monodispersed particles are transferred to the CPC where the particle concentration is determined. The particle size associated with this range of electrical mobility is defined through the following equation for the electrical mobility  $Z_p$ :

$$Z_p = \frac{neC}{3\pi\mu d_m} \quad (2.4)$$

$n$  = number of elementary charges on the particle

$e$  = elementary charge

$C$  = Cunningham slip correction

$\mu$  = gas viscosity

$d_m$  = particle electrical mobility diameter

A particle number distribution ( $dN$  versus  $D_p$ ) is obtained by successive variation of the electrical field and scanning of the corresponding aerosols size classes. The particle number distribution can be used to calculate the volume ( $dV$ ) of the particles:

$$dV = \frac{\pi}{6} D_m^3 dN \quad (2.5)$$

An impactor with a cutoff size of 750 nm is installed in front of the SMPS inlet. Therefore, particles with a diameter between 14 and 750 nm are detected by the SMPS. The detection efficiency for particles with 750 nm is 50%. The detection efficiency reaches 100% for particles of 600 nm diameter and smaller.

The calibration of the SMPS was done using a suspension of polystyrene latex particles (PSL) with known sizes. The solution is atomized with an aerosol generator and the particles are measured with the SMPS. The SMPS size classes are adjusted with respect to the reference values of the PSL.

## 2.8 Particle Density

The density of particles can be estimated for a particle population which is in parallel measured with different equivalent diameter measurements. Simultaneous measurements of the particle mobility diameter  $d_m$  with the SMPS (chapter 2.7) and the particle vacuum aerodynamic diameter  $d_{va}$  with the AMS (chapter 2.6)

can be used for placing constraints on the particle density. Under the assumption of spherical particles particle density  $\rho_p$  can be determined from the measurement of  $d_m$  and  $d_{va}$  using the following equation (DeCarlo et al., 2004):

$$\rho_p = \frac{d_{va}}{d_m} \rho_0 \quad (2.6)$$

$\rho_p$	= particle density	$[\frac{g}{cm^3}]$
$d_m$	= particle electrical mobility diameter	$[nm]$
$d_{va}$	= particle vacuum aerodynamic diameter	$[nm]$
$\rho_0$	= standard density ( $1 \frac{g}{cm^3}$ )	$[\frac{g}{cm^3}]$

For the  $\beta$ -pinene ozonolysis experiment (for details see chapter 4) the particle density was determined as follows. The modes of the particle size distributions  $d_m(n_{max})$  and  $d_{va}(n_{max})$  measured by the SMPS and AMS, respectively, were determined.  $d_m(n_{max})$  and  $d_{va}(n_{max})$  give the particle diameters  $d_m$  and  $d_{va}$  which are measured for the majority of the particles  $n_{max}$  during one measurement.  $d_m(n_{max})$  and  $d_{va}(n_{max})$  were then averaged for two time periods of 60 min (4.77 h to 5.77 h and 25.03 h to 26.03 h after ozone injection) during the chamber experiment. For both time periods a particle density  $\rho_p$  was determined using equation 2.6. The two densities were then again averaged to obtain an average density for the particles formed in the  $\beta$ -pinene ozonolysis experiment.





## 3. Instrument Characterization

In this chapter different aspects of the characteristics and performance of the ACM-GC-MS system are determined. In the following the characterization methods and their results are presented. In chapter 3.1 the performance of the GC-MS system will be determined by direct injection of different compounds into the detector. In chapter 3.2 the transfer efficiency of the valve array and the transfer line of the ACM are analyzed. In the last part (chapter 3.2.3) the collection, desorption and transfer efficiency of test aerosols of the complete ACM-GC-MS system is evaluated. Detection limits, reproducibility and recovery rate of the collected aerosols are determined.

### Characterization setup

In Figure 3.1 the general setup for the characterization measurements is shown. Test aerosols are generated with an aerosol generator and size selected with a differential mobility analyzer (DMA). Thereafter the aerosol stream is split up and directed to the ACM particle inlet and a scanning mobility particle sizer (SMPS). The arrows in the schematic indicate the different regions where the specific characterization measurements are conducted. In the following chapters each experiment will be addressed in detail and the specific variations of this setup will be presented.

### 3.1 GC-MS Characterization

Prior to the characterization of the ACM the GC-MS detector response is determined. A calibration of the GC-MS is necessary to be able to quantify the characterization experiments with the ACM and to evaluate the transfer efficiency of the system and the recovery rate. In the following calibration curves for different compounds will be presented, which will be used to determine linearity,

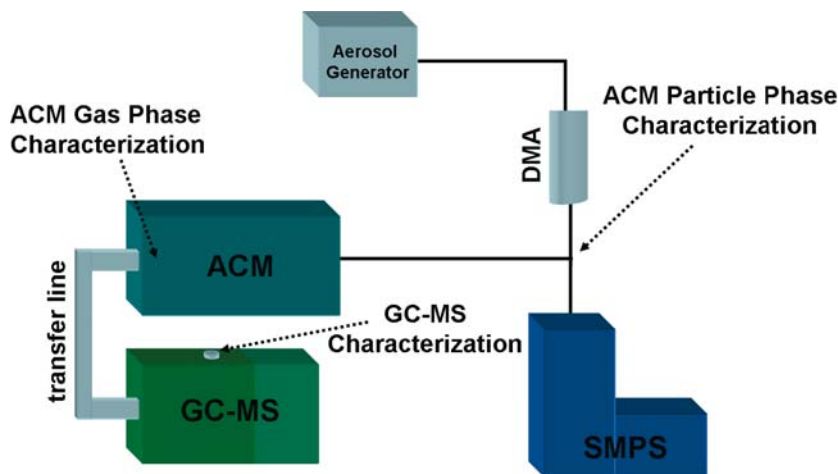


Figure 3.1: This schematic shows the general instrumental setup for the characterization experiments. Test aerosols are generated, size selected and distributed to the ACM and a scanning mobility particle sizer which will provide an independent measurement for comparison. Arrows indicate the different stages in the determination of parameters for the ACM and the GC-MS.

response factors for certain compounds, and detection limits of the FID detector. Also, the correct identification of the standard compounds with the mass spectrometer is tested through comparison with NIST mass spectra.

### 3.1.1 Experimental Setup

For the direct injection of standard compounds the GC-MS setup was altered. The GC-MS was disconnected from the ACM transfer line and the cryofocusing module was removed. Instead of the module a split/splitless liquid injection system was installed. The liquid injection system consists of a carrier gas inlet, a septum, septum purge, injector insert, heater block, inert glass tube, and column connection. A schematic of the GC-MS with the liquid injection system is shown in Figure 3.2. The GC column is installed into the injector so that the beginning of the column reaches about 3 cm into the glass tube. The carrier gas head pressure is kept constant at 2400 hPa. The injector is kept at 230°C. The injector is a split/splitless injector. For a high concentrated sample the needle valve of the split can be opened and set to a specific split ratio so that a well defined amount of the sample is discarded out of the vent and only a small amount enters the column. Since the concentration of the analytes in the solutions used for this characterization experiments were small enough and the retention time of the solvent was small enough compared to the retention time of the analytes all

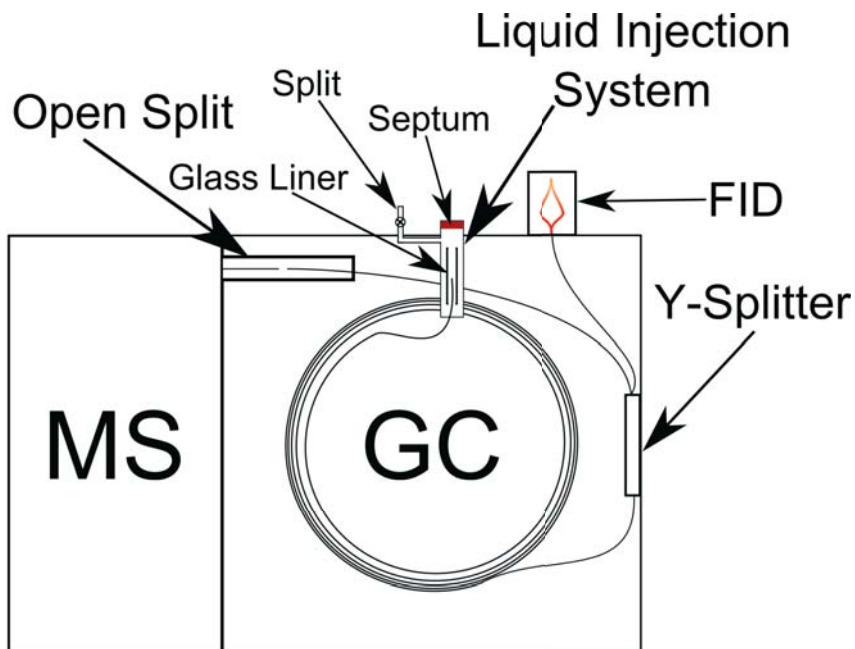


Figure 3.2: GC-MS detector schematic with the liquid injection system installed instead of the cryofocusing module.

measurements were done in the splitless mode. The solutions were injected with a microliter syringe of a maximum capacity of 5  $\mu\text{l}$ . The sample was immediately vaporized and swept onto the column by the carrier gas. The GC oven was programmed for an initial hold of 5 min at 40  $^{\circ}\text{C}$ , temperature increased with 5  $^{\circ}\text{C}/\text{min}$  until a temperature of 200  $^{\circ}\text{C}$  was reached and held for 12 min.

### 3.1.2 GC-MS Detector Calibration

For the calibration of the GC-MS system three different solutions were used. The first solution is a homologous series of alkanes. 5  $\mu\text{l}$  of 14 alkanes from n-Heptane ( $\text{C}_7\text{H}_{16}$ ) to n-Eicosane ( $\text{C}_{20}\text{H}_{42}$ ) are solved in 10 ml n-Hexane ( $\text{C}_6\text{H}_{14}$ ). For the second solution 5  $\mu\text{l}$  of nopinone ( $\text{C}_9\text{H}_{14}\text{O}$ , NIST identifier: Bicyclo[3,1,1]heptan-2-one, 6,6-dimethyl-) is also solved in 10 ml n-Hexane. The third solution consists of 5  $\mu\text{l}$  acetone solved in 10 ml n-Decane. The analytes nopinone and acetone are chosen as a calibration compound because these are important products in the aerosol indoor chamber experiments (see chapter 4). Details about the chemical compounds are listed in Table 3.1.

Multipoint calibration curves were generated separately using direct injections

Chemicals	Purity [%]	Manufacturer
Acetone	99	Aldrich
Ethanol	$\geq 99.5$	Aldrich
Nopinone	98	Aldrich
Hexane	$\geq 96$	Merck
Heptane	99.5	Fluka
Octane	99.5	Fluka
Nonane	99.8	Fluka
Decane	$\geq 98$	Fluka
Undecane	$\geq 99$	Merck
Dodecane	$\geq 99$	Fluka
Tridecane	96	Merck
Tetradecane	$\geq 99$	Fluka
Pentadecane	99	Merck
Hexadecane	99	Merck
Heptadecane	96	WGA
Octadecane	$\geq 98$	Fluka
Nonadecane	98	WGA
Eicosane	$\geq 99$	Backer Chemical

Table 3.1: Chemicals used for the calibration measurements.

of the three solutions. As an example three FID chromatograms for the injection of 0.3  $\mu\text{l}$  of the solutions into the GC-MS are shown in Figure 3.3. The very broad and saturated peaks in each of the chromatograms are the solvents. For the acetone and nopinone chromatograms the difference in the retention times of the solvent peak and the analytes are large enough so that they don't interfere with each other. For the homologous series of the alkanes it could not be avoided that the solvent peak (hexane) interferes with the two adjacent alkane peaks (heptane and octane). All chromatograms are baseline corrected as described in chapter 2.4. In Figure 3.3(a) and 3.3(b) the red curves are shown as an example for the peak fitting with the exponentially modified gaussian function. For all data obtained the fit results are used to calculate the total area under the peaks.

Note the tailing of the acetone peak due to the fact that an almost non-polar column is used. In the GC-MS characterization measurements the cryofocusing module can not be used. Therefore the retention of the acetone is not sufficient at the beginning of the column prior to the start of the GC run. However note that the fit function represents the acetone peak very well.

Calibration curves for the acetone, nopinone and octadecane are shown in Figure 3.4. Octadecane is presented as an example for the alkanes because this compound will be used further on in the characterization of the ACM (for details see chapter 3.2 and 3.2.3). A series of 0.1, 0.3, 0.5  $\mu\text{l}$  of each solution were injected. For nopinone and acetone an additional injection of 1  $\mu\text{l}$  is available. In each

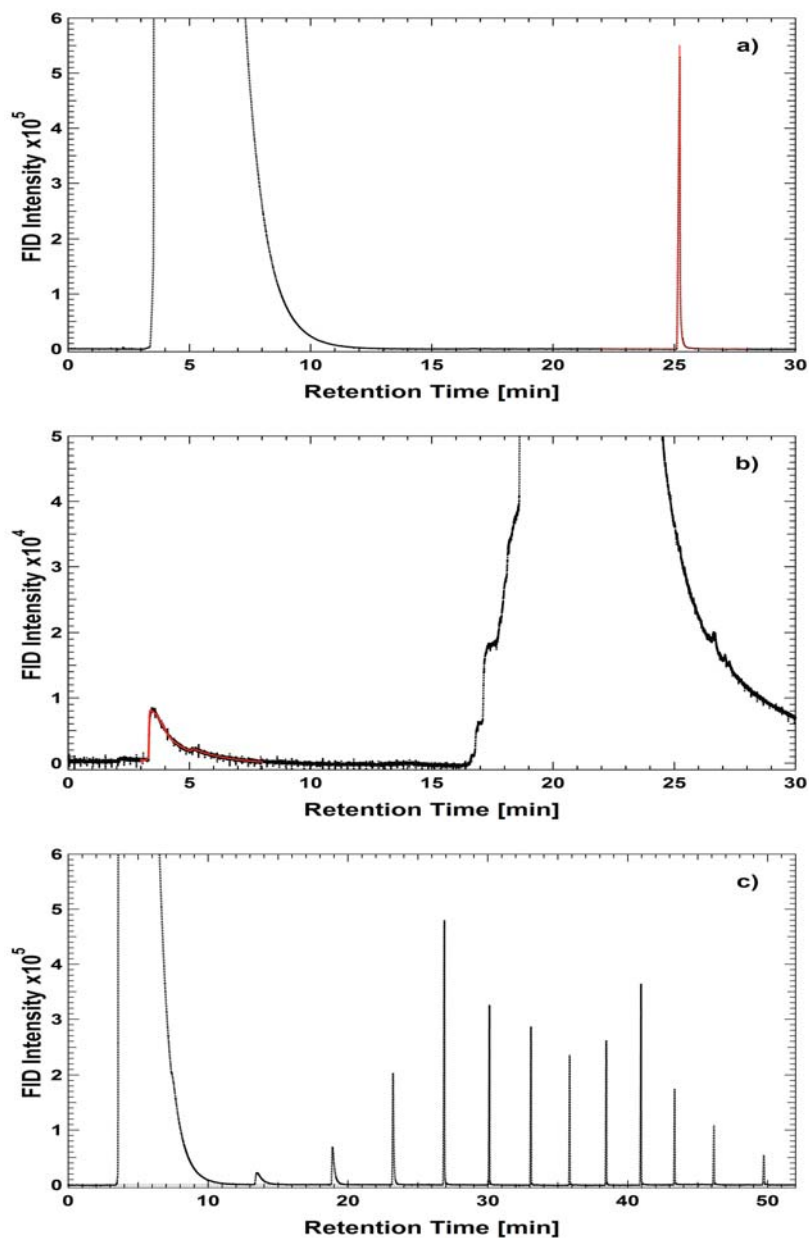


Figure 3.3: Three example chromatograms of the direct injection of  $0.3 \mu\text{l}$  of a) nopinone, b) acetone, and c) homologous series of alkanes with a microliter syringe into the GC-MS. The broad peaks are the solvents. The red curves in Figure a) and b) are examples of the exponential modified gaussian fit through the data points.

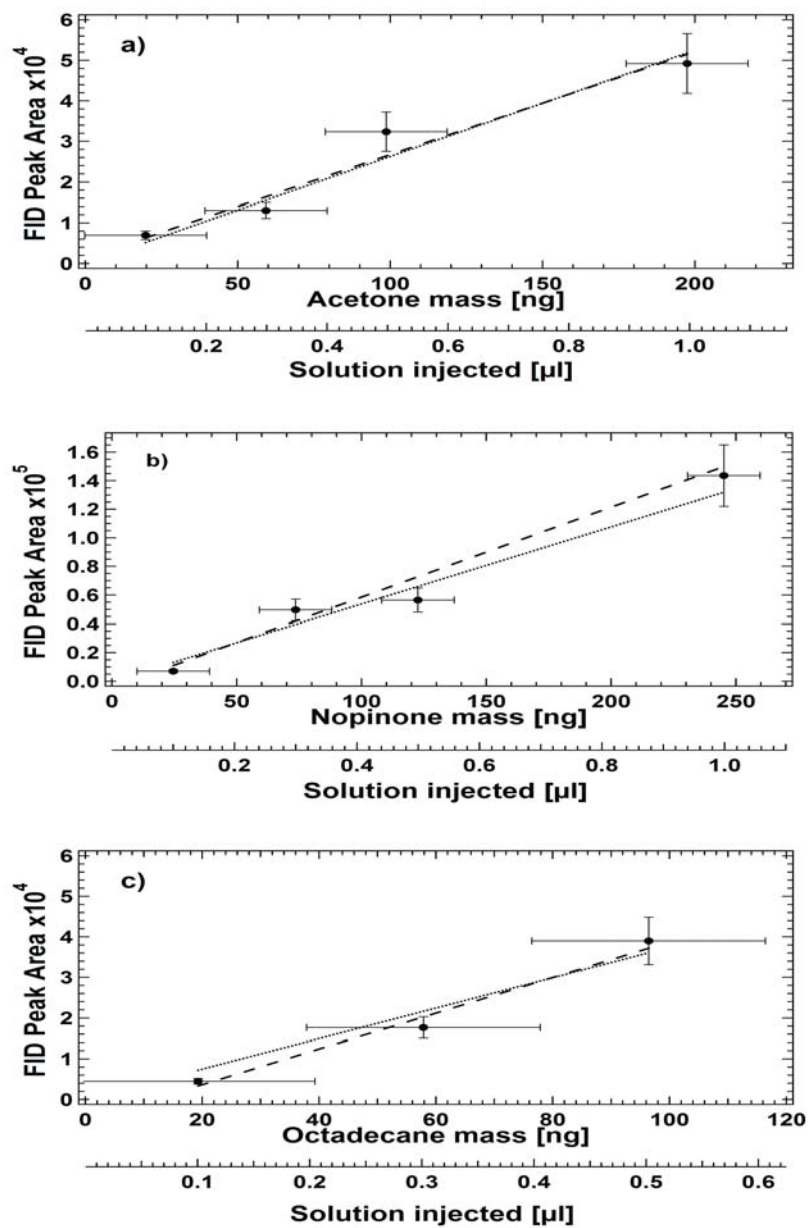


Figure 3.4: Calibration curves for standards compounds a) acetone, b) nopinone, and c) octadecane obtained by direct injections into the GC-MS. For each calibration curve two linear fits are determined. With the first regression line (dashed line) the slope and intercept of the linear relationship are calculated. The second linear fit (dotted line) was calculated where the fit was forced through the point of origin.

figure the areas of the peaks are plotted against the mass of the analytes. The second x-axis gives the amount of solution injected. The mass is calculated using the mixing ratios of the solutions and the density of the analytes.

The error bars for the x-axis show the uncertainty of the amount injected. With the 5  $\mu\text{l}$  microliter syringe it is possible to draw up the solution to an accuracy approximately of 0.05  $\mu\text{l}$ . For the error bars this value was converted to an uncertainty in mass injected. The error bars for the y-axis represent the uncertainty of the area determined from the fit of the peaks. The retention time stability for all GC-MS characterization measurements was 0.1 min. The detection limit for organic compounds is typically defined as the quantity of standard compounds needed to obtain a chromatographic peak area that is three times the baseline noise level (Docherty and Ziemann, 2001; Lamanna and Goldstein, 1999) or empirically by the smallest amount of standard injected. The detection limit was measured using the measurements of the standard compound series to be 10 ng. For all compounds excellent linear responses with  $R^2 > 0.95$  are obtained. For each calibration curve two linear fits are determined. With the first regression line (dashed line) the slope and intercept of the linear relationship are calculated. Taking the error of the each linear fit of the different substances into account it is consistent to assume that the intercept of the fits goes through the point of origin. Hence a second linear fit (dotted line) was calculated where the fit was forced through the point of origin. The second linear fits (dotted lines) for acetone and nopinone will be used to calibrate the response of these substances in the aerosol chamber experiment (chapter 4). The results for the fit coefficient are listed in appendix A. Using for all calibrations the linear fits through the origin, we have the consistent assumption for all calibrations that a compound mass of zero nanogram results in a chromatographic peak area of zero.

The direct injection measurements are also used to verify the capability of the identification of compounds with the quadrupole mass spectrometer. In Figure 3.5 the mass spectra of nopinone, acetone and octadecane are shown. The obtained mass spectra are compared with the EI spectra of the NIST library database. The comparisons achieve good results and the automatic search and compare algorithm of the MS data acquisition software (Masslab 1.4) identifies all compounds with a high probability.



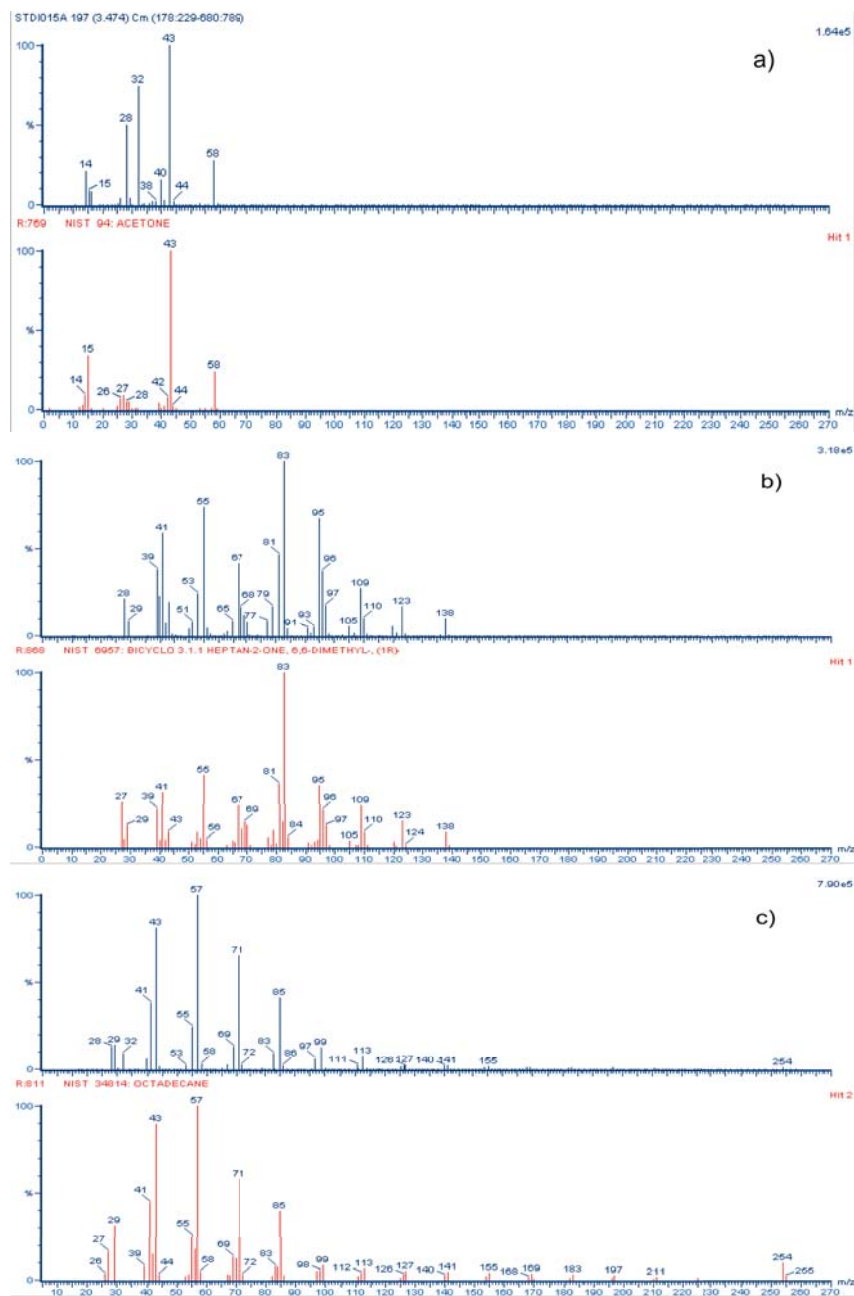


Figure 3.5: Comparison of mass spectra a) acetone, b) nopinone, and c) octadecane obtained through direct injection into the GC-MS (blue mass spectra) to mass spectra of the NIST database (red mass spectra).

## 3.2 ACM Characterization

In the following chapters the ACM will be characterized in two stages. First the transfer efficiency of gaseous compounds from the collector to the detector will be determined. The aim is to identify and quantify possible losses in terms of adsorption of the test compound in the transfer path.

In the second stage aerosols of the same compound are introduced into the ACM. These aerosols will be simultaneously measured by the ACM and a Scanning Mobility Particle Sizer. Comparisons of these measurements will determine the collection efficiency and recovery rate of the ACM.

### 3.2.1 Choice of the Test Compound

In this chapter the choice of octadecane as the test compound will be discussed. For a consistent characterization of the ACM two requirements regarding the test compound had to be considered.

The first requirement was that the test compound could be introduced into the ACM in both forms, as a gas and a particle. Therefore the characterization of the different parts of the ACM (see chapter 3.2.2 and chapter 3.2.3) could be done with the same test compound. Thus any possible effects due to the use of different compounds were avoided in the interpretation of the characterization results. To introduce the test compound as a gas it had to be possible to heat the compound so that it could be used in the diffusion source build inside the valve array of the ACM (chapter 3.2.2). Also it was necessary that the pure compound or the compound solved in a solution could be generated with an aerosol generator for the particle phase characterization of the ACM (chapter 3.2.3). These generated test aerosol needed to be size selectable with a Differential Mobility Analyzer (DMA) before they were injected into the ACM.

The seconde requirement was that the the test compound was detectable with the GC-MS and that the chromatographic peaks of the test compound had no strong tailing.

The compounds tested were oleic acid, stearic acid solved in 2-propanol, triethylene glycol, tetradecane, octadecane solved in 2-propanol, and octadecane solved in ethanol. The compound which fulfilled all requirements was octadecane. Pure octadecane was used in the diffusion source for the gas phase transfer efficiency measurements. For the ACM particle collection, desorption and transfer efficiency measurement octadecane solved in ethanol was used to generated test aerosols with the aerosol generator.

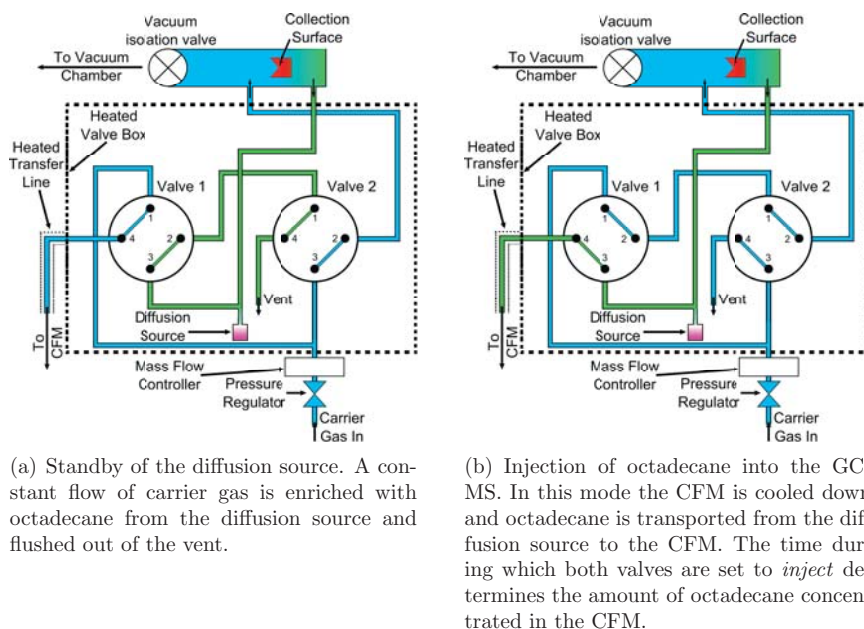


Figure 3.6: Schematic of the modified ACM valve array for diffusion source measurements. The two valve settings for standby and injection of the standard gas for one measurement cycles is shown.

### 3.2.2 ACM Gas Phase Transfer Efficiency

Using a diffusion source with octadecane the transfer efficiency of a gaseous substance is determined for the valve array and the transfer line. These measurement will be compared to the direct injection measurement of octadecane in the GC-MS to determine recovery rate for the test compound.

#### Experimental Setup

For the Gas Phase Transfer Efficiency measurement the ACM was reconnected to the GC-MS detector as shown in Figure 2.4. The liquid injection system was removed and the cryofocusing module reinstalled into the GC-MS.

For the gas phase measurements a standard gas supply is required. This is achieved by adding a diffusion/evaporation source into the valve array. The modified valve array is shown in Figure 3.6. A glass vial filled with octadecane was installed via a T-fitting between the exit of the particle collector and valve 1. Thus the flow path of the standard gas from the diffusion source will be similar to the flow path of desorbed aerosols to the detector. Hence, any losses determined by the measurement of the standard gas can be used to calculate correction fac-

tors which can be applied to aerosol measurements with the ACM.

Since octadecane has a vapor pressure of <0.1 hPa at 20 °C heating of the glass vial is necessary to ensure that enough material is evaporated from the diffusion source. Therefore the glass vial is build inside the heated valve box. The heating of the valve array is used to heat the diffusion source as well. The temperature of the glass vial was controlled separately with a thermocouple. The temperature of the diffusion source was kept constant at  $117 \pm 2$  °C which corresponds to a valve array temperature of 160 °C.

Additionally a mass flow controller (Mass-Flo, 500 sccm, MKS Instruments) is installed after the pressure regulator. The flow of the carrier gas is kept constant at 100 ml/min. This provides a constant flow of carrier gas over the diffusion source and a constant loss of octadecane over a certain period of time. The vial of octadecane is weighted before and after the experiments. The concentration of octadecane in the helium flow can be calculated as follows:

$$C_{C_{18}} = \frac{\Delta m}{f_{He} \cdot t} \quad (3.1)$$

$C_{C_{18}}$	= Concentration of octadecane in the helium flow	$\left[\frac{ng}{ml}\right]$
$\Delta m$	= weight difference of the diffusion source	$[ng]$
$f_{He}$	= helium flow over the diffusion source	$\left[\frac{ml}{min}\right]$
$t$	= time the diffusion source is active	$[min]$

The octadecane concentration in the helium flow is calculated to  $C_{C_{18}} = 5.32 \frac{ng}{ml}$ .

### Diffusion Source Measurements

The measurement procedure for the diffusion source deviates from the described procedure in 2.1.4. As shown in Figure 3.6 the desorption step is skipped. In the standby mode (Fig. 3.6(a)) octadecane is constantly flushed out of the vent. Prior to each measurement the CFM is cooled down to -120 °C. When the measurement starts both valves switch to the *inject* position and octadecane is transferred from the diffusion source to the CFM (Fig. 3.6(b)). The flow of the carrier gas to the CFM is  $f_{CFM} = 3 \frac{ml}{min}$ . The quantity of octadecane concentrated in the CFM is controlled by the time span the valves are in the *inject* position. After the sampling in the CFM is completed the valves switch back to the standby mode and the CFM is rapidly heated to 220 °C. The optimal GC program for this measurement was: oven temperature held at 50 °C for 5 min; ramped at a rate of 10 °C min<sup>-1</sup> to 220 °C; isothermal hold at 220 °C for 8 min. The GC temperature program is longer than necessary to elute the octadecane. However the long run

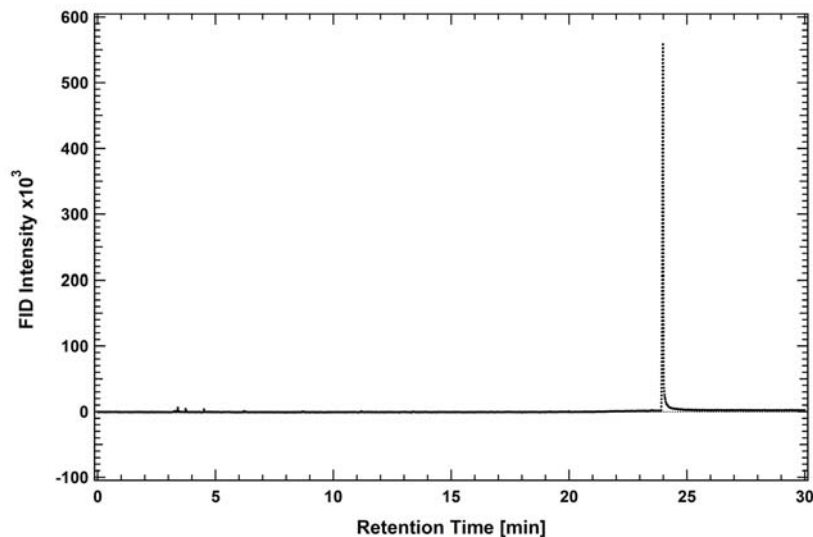


Figure 3.7: *Example chromatogram of 10 min sampling of octadecane with the diffusion source. No significant impurities or artifacts can be seen in the chromatogram.*

is also used to test if impurities are detected or artifacts occur. The transfer line is kept at a temperature of 230 °C.

The measurements were conducted for different sampling times. An example chromatogram of these measurements is shown in Figure 3.7. The octadecane peak is the only peak in the chromatogram which is detectable. No significant impurities or artifacts were observed. This was true for all chromatograms measured. The different sampling times are converted into total octadecane mass using equation 3.1 and the flow to the CFM.

In Figure 3.8 the results of all measurements are summarized. The peak areas measured by the GC-MS (filled symbols) is plotted against the mass. The relationship is linear. Again two linear fits are applied to the data, one unrestricted fit (dashed line) and the other is forced through the origin (dotted line). Considering the error of the intercept it is valid to assume that zero octadecane sampled yields a peak area of zero. Therefore the linear fit forced through the point of origin will be used as the calibration curve for the data obtained for the octadecane aerosol measurements (chapter 3.2.3). The results for the fit coefficient are listed in appendix A.

These results are also compared with the direct injection of octadecane into the GC-MS (open symbols in Fig. 3.8). The octadecane mass detected by the GC-MS in both experiments matches within the margin of error. This shows that

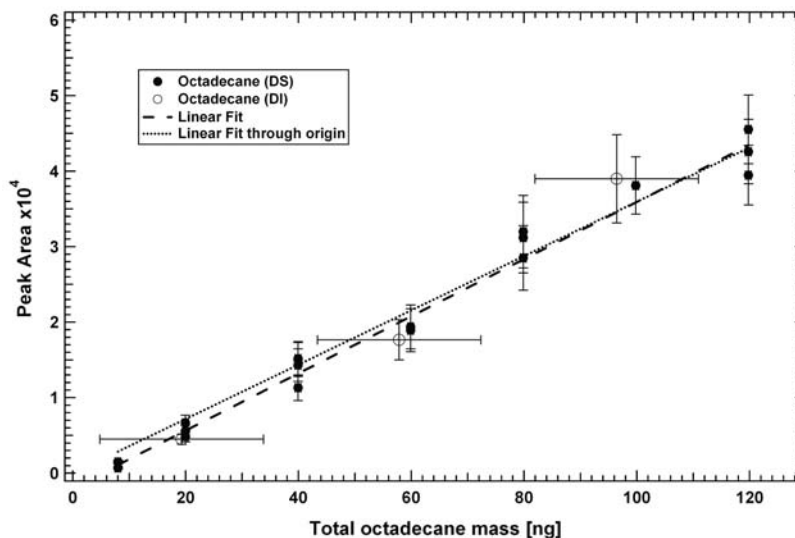


Figure 3.8: Results of the diffusion source measurements and comparison with the direct injection of octadecane into the GC-MS system. Note that the x-error bars ( $\pm 0.5$  ng) for diffusion source measurements (DS) are smaller than the data points.

there are no significant losses of octadecane in the valve array and the transfer line. The transfer efficiency is close to 100%.

### 3.2.3 ACM Particle Collection, Desorption and Transfer Efficiency

In the next stage octadecane aerosols are introduced into the ACM and simultaneously measured by a SMPS system. By comparing these independent measurements of the same particle distributions, the collection and transfer efficiency can be evaluated. Variations in collector temperatures will determine lower limits for the capability of desorbing aerosols from the collector.

#### Experimental Setup

In Figure 3.9 the complete experimental setup for producing and measuring octadecane aerosols with the ACM is shown. The aerosols are generated with a TSI constant output aerosol generator (3076). The particles were transferred to a delay tube. The particle production with a atomizer favors the generation of smaller aerosol diameters. In the delay tube the particles get time to coagulate.

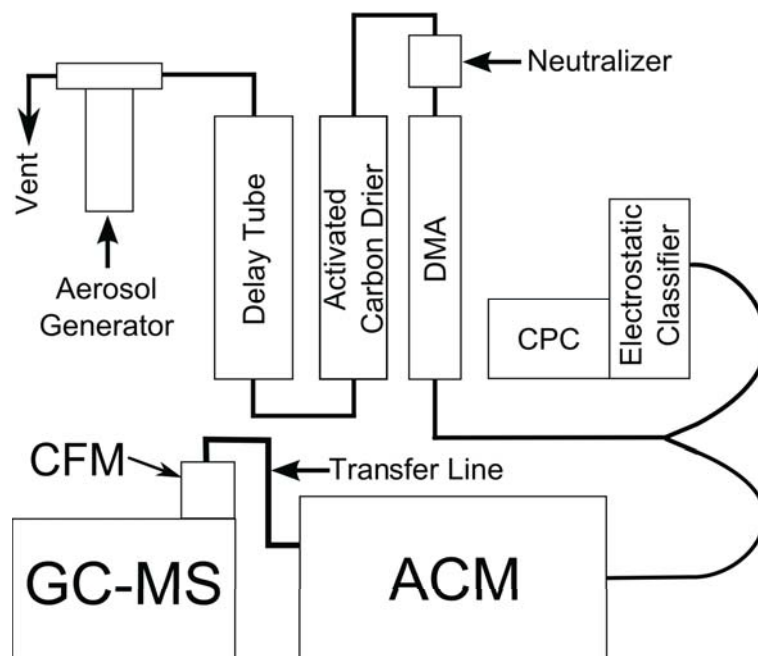


Figure 3.9: Schematic of the experimental setup for measuring octadecane aerosols simultaneously with the ACM and a SMPS. The aerosols are generated with an aerosol generator, dried, size selected and transferred to the two systems.

Thereby the particle size distribution is shifted to larger diameters. This will accelerate the measurement since more mass adds up on the ACM collector in a shorter time span for each sample collected. After the delay tube the octadecane aerosols can still consist of a significant amount of ethanol. The aerosols are lead through a activated carbon drier. The drier consist of a cylindrical wire mesh tube which is surrounded by activated carbon. The wire mesh is covered with a layer of GOR-TEX<sup>®</sup>. The wet aerosols pass through the tube and the volatile solvent penetrates the GOR-TEX<sup>®</sup> layer and is adsorbed on the carbon. Thereafter the aerosols are size selected with a DMA. The DMA voltage is kept constant so that only particles with a particle diameter of 250 nm are selected. Drying the aerosols before they are size selected is important because the amount of the octadecane which is collected by the ACM is calculated using the particle diameter of the aerosols measured by the SMPS. If the aerosol would still consist of large quantities of ethanol after size selection the solvent might evaporate inconsistently in the vacuum chamber of the ACM compared to the DMA in the SMPS. The particle diameter which is measured in this case with the SMPS would be larger compared to a dry aerosol. The total mass of the aerosol calculated from the SMPS measurements would be to large thus overestimating the aerosol loading

on the ACM collector. After the size selection the aerosol flow is then split to be characterized simultaneously with the ACM-GC-MS and the SMPS (TSI 3934, see chapter 2.7).

### Octadecane Aerosol Measurements

Previous to the experiments the DMA was calibrated using a solution of 200 ml of particle free water (Millipore Mili-Q®) with 0.9 g ammonium sulfate. Ammonium sulfate particles were atomized, dried and size selected with the DMA. A sequence of voltages was applied to the DMA and the corresponding particle diameter of the ammonium sulfate aerosols were measured with the SMPS system. Thereafter the DMA was set to a voltage so that particles with a diameter of 250 nm are selected for all octadecane particle measurements.

A series of experiments was conducted with aerosols generated from the solution of 0.5 g octadecane solved in 100 ml ethanol. After the generation of aerosols is started the delay tube starts to fill up with the octadecane particles. It takes about one minute until enough particles are in the delay tube and a well defined size distribution is measurable. Thereafter the measuring sequence of the ACM is started and the particle collector is cooled. As soon as the collector reaches the desired temperature the vacuum isolation valve opens and the sampling onto the collection surface starts. Simultaneously the data acquisition of the SMPS is also started. This ensures that the particle size distributions measured with the SMPS are consistent with the distribution collected with the ACM. The time resolution, i.e. one complete scan of the size distribution of the SMPS, is 3 minutes. The sampling of the ACM is stopped matching the end of a completed scan of the SMPS. For all experiments the collection temperature of the ACM collector is  $-30\text{ }^{\circ}\text{C}$ . However the desorption temperature was varied between  $150\text{ }^{\circ}\text{C}$  and  $270\text{ }^{\circ}\text{C}$  during these experiments to evaluate the desorption efficiency of aerosols from the collector. The temperature of the valve array and the transfer line were always matched with the desorption temperature. The desorption time, i.e. the time the collector was heated and the valve array was in the inject mode, was kept constant at 6 minutes. The desorbed aerosols were then concentrated again in the cryofocusing module at  $-120\text{ }^{\circ}\text{C}$  for one more minute after the desorption was completed. Then the CFM was heated in 2 minutes to a temperature of  $220\text{ }^{\circ}\text{C}$  and the sample was injected into the GC-MS for analysis. The temperature program of the GC oven was the same as described for the diffusion source measurements (chapter 3.2.2).

The series of experiments consists of different sampling times which results in different mass loadings on the ACM collector. The collector loading is calculated



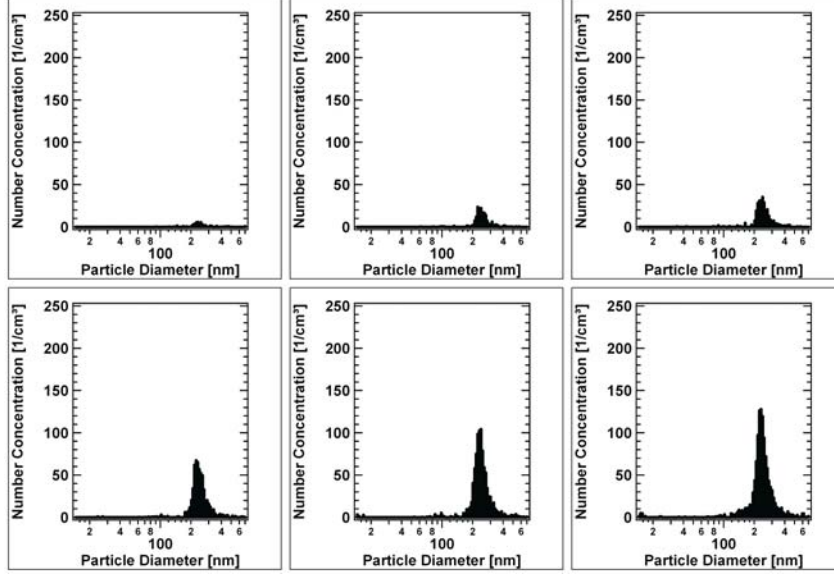


Figure 3.10: Series of size distribution of octadecane particles measured by the SMPS. The particle diameter is on a logarithmic scale. Note that the mode of the particles are centered around 250 nm. However also smaller and larger particles can be measured. Therefore the integrated size distributions will be used for calculations of the corresponding ACM collector loading.

using the SMPS distribution. Figure 3.10 shows an example of the particle size distribution from a measurement. The graphs show the particle number concentrations ( $dN$ ) versus the particle diameters ( $D_p$ ). Note that the mode of the particles is centered around 250 nm. However due to the SMPS transfer function the distribution consist also of smaller and larger particles. Particles with a large diameter contribute significantly to the total mass of the collected aerosols. Therefore, the complete distribution has to be considered to calculate the average mass loading which is sampled on the ACM collector. Using equation 2.5 the number distribution is converted into the volume of the particles. The total volume distribution is derived by integrating each scan. Figure 3.11 shows the time series for the integrated total volume concentration for this measurement. The mass introduced into the ACM is then calculated using the following equation:

$$M_{ACM} = \overline{C_{V_{SMPS}}} \cdot 10^{-21} \cdot \rho_{C_{18}H_{38}} \cdot f_{ACM} \cdot t_s \quad (3.2)$$

$M_{ACM}$	= ACM collector mass loading	$[\mu g]$
$\overline{C_{V_{SMPS}}}$	= Average total particle volume concentration	$\left[\frac{nm^3}{cm^3}\right]$
$\rho_{C_{18}H_{38}}$	= Density of octadecane	$\left[\frac{g}{cm^3}\right]$

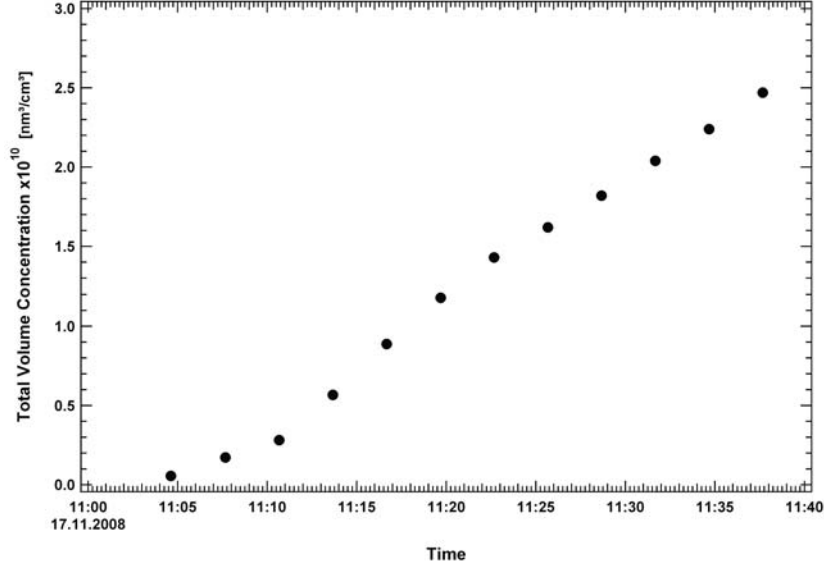


Figure 3.11: Time series of the calculated total volume concentration of octadecane particles. The data points represents the integration of the scans in Fig. 3.10 converted to the particle volume using equation 2.5.

$$\begin{array}{ll}
 t_s & = \text{Sampling time} & [s] \\
 f_{ACM} & = \text{Flow into the ACM} & [\frac{cm^3}{s}]
 \end{array}$$

As seen before in the diffusion source measurements no impurities or artifacts can be observed in the GC-FID chromatogram for all octadecane aerosol measurements. The collection of the aerosol under low temperature conditions and the desorption from the collector did not lead to a thermal degradation of the octadecane.

The peaks of all octadecane samples measured with the ACM-GC-MS are integrated and the peak areas are converted into octadecane mass using the calibration of the diffusion source measurements (Fig. 3.8). Figure 3.12 shows the calculated mass loading from the SMPS data versus the mass measured with the GC-FID. The linear fit to the data shows that the slope is one. The recovery rate for octadecane is 100%. Possible losses of octadecane at all temperatures over the complete pathway of the ACM system are minimal. Additionally the desorption temperature was changed between 150 °C and 270 °C (numbers at each data point). The temperature of the valve array and the transfer line were changed accordingly to match the desorption temperature. Within this temperature range the octadecane is completely desorbed from the collector and transferred without losses to the GC-MS detector. Additionally no thermal degradation, impurities

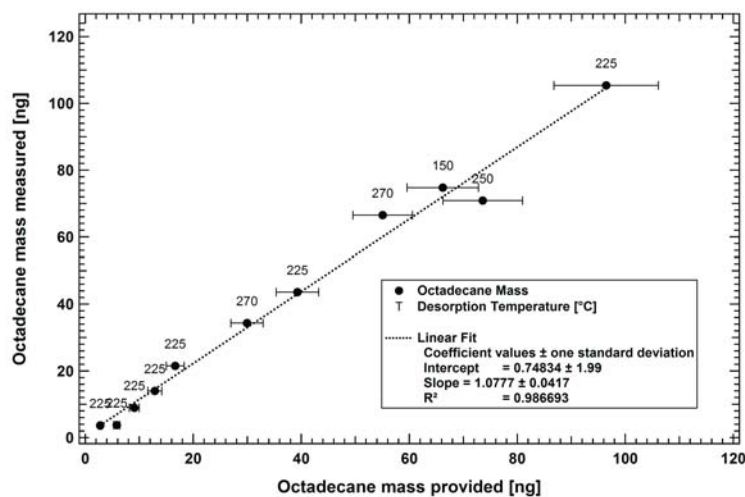


Figure 3.12: Octadecane mass measured with the GC-FID vs. the collector loading (calculated from SMPS measurements) lie on a line through the origin with slope one. Numbers show the different desorption temperatures for each measurement.

or artifacts resulting from the sampling or desorption of octadecane could be observed. It could be demonstrated that the ACM-GC-MS is linear over a mass range of 2 to 100 ng.

## 4. Secondary Organic Aerosol Formation from $\beta$ -pinene Ozonolysis

In this chapter the formation of secondary organic aerosol (SOA) from the oxidation of  $\beta$ -pinene with ozone in an atmosphere simulation chamber experiment is presented and discussed. The experiment was conducted in the aerosol chamber of the Forschungszentrum Jülich (FZJ). In the following the set up of the chamber and the experiment are described in detail. Results obtained for gas phase measurements of ozone and VOC are presented. The SOA were measured and analyzed using different aerosol measurement techniques such as ACM-GC-MS, SMPS, filter samples, and AMS measurements. Products of the  $\beta$ -pinene ozonolysis in the SOA were identified and the partitioning of nopinone between the gas and particle phase was analyzed. Temporal evolution of the organic composition of the SOA were determined applying the Positive Matrix Factor (PMF) Analysis to AMS measurements.

### 4.1 Aerosol Chamber of the FZJ and Experimental Set Up

#### 4.1.1 Description of the Aerosol Chamber of the FZJ

Atmosphere simulation chambers are used to study atmospheric chemical processes. An atmospheric simulation chamber is a closed system. A variety of different gas mixtures can be studied inside the chamber without influences from unknown sources and sinks of atmospheric trace gases and without the interferences due to meteorological processes.

The aerosol chamber of the Forschungszentrum Jülich (FZJ) (Mentel and Wah-

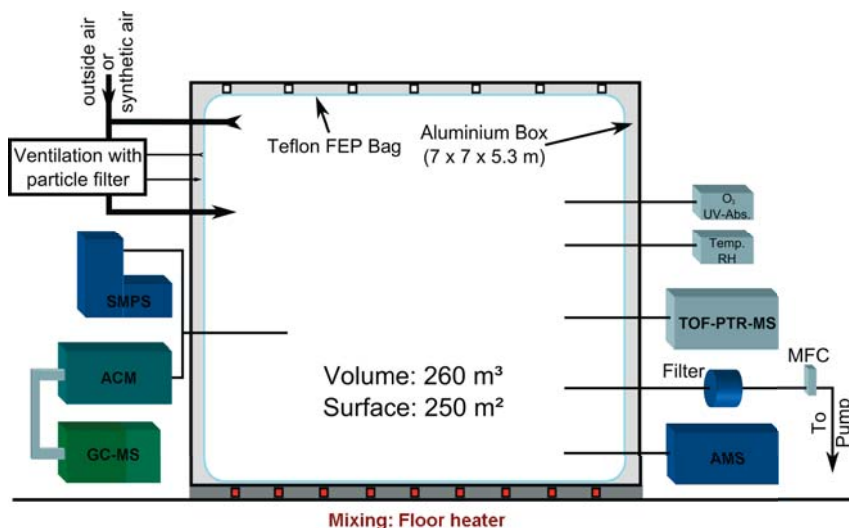


Figure 4.1: Schematic of the FZJ aerosol chamber and the instrumental set up for the  $\beta$ -pinene ozonolysis experiment.

ner., 1996) was used for experiments characterizing SOA with the ACM-GC-MS system. In the following the chamber will be described in detail.

A schematic of the aerosol chamber and the instruments applied in this study is shown in Figure 4.1. The chamber is designed for studying atmospheric nighttime chemistry. Additionally, the chamber can be used to study the formation of SOA from the oxidation of trace gases such as monoterpenes.

The aerosol chamber consists of an aluminium box. The inner walls are lined with chemically inert FEP (Fluorinated Ethylene Propylene) teflon foil. The FEP foil is permeable for gas so that the interspace between the aluminium box and the foil is constantly flushed with pure synthetic air (Linde® 6.0) to avoid contamination of the chamber. The pressure inside the chamber is slightly higher than ambient pressure. This inhibits contamination of the aerosol chamber by diffusion of external air.

The chamber has a volume of  $260 \text{ m}^3$  and a surface of  $250 \text{ m}^2$ . Thus the chamber has a surface to volume ratio of  $0.96 \text{ m}^2 / \text{m}^3$ . A small surface to volume ratio ( $< 1$ ) minimizes potential wall loss such as deposition of aerosols or trace gases.

Homogenous mixing inside the chamber is achieved by convection. This is provided by a floor heating system which is set to  $30 \text{ }^\circ\text{C} \pm 4 \text{ }^\circ\text{C}$ . The temperature of the heating is periodically changed in this temperature range over the duration of 2 h. Thus the mixing time inside the chamber is less than 10 minutes and the change of the gas temperature inside the chamber is approximately  $0.25 \text{ }^\circ\text{C}$ .

### 4.1.2 Instrumentation for the Aerosol Chamber Experiment

Temperature, relative humidity, and pressure inside the aerosol chamber were permanently monitored during the experiment. Instrumentation for measuring both the gas phase and the particle phase was available. All instruments can be connected to the chamber using separate stainless steel or PFA tubing (both have an inner diameter of 4 mm) which extend approximately between 0.5 and 1.5 m into the chamber. This ensures that all samples taken are from the homogeneously mixed content of the chamber.

The ozone mixing ratio in the chamber was monitored with an ozone analyzer (Ansyco, 41M) by UV absorption with a time resolution of 5 minutes.

The monoterpene concentration and the mixing ratios of oxidation products were measured with a Proton Transfer Time of Flight Mass Spectrometer (Ionicon, HRS PTR-TOF-MS). The PTR-TOF-MS inlet was connected to the chamber through a 1 m long PFA tube. The sample flow was 400 ml/min. A teflon filter (Sartorius, pore size 0.45  $\mu\text{m}$ ) was installed between the PTR-TOF-MS inlet and the sampling line to ensure that no particles enter the PTR-TOF-MS. The inlet and the drift tube of the PTR-TOF-MS were heated at 60 °C. The mass spectra were recorded over a range from 10 to 420 amu.

The particle number concentration was measured with a CPC (TSI, 3687). The flow of the CPC was 600  $\frac{\text{ml}}{\text{min}}$ . The CPC was measuring continuously during the experiment. The smallest particle diameter the CPC is able to detect is 3 nm. The CPC was connected with a T-fitting to the sampling line of the AMS.

The particle size distribution was measured with a SMPS system (TSI 3934, see chapter 2.7). The time resolution of the SMPS system was set to 3 min. The SMPS was measuring the particle diameters between 14 nm and 750 nm. The sample flow of the SMPS system was 300  $\frac{\text{ml}}{\text{min}}$ . The SMPS was connected to the ACM with a Y-splitter. The Y-splitter itself was connected to the chamber with a 1 m stainless steel sampling line. Both instruments were sampling with a total flow of 380  $\frac{\text{ml}}{\text{min}}$  from the chamber. This results in residence time for the particles in the sample line of approximately 2 s.

The particle composition was measured with the Aerosol Mass Spectrometer (AMS). The AMS has a sample flow of 80  $\frac{\text{ml}}{\text{min}}$ . The time resolution of the AMS data was set to 10 min. The mass spectra were recorded over a range from 10 to 300 amu. The temperature of the oven for the flash evaporation of the aerosols was set to 600 °C. The sampling lines of the CPC and the AMS were connected through a T-connector to a 1 m stainless steel tubing which led into the chamber. Both instruments were sampling over this tubing so that in total the flow through

this sample line was  $680 \frac{ml}{min}$ . This results in a residence time for the particles in the sample line of approximately 1.2 s.

During the experiment aerosol samples were taken regularly with the ACM-GC-MS system. The collection time for each sample was 60 min. The collection temperature of the collector was -30 °C and the desorption temperature 225 °C. The aerosol sample was desorbed for 6 min from the collector. The temperature of the valve array and the transfer line were kept constant at 230 °C. The aerosols were focused after desorption in the CFM for 1 min at -120 °C and injected into the GC-MS at 225 °C. The temperature program of the GC oven for each sample was as follows: start oven temperature was held at 40 °C for 5 min; ramped at a rate of 5 °C min<sup>-1</sup> to 200 °C; isothermal hold at 200 °C for 12 min. The total GC run was 54 min. With the desorption time of 6 min the total ACM-GC-MS measuring cycle was 60 min. Since the GC needed about 30 min to get back to the start temperature of 40 °C a sample could be measured approximately every 90 min. After each desorption the ACM was operated in the backflush mode with a temperature of 250 °C for 10 min.

During the experiments aerosol filter samples were taken regularly. The aerosols were sampled on quartz fiber filters (Millipore, 47 mm diameter). The filters were preheated 10 h at 600 °C before sampling. The filter holders were connected to the chamber with a 1 m long stainless steel tubing. The flow through the filter was  $25 \frac{l}{min}$  and was regulated with a mass flow controller (MKS Instruments, Type 579). After sampling the filters were stored in a 55 mm Petri dish, wrapped in aluminium foil, and stored in a freezer at -18 °C for the later analysis.

All sample lines to the instruments were at the same temperature as the temperature in the aerosol chamber. Thus changes in the aerosol composition due to evaporation or condensation of semivolatile components in the sample lines were avoided.

### 4.1.3 Experimental Conditions and Procedure

In the aerosol chamber experiment the formation of secondary organic aerosol (SOA) from the oxidation of  $\beta$ -pinene with ozone was studied. The experiment was conducted at ambient pressure and temperature. Prior to the experiment the chamber was flushed with particle free outside air for 16.5 hours. The air flow through the chamber during flushing was 25 m<sup>3</sup>/h. The humidity of the chamber was determined through the humidity of the outside air used for flushing the chamber. No additional humidification was applied. The initial conditions inside the chamber after flushing were 26.76 % relative humidity, a temperature of

#### 4.1. AEROSOL CHAMBER OF THE FZJ AND EXPERIMENTAL SET UP

---

20 °C, and an ozone concentration of approximately 20 ppb. The CPC measurements were used to check if the aerosol chamber was particle free. The particle concentration was  $<20\text{ cm}^{-3}$ .

Pure  $\beta$ -pinene (Aldrich, purity of 99%) was introduced into the chamber as a liquid with a microliter syringe. 1 ml of  $\beta$ -pinene, which is equivalent to 584 ppb, was injected in 10 steps through an opening in the chamber wall approximately 4 m above the chamber floor. After the content of the chamber was well mixed 1 ppm ozone was injected. The ozone was generated from pure oxygen (Linde, 4.8) through electrical discharges and introduced into the chamber with two inlets, one near a wall and the other at the center of the chamber. After the ozone was added the reaction inside the chamber started immediately.

Note that the initial monoterpene and ozone concentrations are orders of magnitude above ambient levels (Guenther et al., 1995; Kesselmeier and Staudt, 1999). The hydroxyl radical chemistry occurring in the chamber is largely independent on the concentration regarding the chemical mechanism and the products formed (Atkinson, 1997). However, the high concentrations do have an influence on the relative importance of competing reactions of organic species with ozone, OH and  $\text{NO}_x$ . Hence the observed yields for products formed in this experiment not necessarily represent ambient yields.

The high concentrations of the gas phase precursors were chosen in order to ensure sufficient aerosol mass for the experiment. An excess of ozone was used to ensure that all of the  $\beta$ -pinene is consumed during the experiment.

Due to the fact that in the oxidation of monoterpenes hydroxy radicals are formed (Atkinson and Arey, 2003) OH scavengers are often added to the precursor mixture (e.g., Lee et al., 2006; Ma and Marston, 2008). In this experiment no scavenger was used so that the oxidation of the precursor and to some extent of the products was due to ozone and OH radicals.

All instruments were measuring continuously during the experiment. The filter samples were taken in parallel to the ACM-GC-MS sampling. 16 ACM-GC-MS measurements with a 60 min sampling interval were taken over a time period of 60 h after starting SOA formation. Details of the ACM-GC-MS and filter measurements are shown in Table 4.1. The time for each sample indicates the time when the sampling for the ACM-GC-MS and the filters were started.

Prior to the injection of  $\beta$ -pinene a filter and ACM-GC-MS sample were taken from the empty chamber. ACM-GC-MS blank measurements were conducted regularly between the chamber samples. For the blank measurement a High Efficiency Particulate Airfilter (HEPA) was installed between the chamber sampling tubing and the ACM-GC-MS inlet. The same measurement cycle of the ACM-GC-MS was repeated with the installed filter. The blank measurement were used



CHAPTER 4. SECONDARY ORGANIC AEROSOL FORMATION FROM  
 $\beta$ -PINENE OZONOLYSIS

---

Table 4.1: *Overview of the course of the  $\beta$ -pinene experiment and the samples collected with the ACM-GC-MS and filter measurements. The times define the start of the sampling. S indicates that a chamber sample is collected and B indicates that a blank measurement was done.*

Date and Time	Time after ozone injection [h]	ACM sample	Filter sample	Comment
25.11.08 15:30	-	-	-	Start flushing aerosol chamber
26.11.08 07:30	-	-	-	Stop flushing aerosol chamber
26.11.08 08:00	-	S1	S1	chamber blank measurement
26.11.08 09:15	-	-	-	injection of 584 ppb $\beta$ -pinene
26.11.08 10:00	-	-	-	injection of 1 ppm ozone
26.11.08 11:18	1.3	S2	S2	-
26.11.08 13:02	3.03	B1	-	-
26.11.08 14:46	4.77	S3	S3	-
26.11.08 16:28	6.47	B2	-	-
26.11.08 18:03	8.05	S4	S4	-
26.11.08 19:49	9.82	B3	-	-
27.11.08 07:58	21.97	S5	S5	-
27.11.08 09:34	23.57	B4	-	-
27.11.08 11:02	25.03	S6	S6	-
27.11.08 12:33	26.55	S7	S7	-
27.11.08 14:07	28.12	S8	S8	-
27.11.08 15:43	29.72	S9	S9	-
27.11.08 17:19	31.32	S10	S10	-
27.11.08 18:41	32.68	B5	-	-
28.11.08 08:02	46.03	S11	S11	-
28.11.08 09:31	47.52	B6	-	-
28.11.08 11:03	49.05	S12	S12	-
28.11.08 12:36	50.60	S13	S13	-
28.11.08 14:07	52.12	S14	S14	-
28.11.08 15:38	53.63	S15	S15	-
28.11.08 17:07	55.12	S16	-	-
28.11.08 18:37	56.62	B7	-	-

to check for contaminations or residues inside the ACM-GC-MS and for adsorptions from the gas phase onto the collector.

## 4.2 Results of the Gas Phase and Particle Phase Measurements

### 4.2.1 Results of the PTR-TOF-MS Measurements

During the experiment the gas phase concentration of the precursors VOC and its oxidation products was measured with a Proton Transfer Reaction Time of Flight Mass Spectrometer (PTR-ToF-MS) and an ozone analyzer. In Figure 4.2 the evolution of the gas phase concentrations in the chamber during the experiment are shown. Additionally the evolution of the temperature and the relative humidity (RH) in the chamber are presented. The temperature during the experiment was almost constant and varied only between 20.5 °C and 22 °C. At the beginning of the experiment the relative humidity was 27% and slightly decreased during the experiment to approximately 20% at the end of the experiment. The temperature and the relative humidity show an oscillating behavior during the experiment which is due to the periodically change of the floor heating system to ensure a homogenous mixing inside the chamber.

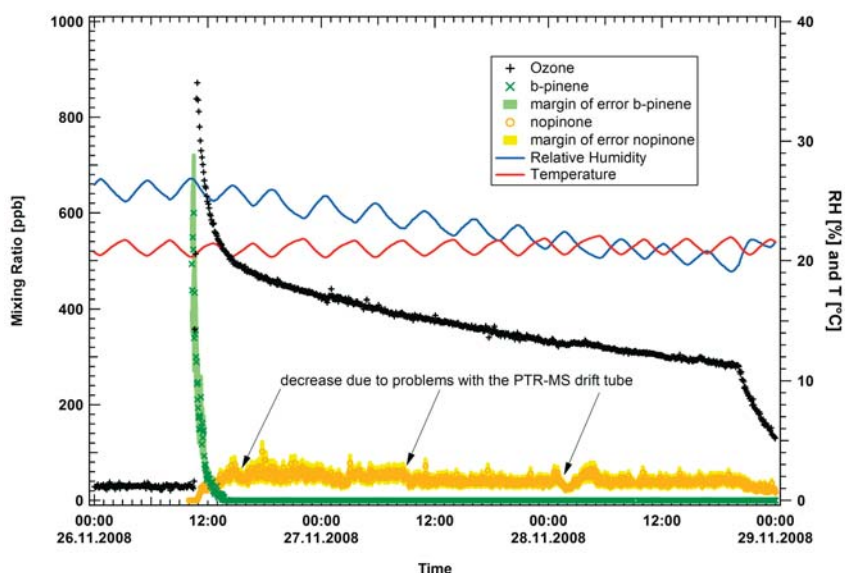


Figure 4.2: Gas phase measurements of the  $\beta$ -pinene ozonolysis experiment.

Prior to the start of the experiment the ozone concentration inside the chamber was approximately 30 ppb. At 10.30 h ozone was injected into the chamber for 6 minutes. The ozone concentration increased rapidly and reached its maximum of 872 ppb 20 minutes after the ozone injection was started. Afterwards the ozone concentration decrease again quickly for approximately 6 hours. Thereafter the ozone loss was significantly smaller. The ozone loss from the end of the first day till the end of the experiment is mainly due to the chamber wall loss processes and dilution due to sampling. Note that the steep decrease in the ozone concentration at the end of the experiment is due to the start of flushing the chamber with clean air.

The  $\beta$ -pinene concentration prior to the injection of ozone was approximately 600 ppb. After the ozone was added to the chamber the  $\beta$ -pinene concentration decreased steeply. Within 4 hours most of the  $\beta$ -pinene was consumed in the ozonolysis reaction in the chamber.

Approximately 30 min after the reaction was initiated the nopinone concentration inside the chamber started to increase. The increase was not as steeply as the decrease of  $\beta$ -pinene or ozone. 6 hours after the reaction was started the nopinone concentration reached its maximum of 60 ppb and stayed nearly constant over the whole rest duration of the experiment. Note that the sudden drops in the nopinone concentration during the experiment were due to problems with the PTR-ToF-MS drift tube.

#### 4.2.2 Results of the CPC and SMPS Measurements

During the  $\beta$ -pinene experiment the particle concentration inside the chamber was measured with a Condensation Particle Counter (CPC). Figure 4.3(b) shows the temporal development of the particle concentration. Prior to the experiment the chamber was flushed with clean air and the particle concentration was approximately  $20 \text{ cm}^{-3}$  before the precursors were injected into the chamber. After the  $\beta$ -pinene was injected into the chamber the particle concentration did not change. At 26.11.08 10:30 h the ozone was injected in the chamber and new particle formation started almost instantaneously. Within two minutes the maximum in particle concentration of  $2.23 \cdot 10^5 \text{ cm}^{-3}$  was reached. Then the particle number concentration decreased continuously until the end of the experiment. The reduction in the particle number concentration is due to particle losses in the chamber (wall losses, dilution and sedimentation) and coagulation of the particles. Coagulation of particles became less important with decreasing concentration so that after several hours the main reason for the reduction in particle concentration

## 4.2. RESULTS OF THE GAS PHASE AND PARTICLE PHASE MEASUREMENTS

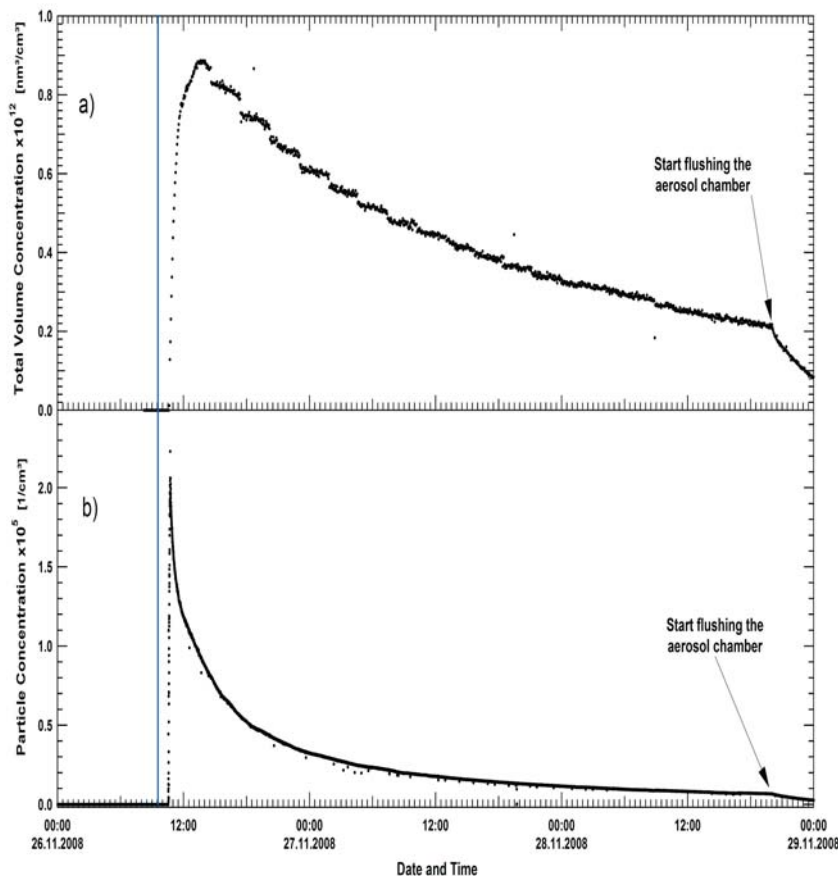


Figure 4.3: (a) Total volume concentration and (b) particle concentration during the aerosol chamber experiment. The blue vertical line marks the injection of  $\beta$ -pinene into the chamber. Note that the sharp bend in both graphs at the end of the experiment is due to the start of flushing the chamber.

were the other loss processes in the chamber. Note that at 28.11.08 20:00 h the experiment was concluded and the stronger decrease in particle number concentration is due to the flushing of the chamber with clean particle free outside air.

With the Scanning Mobility Particle Sizer (SMPS) the particle size distribution of the SOA formed during the reaction was measured. The SMPS measured the number distribution (dN versus particle diameter  $D_p$ ) which is used to calculate the particle volume distribution using equation 2.5. As described in chapter 3.2.3 the total particle volume concentration was calculated by integrating the particle volume distribution for each sample measured with the SMPS. In Figure 4.3(a) the time series of the total particle volume concentration obtained with the SMPS

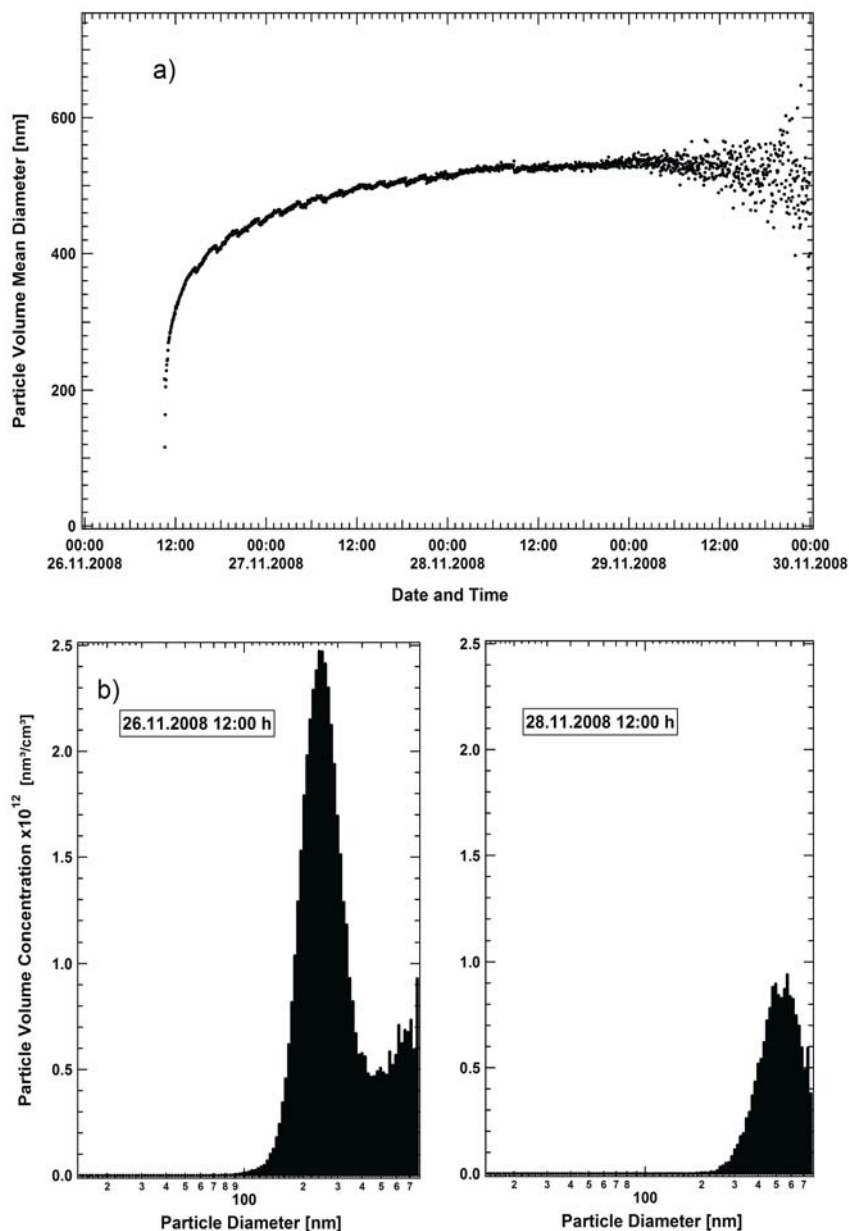


Figure 4.4: a) Time evolution of the mean particle diameter of the SOA during the experiment which shows the grow of the SOA due to coagulation of the particles and condensation of organic vapors. b) Example of two SMPS measurement of the particle volume distribution. Note that during the experiment the particle mode moves beyond the upper detection limit of the SMPS.

is shown. The particle volume concentration increased rapidly after the ozone was injected into the chamber and reached its maximum approximately 3 h after the reaction was initiated. Thereafter the concentration decreased due to the particle loss processes described before.

In Figure 4.4(a) the development of the particle mean diameter is shown. In the first two minutes, as shown in the CPC data, the majority of the particles are formed which afterwards grew due to coagulation of the particles and condensation of semivolatile and low volatile oxidation products onto the particles. In the first SMPS measurement after the injection of ozone the particle were 100 nm in diameter. Within 24 h the particle diameter increase to 500 nm and thereafter stayed nearly constant. Note that the accuracy in the determination of the mean particle diameter during the last 12 hours of the experiment decreased significantly due to the low particle concentration in the chamber which results in the larger scatter in the graph to the end of the experiment.

In Figure 4.4(b) two examples of the particle volume distributions are shown. Note that the majority of the particles were centered around a mode. The particles were growing equally during the experiment and the mode of the particles constantly moved to larger diameters until the particles mean diameter was approximately 530 nm. However the particle distribution also consists of larger particles which exceeds the upper detection limit (750 nm) of the SMPS. After approximately 12 h the diameter of the particles had increased to over 500 nm so that the particle mode partly moved beyond the detection limit of the SMPS. Thus the particle mass determined in the further analysis is an lower limit of the mass in the chamber.

### 4.2.3 Results of the ACM-GC-MS Measurements

In the following the results of the ACM-GC-MS system are presented. Figure 4.5 shows the FID chromatogram of sample S1, the empty chamber particle background. This sample was taken prior to the injection of the  $\beta$ -pinene when the aerosol chamber was almost particle free. The chromatogram consists of five peaks. However the origin of these peaks are not due to the content of the aerosol chamber. The peaks are due to a contaminated valve rotor replacement. The peaks occurred right after the exchange. A damaged rotor was exchanged with a previously repaired rotor. Presumably the repaired valve rotor was cleaned with unknown solvents which continually evaporated from the rotor after installation into the ACM. The contamination was more pronounced in the morning after the substances had time to accumulate over night at the beginning of the

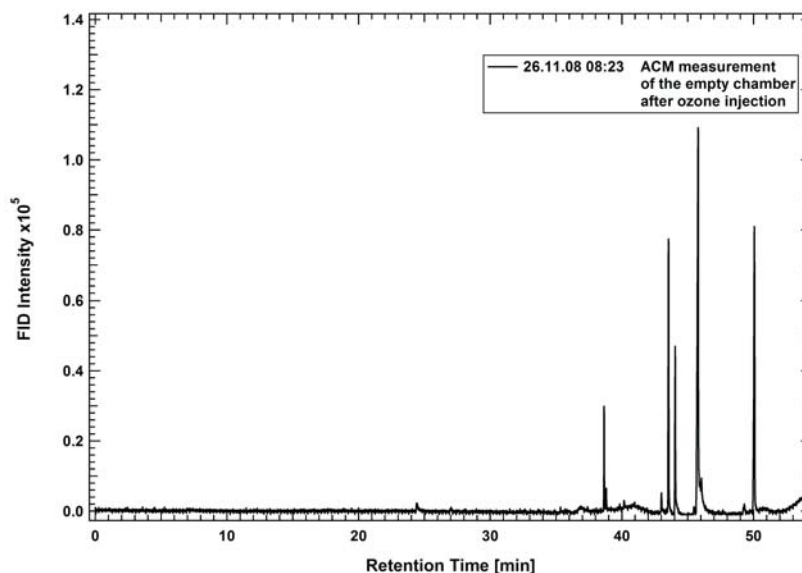


Figure 4.5: ACM-GC-MS FID chromatogram of the empty aerosol chamber. The measurement was done prior to the injection of the precursors. The peaks in the chromatogram are due to contamination of a rotor in the valve array of the ACM-GC-MS.

GC column. During the day with several experiments conducted the contamination were reduced successively and vanished completely. Also before the rotor needed to be exchanged no artifacts or contamination could be observed. Since the particle concentration in the aerosol chamber prior to the introduction of the precursors was very low (chapter 4.1.3) it is unlikely that the amount of aerosol sample during the blank could result in such high signals. Since the retention time for those peaks are constant they were omitted from the further analysis of the chromatograms.

The ACM measurements of the SOA from the chamber was successful for all samples taken during the experiment. Figure 4.6(a) shows the first sample measured with the ACM after the reaction in the chamber was started. The sample was taken 78 minutes after ozone injection. The FID chromatogram shows a variety of compounds. The majority of peaks are between 3 to 8 min and 15 to 33 min retention time. Two peaks, at 3.44 min and 25.3 min respectively, are the major products dominating the aerosol composition at this early stage in the reaction. Note that the contaminations from the rotor are reduced significantly after three consecutive measurements with the ACM.

Figure 4.6(b) and (c) shows examples of the following samples taken with the ACM, 22 h and 57 h after the ozone injection, respectively. The intensity of all

#### 4.2. RESULTS OF THE GAS PHASE AND PARTICLE PHASE MEASUREMENTS

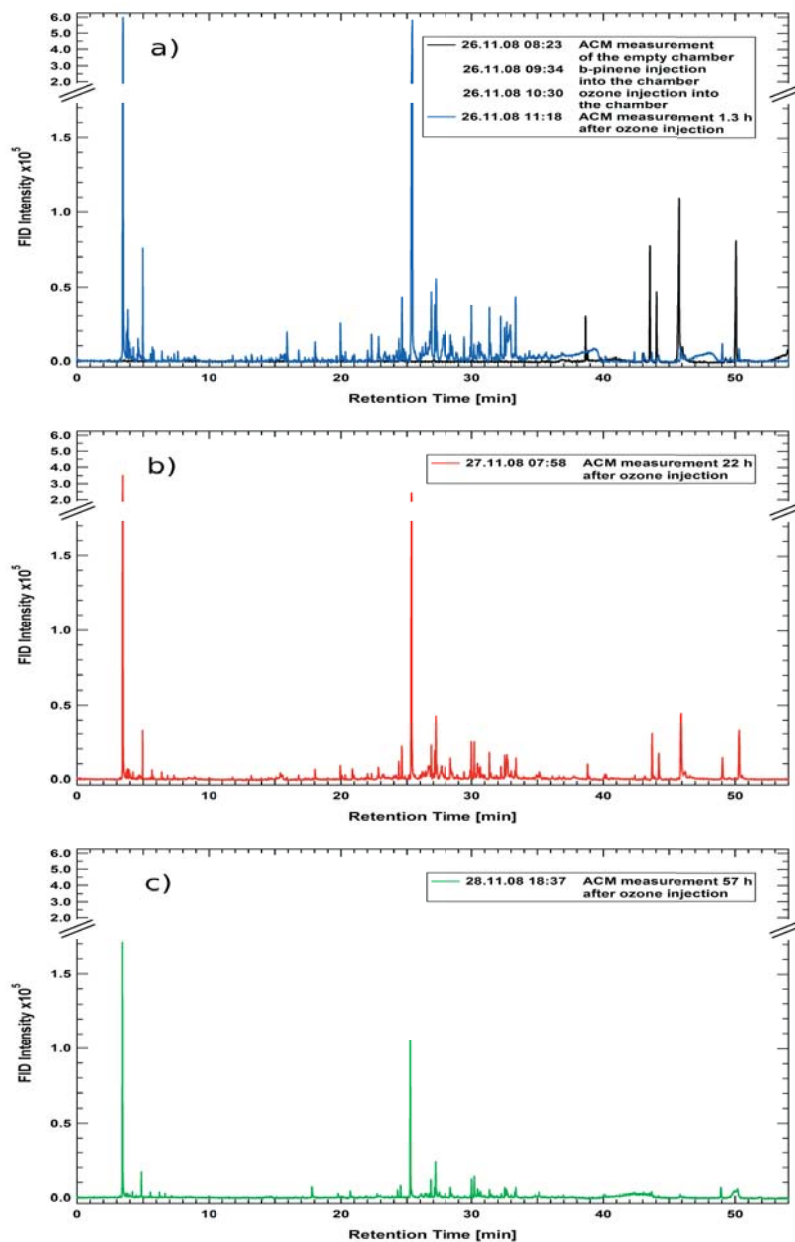


Figure 4.6: Comparison of three ACM-GC-MS FID chromatograms measured at (a) the beginning, (b) 22 h after the reaction started, and at (c) the end of the experiment. Note that aerosol mass in the chamber is decreasing over time. However the reduction of the peak intensity is not equal for all compounds which indicates changes in the SOA composition.



peaks was reduced during the experiments due to aerosol losses in the chamber (see chapter 4.2.2). After 57 h for example the peaks at 16 min, 20 min, and 22.34 min are below the detection limit of the GC-MS system. Note that the reduction of intensity is not the same for all compounds which indicates different composition of the sampled aerosols over the duration of the experiment. This is a good indication that the aging of the SOA could be observed with the ACM-GC-MS. All 16 FID chromatograms are presented in the appendix B.

For the further analysis of the chromatograms only peaks with a signal height of 5000 counts, based on the FID measurements, were chosen. All peaks smaller than 5000 counts could not be fitted well enough with the exponentially modified gaussian function (equation 2.2). The area under the peaks were calculated as described in chapter 2.4.

#### 4.2.4 Results of the Filter Sample Measurements

During the chamber experiment filter samples were taken in parallel to the ACM measurements. All filter samples were taken with the set up using a front and a back filter as described in chapter 2.5. Afterwards all front and back filter samples were analyzed using the Gas Chromatograph - Isotopic Ratio Mass Spectrometer (GC-IRMS) (chapter 2.5). Note that the desorption temperature of the GC-IRMS system for evaporating the aerosols from the filters was matched with the desorption temperature of the ACM collector of 225 °C. The total amount of nopinone in the SOA sampled with the filters was determined. The SOA were sampled onto the filters with an sampling flow of 25 l/min for 60 min (total sampling volume of 1500 l). However the sampling flow of the ACM was 0.08 l/min for 60 min (total sampling volume of 4.8 l). To be able to compare the filter measurements with the ACM-GC-MS measurements the result for the total nopinone mass on the filters was calculated for a sampling volume of 4.8 l. That means, that the nopinone mass of the filters was multiplied with a conversion factor of  $C_{IRMS,ACM} = \frac{4.8}{1500} = 0.0032$ . In Figure 4.7 the results of the filter analysis is shown. Note that the data points shown in Figure 4.7 already included the conversion factor. The red triangles show the total nopinone mass of the front filters measured with the GC-IRMS. The blue circles are the total mass of nopinone on the back filters due to gas phase adsorption. The purple crosses are the nopinone mass of the front filter corrected for the gas phase adsorption. The error bars shown in the graph include the standard deviation of the measurement and the uncertainty of the size of the filter piece that was cut out of the whole filter (chapter 2.5). The nopinone concentration on the filters was highest at the beginning

### 4.3. IDENTIFICATION AND TEMPORAL EVOLUTION OF $\beta$ -PINENE OZONOLYSIS PRODUCTS IN THE SOA

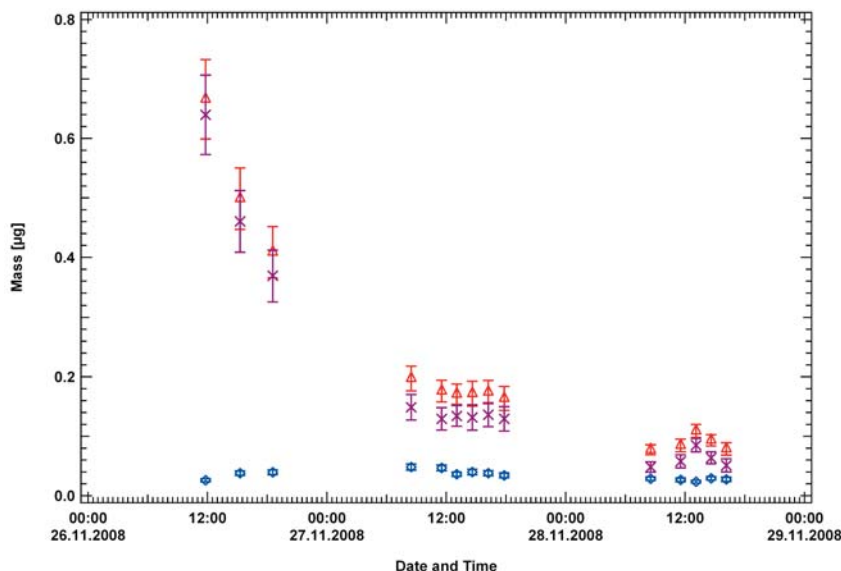


Figure 4.7: Total mass of nopinone measured for the front filter sample (red triangles) taken during the  $\beta$ -pinene ozonolysis experiment. The blue diamonds is the total nopinone mass on the back filters due to gas phase adsorption. The purple crosses shows the nopinone mass on the front filter corrected for the gas phase adsorption.

of the experiment and drops continuously over the course of the experiment due to aerosol loss in the chamber (chapter 4.2.2). The amount of nopinone due to gas phase adsorption onto the back filter is over the course of the experiment almost constant. Note that during the experiment the total amount of nopinone on the back filter ranged between 3 to 40% of the total nopinone mass sampled on the front filter. The total nopinone mass measured with the filter samples will be further compared with the ACM-GC-MS measurements in chapter 4.5.

## 4.3 Identification and Temporal Evolution of $\beta$ -pinene ozonolysis products in the SOA

### 4.3.1 Identification of $\beta$ -pinene ozonolysis products

For the identification of the chromatographically separated compounds the averaged mass spectra of the peaks measured with the MS were used. The procedure to obtain these mass spectra is described in chapter 2.4. Two approaches were used to identify components in the chromatograms. The first approach is to

identify the peaks by comparison of the averaged mass spectra measured with the MS with the content of the NIST database. However the content of the NIST database (version from 1992) which was available for the identification does not contain all compounds formed during the  $\beta$ -pinene ozonolysis. Only the two major peaks in the chromatogram could be reliably identified as acetone (3.54 min retention time) and nopinone (25.34 min retention time). The identification of both peaks was also verified by comparison of the mass spectra with the spectra obtained for the calibration of the GC-MS detector.


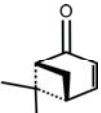
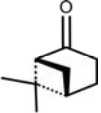

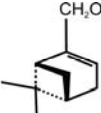
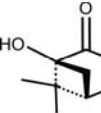
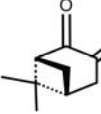
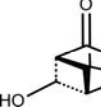
Nopinone had been previously identified as a major product of the  $\beta$ -pinene ozonolysis (Grosjean et al., 1993; Hakola et al., 1994) in the gas phase (Lee et al., 2006; Winterhalter et al., 2000) and also in the aerosol phase (Yokouchi and Ambe, 1985; Jaoui and Kamens, 2003b). Also acetone was found as a major product formed in the reaction of  $\beta$ -pinene with ozone (Orlando et al., 2000; Larsen et al., 2001; Wisthaler et al., 2001; Jaoui and Kamens, 2003a). However the acetone in these studies was only measured in the gas phase not in the aerosol phase. Acetone is the second major compound in the composition of the SOA measured with the ACM-GC-MS. However it is unlikely that the acetone partitions from the gas phase into the SOA due to its high vapor pressure. The possible source of the acetone will be further analyzed in chapter 4.3.2.

For the second approach peaks were tentatively identified by comparing the results with literature. Since one aim of the aerosol chamber experiment was to determine the performance of the ACM-GC-MS system in measuring the composition of the SOA the data provided by literature will be used to search for peaks corresponding to compounds which were previously identified by others in SOA resulting from the oxidation of  $\beta$ -pinene with ozone and OH (Jaoui and Kamens, 2003b,a; Yu et al., 1999; Larsen et al., 2001). Since the chamber was flushed with particle free outside air it can be assumed that with the beginning of the experiment a typical ambient  $\text{NO}_x$  concentration had been established inside the chamber. As mentioned earlier (chapter 4.1.3) also products from the oxidation of the precursors with OH radicals were to be expected.

For all major peaks measured with the ACM-GC-MS average background subtracted mass spectra were created and analyzed. Jaoui and Kamens (2003b) work focused on the characterization of the gas and particle phase reaction products from the reaction of  $\beta$ -pinene with ozone and  $\beta$ -pinene with OH radicals in the presence of  $\text{NO}_x$  and natural sunlight. Their findings for the nighttime reaction products will be compared to the ACM-GC-MS measurements. For the identification the three major ion fragments in the EI mass spectra were used. In appendix C the ACM-GC-MS mass spectra are shown which could be tentatively identified. Bicyclo[3,1,1]hept-3-ene-2-one, bicyclo[3,1,1]heptane-2-carboxaldehyde (also

#### 4.3. IDENTIFICATION AND TEMPORAL EVOLUTION OF $\beta$ -PINENE OZONOLYSIS PRODUCTS IN THE SOA

Table 4.2: Retention time, structure, molecular weight, and major ion fragments of the identified products in the  $\beta$ -pinene ozonolysis experiment listed in the order of ascending retention time.

Identification	Retention Time	Structure	MW (g mol <sup>-1</sup> )	m/z (EI)
acetone	3.44		58	43, 15, 58
bicyclo[3,1,1]hept-3-ene-2-one	24.59		136	93, 121, 77
nopinone	25.34		138	83, 95, 55
myrtanal	26.81		152	69, 82, 41
myrtenol	27.18		152	79, 91, 108
1-hydroxynopinone	28.35		154	83, 95, 136
3-oxonopinone	31.35		152	83, 55, 152
3,7-dihydroxynopinone	33.33		170	83, 111, 55

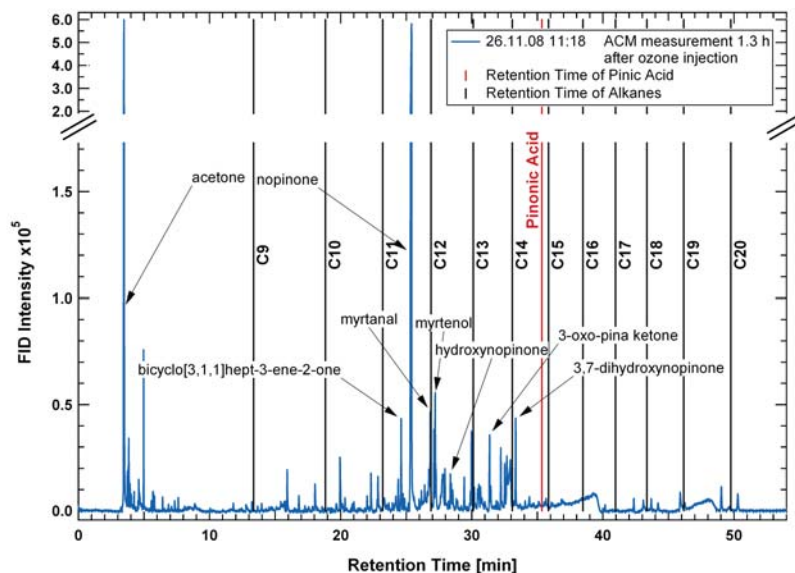


Figure 4.8: ACM-GC-MS FID chromatogram of S2. The retention time of the homologous alkane series are indicated through black vertical lines. The retention time of pinonic acid, determined through direct injection into the GC-MS, is indicated through the red vertical line.

known as myrtanal), myrtenol, 1-hydroxynopinone, 3-oxonopinone (also known as 3-oxo-pina ketone) and 3,7-dihydroxynopinone could be assigned to peaks in the chromatogram.

In addition the EI mass spectra of 1-hydroxynopinone was compared to the mass spectra presented in Jaoui and Kamens (2003a) which back up the identification of this compound. In Table 4.2 the structure, molecular weight, the major ion fragments, and the retention time of these compounds are summarized. Some of these products were also identified as compounds in the particle phase by Yu et al. (1999); Larsen et al. (2001). However myrtenol was previously only detected in the gas phase but not in the aerosol phase.

To strengthen the identification of myrtenol and myrtanal the retention index (RI) of these compounds were calculated and compared to literature data. The definition of the linear retention index and calculation of the linear retention index used in this study are described in appendix D. In Figure 4.8 the retention times of the homologous series of alkanes (for details see chapter 3.1.2) were added to the chromatogram of sample S2. The linear retention indices for the identified compounds were calculated and are summarized in Table 4.3. The linear retention indices for nopinone and myrtanal calculated in this work are slightly higher than the reported literature value. The linear retention indices for myrtenol reported

#### 4.3. IDENTIFICATION AND TEMPORAL EVOLUTION OF $\beta$ -PINENE OZONOLYSIS PRODUCTS IN THE SOA

Table 4.3: *Comparison of determined linear retention indices of the identified products with literature values.*

Compound Name	RI This work	RI Other Studies (type of column)	Reference
bicyclo[3,1,1]hept-3-ene-2-one	1138	-	-
nopinone	1158	1137 (HP-5MS)	Papandreou et al. (2002)
		1139 (HP-5MS)	Kallio et al. (2006)
myrtanal	1198	1180 (HP-5MS)	Papandreou et al. (2002)
myrtenol	1209	1202 (DB-5MS)	Kowalski and Wolski (2005)
		1214 (DB-5MS)	Wang et al. (2005)
1-hydroxynopinone	1158	-	-
3-oxonopinone	1342	-	-
3,7-dihydroxynopinone	1408	-	-

by Kowalski and Wolski (2005) and Wang et al. (2005) correspond well with the indices determined. Note that the chromatographic column which is used in the studies by Papandreou et al. (2002) and Kallio et al. (2006) is a HP-5MS. This column has an equivalent stationary phase ((5%-Phenyl)-methylpolysiloxane) as the DB-5ms column which was used with the ACM-GC-MS system, but is from a different manufacturer which can explain the minor deviation between the retention indices. Unfortunately only retention indices for three compounds could be found in the literature.

No acids such as pinonic acid or pinic acids which are also important products of the  $\beta$ -pinene ozonolysis were identified in the ACM-GC-MS measurement. To proof the absence of these compounds in the SOA sample chromatograms pinonic acid (purity 98%) was measured with the GC-MS system through direct injection. In Figure 4.8 the retention time of pinonic acid is indicated. Pinonic acid eluted from the GC column at 35.35 min. The peak with largest retention time measured during the SOA experiment was 3,7-dihydroxynopinone which eluted at 33.33 min. Previous studies analyzed the composition of  $\beta$ -pinene SOA with respect to polar compounds such as acids by solvent extraction of the filters with subsequent derivatization of the compounds (Yu et al., 1999; Jaoui and Kamens, 2003b,a). The ACM-GC-MS system measures the compounds directly without these steps. Presumably the ACM-GC-MS system in this specific set up is not capable to transfer and/or measure the acids.

Eight products of the  $\beta$ -pinene ozonolysis in the SOA could be identified with

the ACM-GC-MS system by comparison with literature values of the main  $m/z$  fragments. Myrtanal, myrtenol and nopinone were also identified by determining their retention indices and comparison with literature values. Acteone and nopinone were additionally identified using the NIST database.

### 4.3.2 Source of Acetone in the SOA

As presented previously (chapter 4.3.1) acetone is found to be a major compound in the SOA measured with the ACM-GC-MS. However it is unlikely that the acetone partitioned from the gas phase into the SOA due to its high vapor pressure. To further investigate the source of acetone in the ACM-GC-MS experiments, particles sampled on quartz fiber filters were measured with a thermal desorption system coupled to a gas chromatograph isotope ratio mass spectrometer (GC-IRMS) (Fisseha et al., 2009). The SOA was analyzed by evaporating the collected particles from the filters and subsequent analysis of the composition with the GC-IRMS. The analysis showed also high amount of acetone in SOA formed in the  $\beta$ -pinene ozonolysis experiment.

Measurements of blank filters and blanks measurements of the GC-IRMS system were performed to exclude contaminations of the filters and the system as a possible source. Additionally an experiment in the aerosol chamber was performed to exclude that the acetone is result of ozone reacting with the chamber wall or any contaminations in the chamber. The acetone concentration of the filters from this blank experiment was below the detection limit of the GC-IRMS. This results shows that the acetone was directly related to the SOA from the  $\beta$ -pinene.

To further characterize the acetone from the SOA one set of analysis was performed in which the filters were heated in a stepwise manner between 30 °C and 240 °C. It was shown that acetone needed a higher temperature to be desorbed from the filter than nopinone. Thus we concluded that the acetone measured during the analysis might be due to a thermal decomposition of a an oligomer or from a partial decomposition of high molecular compounds which contain a C = O functional group. Since the samples collected with the ACM were also evaporated from the collector at 225 °C it is reasonable to assume that the acetone measured with the ACM-GC-MS is also due to a thermal breakdown of a high molecular compound.

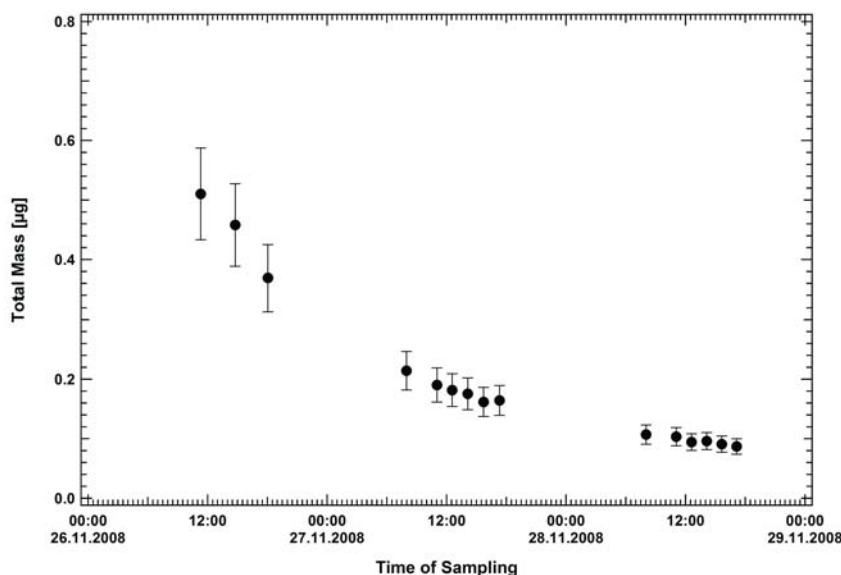


Figure 4.9: *Time series of the total SOA mass measured by the ACM-GC-MS system.*

### 4.3.3 Time Series of Aerosol Composition

The peak areas determined for all selected peaks were converted into mass using the calibration curves derived in chapter 3. For acetone and nopinone the according response factors from calibration of the direct injection into the GC-MS system (chapter 3.1) were applied. For all other compounds the calibration derived for the octadecane (chapter 3.2.2) is used. Note that the response factor of the FID detector is different for oxidized compounds. Organic compounds with functional groups such as carbonyl, alcohol, and halogens give a weaker signal when they enter the FID detector and are underestimated compared to non oxygenated species (Komenda et al., 2001, and references therein). Therefore, by applying the octadecane calibration to the ACM-GC-MS measurements the mass determined for each individual compound and the total mass of each sample represents a lower limit.

In Figure 4.9 the variation over time in the total mass collected with each sample is shown. The total mass was calculated by integrating the areas of all peaks in the FID chromatograms for each sample. Note that only peaks selected as stated in chapter 4.1.3 were considered to contribute to the total mass. The time for each data point corresponds to the middle of the sampling interval. The total aerosol mass measured by the ACM-GC-MS is at its maximum at the beginning



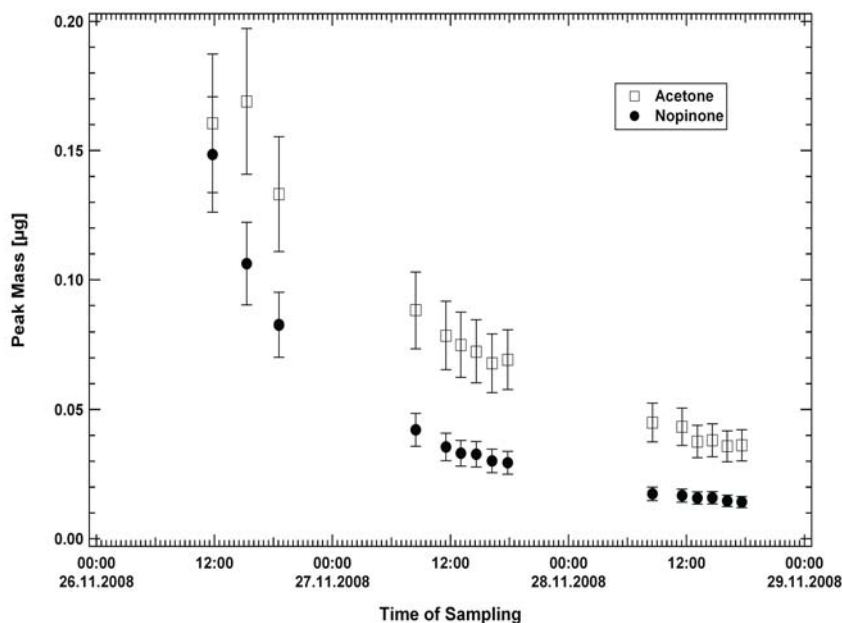


Figure 4.10: *Time series of the nopinone (circles) and acetone (squares) mass determined from the ACM-GC-MS FID chromatograms.*

of the experiment and afterwards decays over time. Since the collection time of the ACM-GC-MS was kept constant at 60 min with a sampling flow of 80 ml/min for all samples the time series shows the reduction of the aerosol mass inside the aerosol chamber during the experiment. The reduction is due to wall losses, dilution and sedimentation of aerosols. Also the continuous sampling reduced the aerosol concentration in the chamber. In Figures 4.10 and 4.11 the temporal variation for the single compounds of the SOA is presented. The time series are presented for the previously identified compounds. For a better overview acetone and nopinone are displayed separately from the other compounds. The masses of nopinone, bicyclo[3,1,1]hept-3-ene-2-one, and 3,7-dihydroxynopinone shows the same variation over time as the total mass. However not all peaks follow the same trend. The masses of the acetone, myrtanal, 1-hydroxynopinone, and 3-oxonopinone initially increase for the first 2 samples before they also decrease. Note that acetone and nopinone together contribute 60% to the total mass detected by the ACM-GC-MS.

The different curve shapes indicate changes in the aerosol composition. This aspect is discussed in detail in chapters 4.4 and 4.7 in comparison of the ACM-GC-MS results to the results obtained with the SMPS and AMS.

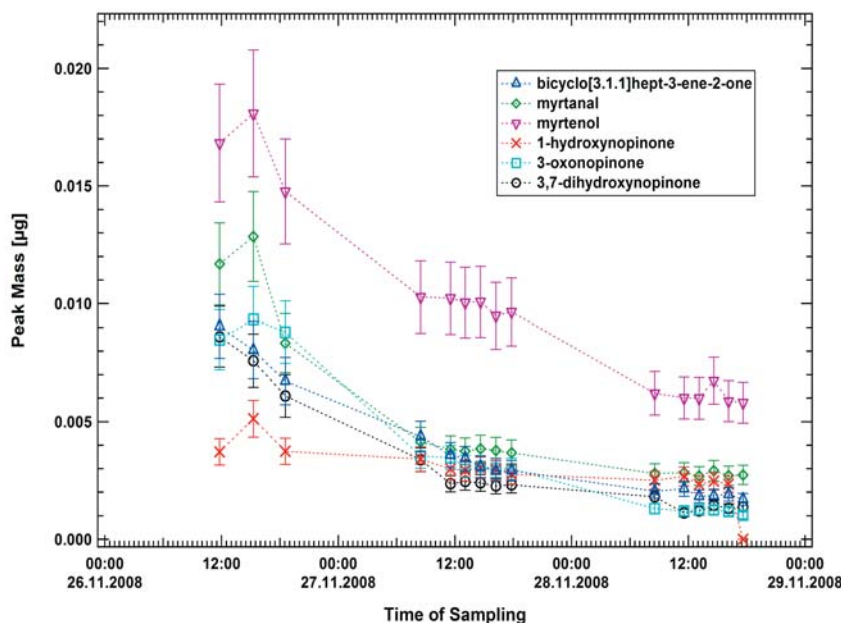


Figure 4.11: Time series of the identified peaks determined from the ACM-GC-MS FID chromatograms. Note that the different curve shapes indicate a change in the SOA composition.

## 4.4 Intercomparison of ACM-GC-MS and SMPS

In this chapter the total mass measured with the ACM-GC-MS is compared to the mass loading of the collector derived from the SMPS measurements. Also the temporal evolution of the mass fractional abundances of the compounds in the SOA will be analyzed and discussed.

### 4.4.1 Total Mass measured by ACM-GC-MS

In Figure 4.12(a) the total mass measured with the ACM-GC-MS for each sample is compared to the collector mass loading derived from the SMPS measurements. The collector mass loading was determined using equation 3.2. Instead of using the density of octadecane in equation 3.2 the average density of the SOA of  $1.2 \text{ g/cm}^3$  determined as described in chapter 2.8 was used. In general the total mass measured with the ACM-GC-MS and the collector mass loading have the same temporal variation except for the first three samples. In Figure 4.12(b) the total mass measured with the ACM-GC-MS was normalized to the collector mass loading. The mass fraction measured with the ACM-GC-MS was 11% at

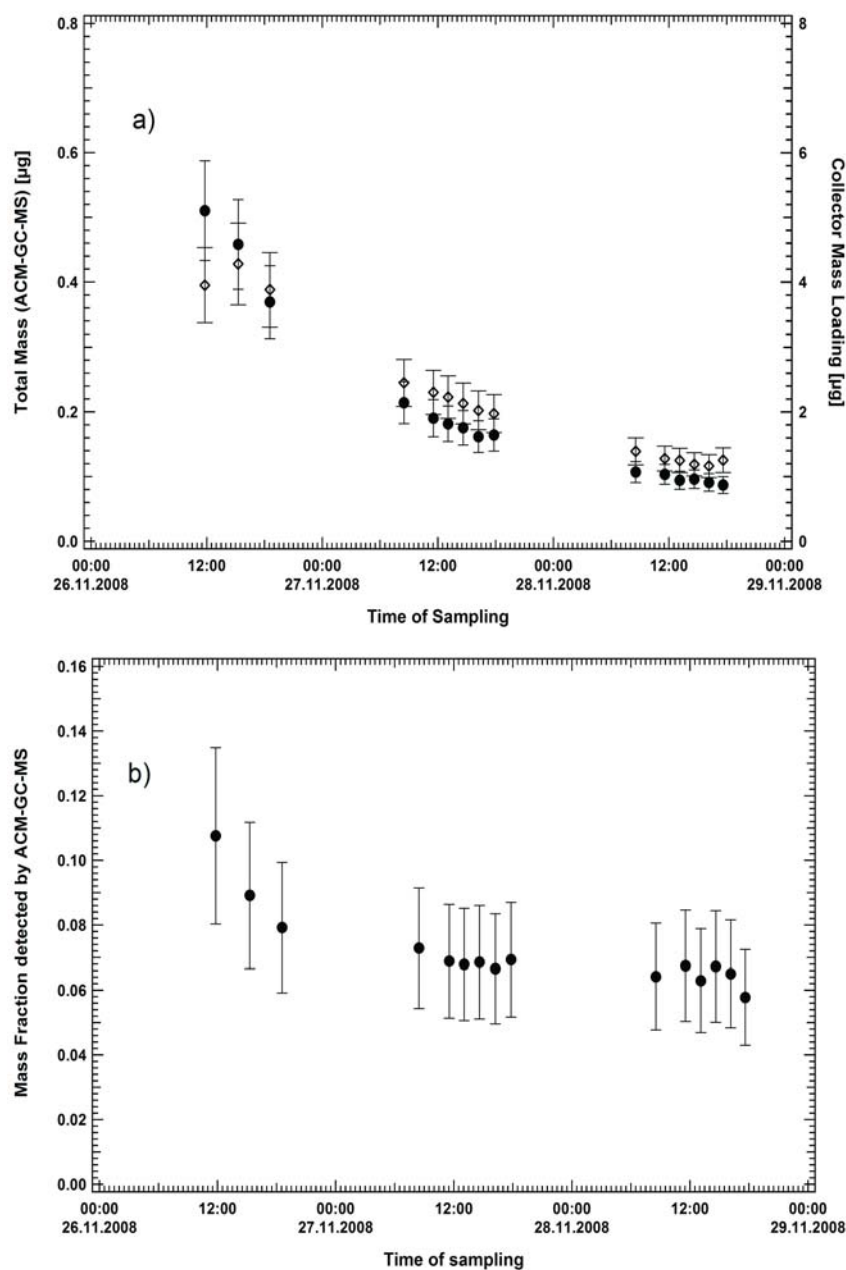


Figure 4.12: Figure (a) shows the Comparison of the ACM collector mass loading (open diamonds) and the total mass measured with the ACM-GC-MS (filled circles). Note that scale of the y-axis have one order of magnitude difference. In Figure (b) the time series of the fraction of the aerosol mass detected by the ACM-GC-MS is presented.

the beginning of the experiment and decreased during the first day to 6% and was nearly constant for the next two days. In part the low (6-11%) recovery of SOA mass with the ACM-GC-MS can be explained by the compound detection capabilities of the ACM-GC-MS. In chapter 4.3.1 it was shown that higher oxygenated products of the  $\beta$ -pinene ozonolysis such as acids are not measurable with this specific ACM-GC-MS set up. Additionally the gas phase measurements (see 4.2) show that during the first hours after the reaction was started the ozone concentration decreased rapidly. During this period the successive oxidation of the  $\beta$ -pinene and the products led to an increase in the compounds which are not measurable with the ACM-GC-MS set up. It can be assumed that this trend is reflected in the curve shape in Figure 4.12(b) which shows that the mass fraction measured by the ACM-GC-MS decrease during the first three samples. On the second and third day the ozone was, except for chamber wall losses, nearly constant as was the ACM-GC-MS detected mass fraction.

Furthermore the GC-MS technique is limited with regard to measuring high molecular weight compounds. The evidence for oligomer formation in SOA from the photooxidation and ozonolysis of  $\alpha$ -pinene were measured during different smog chamber studies (Gao et al., 2004; Baltensperger et al., 2005; Müller et al., 2008). Baltensperger et al. (2005) additionally found increasing abundances of high molecular weight compounds (up to 1000 Da) with increasing aging time of the SOA. They also estimated that after 20 h of aging about 50% of the particle mass consisted of oligomers. Under the assumption that in the  $\beta$ -pinene ozonolysis also oligomerization occurred these high molecular compounds in the SOA would not have been detected by the GC-MS system.

#### 4.4.2 Temporal evolution of the mass fractional abundances of SOA compounds

In Figure 4.13 the mass fractional abundance of the identified compounds in the aerosol is shown. The masses for these compounds determined in chapter 4.3.3 were normalized to the collector mass loading determined from the SMPS measurements. In Figure 4.13(a) the contributions of acetone and nopinone to the SOA of each sample measured during the experiment are presented. The fraction of nopinone in the aerosol had its maximum at the beginning of the ozonolysis and continuously decreased over the first two days of the experiment. The last 6 samples measured with the ACM-GC-MS had a nearly constant nopinone fraction. The largest change of the nopinone fraction in the aerosol was ob-

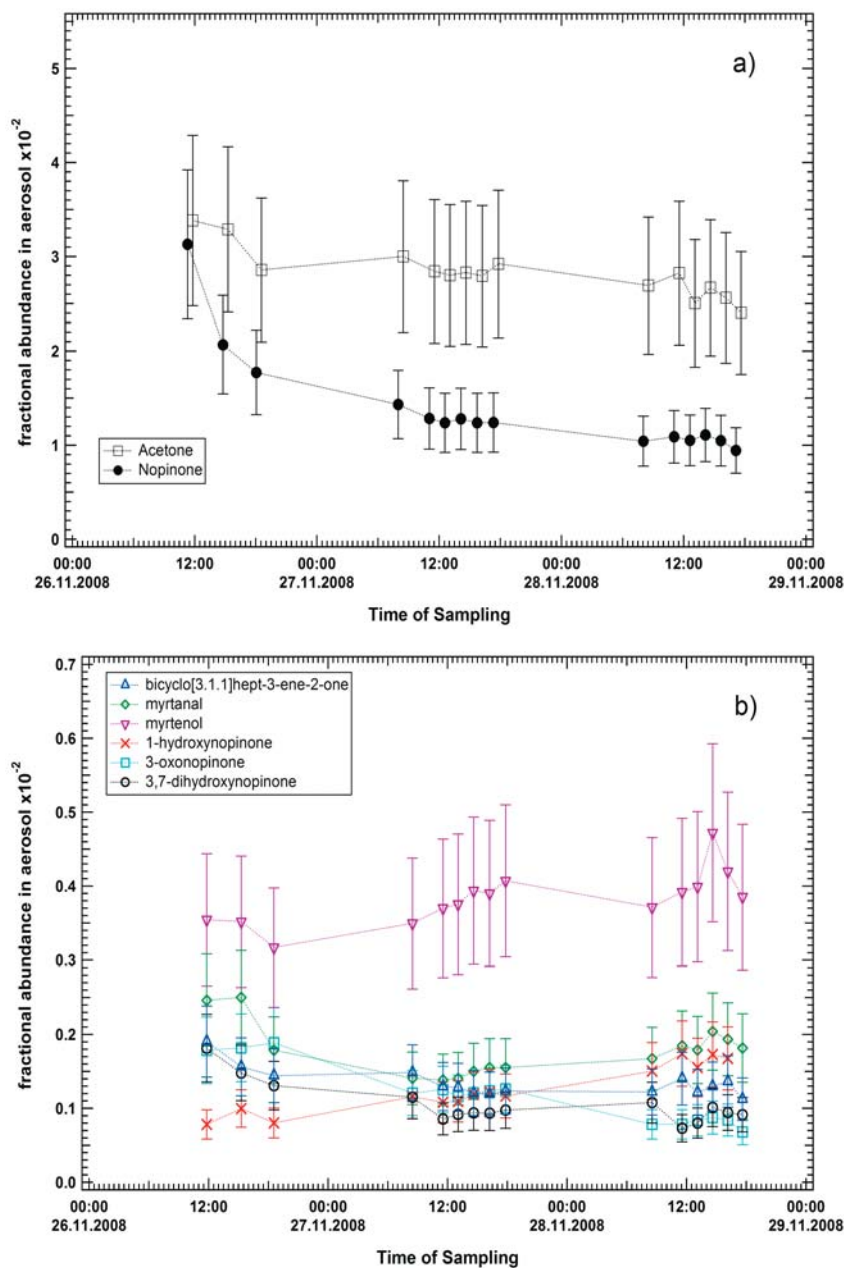


Figure 4.13: Fractional abundances of identified compounds in the SOA. Note that for overview reasons the two main compounds are presented separately from the other compounds. a) Fractional abundances for the two main compounds nopinone and acetone in the ACM-GC-MS chromatograms. b) Fractional abundances for the other identified compounds.

served in the first four samples with a decrease from 3% to 1% within 24 h. However the gas phase nopinone concentration stayed quite constant 5 hours after the reaction was started until the end of the experiment (see Figure 4.2) which is reasonable since nopinone does not react with ozone (Calogirou et al., 1999). However during the first 24 hours the large decrease in ozone indicates the continuous progress of the oxidation of the  $\beta$ -pinene and other products which results in an increase in other species. Therefore the mass fractional decrease of nopinone in the SOA can be explained due to the relative change in composition of the SOA that is more species partitioned into the SOA so that the relative contribution of the nopinone decreased. The time trend of the acetone fraction is similar however the total decrease in the acetone fraction of the aerosols is approximately 1% from 3.5 to 2.5%. In Figure 4.13(b) the time series of the other identified peaks are shown. Note that these compounds show distinctively different time trends. While bicyclo[3,1,1]hept-3-ene-2-one and 3,7-dihydroxynopinone show similar temporal evolutions as nopinone and acetone, the fractions of myrtanal and 3-oxonopinone of the SOA first increase in the first two to three samples before they decrease. The fraction of 1-hydroxynopinone and myrtenol even increase continuously during the experiment.

For the further analysis also the time series of the mass fraction of the unidentified compounds were analyzed. As described for the identified compounds the mass determined for the unidentified compounds were normalized to the collector mass loading. The compounds were grouped according to similar time evolution of the mass fractional abundance in the SOA. In Figure 4.14 each graph shows a group of compounds which had the same or similar temporal behavior. The majority of the peaks could be grouped together according to the three trends previously described for the identified compounds. Figure 4.14(a) contains unidentified peaks with a time series comparable to nopinone, acetone, bicyclo[3,1,1]hept-3-ene-2-one, and 3,7-dihydroxynopinone. These compounds contribute the largest fractional mass at the beginning of the experiment and decrease over time. In Figure 4.14(b) the compounds show the same time trend as myrtanal and 3-oxonopinone. The mass fraction of the aerosol rise during the first samples before it decreased again. The compounds showing continuous increase over the duration of the experiments are presented in Figure 4.14(c). Note that for reasons of clarity only two or three example time series are presented in Figures 4.14(a), 4.14(b), and 4.14(c). In appendix E all measurable peaks are grouped according to their time trends. Also peaks which could not clearly be assigned to a group are presented in appendix E.

Group 1 to 3 will be analyzed further in comparison with the AMS measurements in chapter 4.7.2. However peaks which could not clearly be assigned to one of the

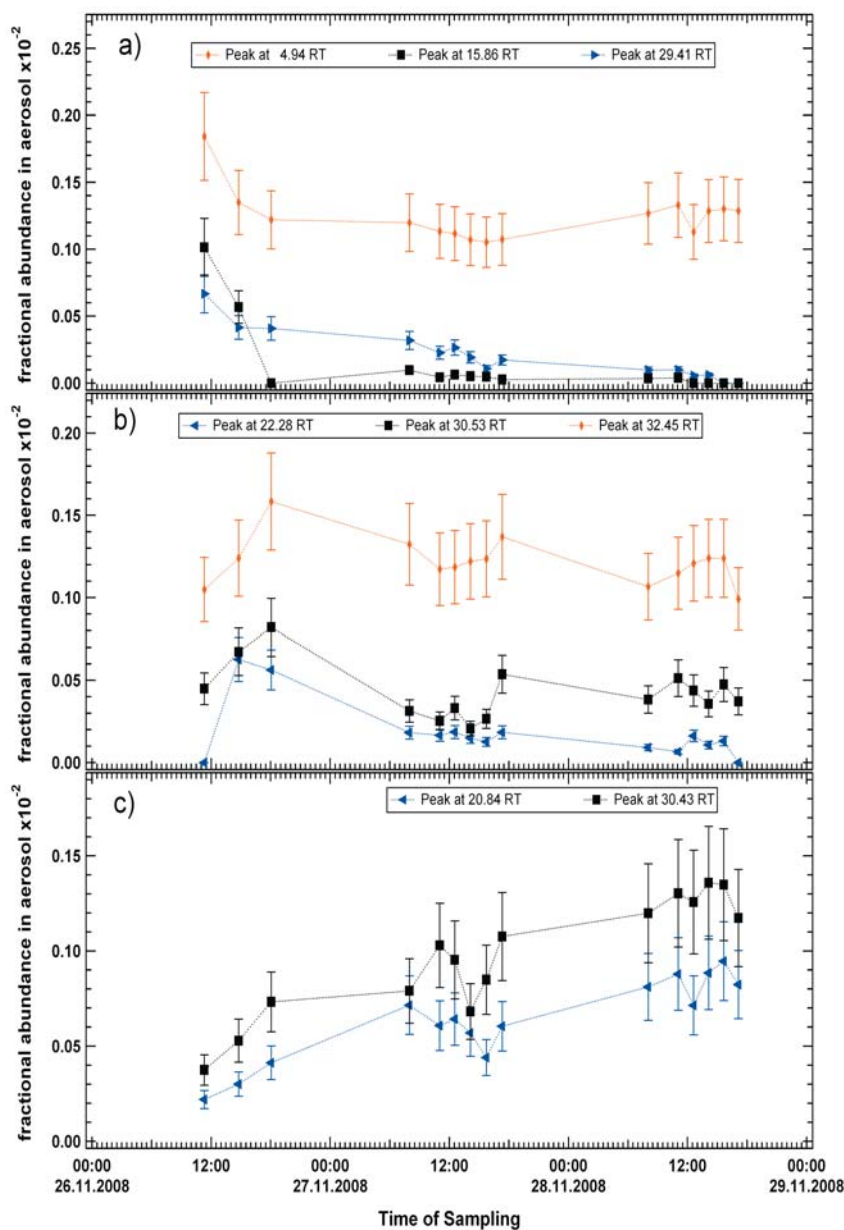


Figure 4.14: Fractional abundance of the unidentified peaks group together according to their specific temporal evolution. Note that for overview reasons only the time series for three example peaks in Figure a) and b) and two example peaks for Figure c) are shown. The graphs with all peaks assigned to the groups is presented in appendix E.

groups will be not included in this comparison since no identified peak shows a similar trend and therefore no further analysis with regard to compound specific analysis such as O/C ratios can be applied.

## 4.5 Intercomparison of ACM-GC-MS and Filter Samples

In Figure 4.15 the total nopinone mass measured with the filter samples is compared to the total nopinone mass measured with the ACM-GC-MS. As described previously the total nopinone mass measured with the filters (red triangles) was corrected by subtracting the total amount of nopinone measured on the back filters (blue diamonds). However an additional correction had to be applied to the nopinone mass from the filter measurements to be comparable to the ACM-GC-MS measurements (black circles). The ACM inlet has a particle transmission efficiency for particles in the size range between 70 and 500 nm in diameter of 100%. Quartz fiber filters have collection efficiency of 100% for particles larger

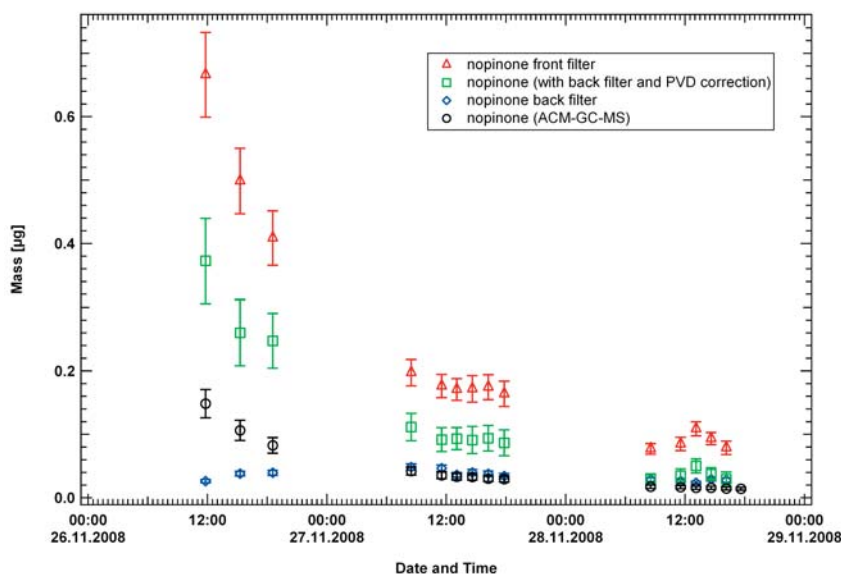


Figure 4.15: Comparison between the total nopinone mass sampled with filters (red triangles: uncorrected and green squares: corrected) and the total nopinone mass measured with the ACM-GC-MS (black circles). Also the total amount of nopinone on the back filter (blue diamonds) due to nopinone gas phase adsorption is shown.



than 100 nm. During the  $\beta$ -pinene ozonolysis experiment the particles grew such that a significant fraction of the particles had a diameter larger than 500 nm (see Figure 4.4). Therefore also particles with larger diameter than 500 nm will contribute significantly to the total nopinone mass collected with the filters. For a better comparison of the filter samples to the ACM-GC-MS samples the nopinone mass on the filter was corrected using the SMPS measurements. The SMPS particle volume distributions were fitted with a lognormal function. For each filter sample the fraction of particles with a larger diameter than 500 nm was determined. The total nopinone mass measured with the filters was then corrected for the fraction of nopinone mass which could not be sampled with the ACM-GC-MS. In Figure 4.15 the total nopinone mass after both corrections, the back filter correction and the particle volume distribution (PVD) correction, were applied is represented by the green squares. The amount of nopinone measured with the both method follow a similar temporal trend. However the corrected nopinone mass measured with the filter samples was during the first two days more than two times larger than the nopinone mass measured with the ACM-GC-MS. On the last day both measurements show a similar nopinone mass. Note that the amount of nopinone on the back filter is for the second and third day approximately the same as the amount measured with the ACM-GC-MS. The comparison show that either the ACM-GC-MS underestimated the nopinone mass or that the filter samples overestimated the amount of nopinone in the SOA. Since octadecane test aerosols were sampled, desorbed and transferred with a recovery rate of 100% with the ACM-GC-MS it can be assumed that no significant amount of nopinone is lost in the ACM-GC-MS system. However positive artifacts for filter samples due to gas phase adsorption is a known complication for filter collection of organic aerosols (Turpin et al., 2000; Kirchstetter et al., 2001). Positive artifacts appear to dominate samples taken with quartz filters and are estimated of over 50% of the particulate organic matter (Turpin et al., 1994; Kirchstetter et al., 2001). Subramanian et al. (2004) and Kirchstetter et al. (2001) showed that a quartz backup filter provides a good estimate of the positive artifact on the sampling (front) quartz filter when the sampling period is long (24 h and 14 h, respectively). However they also showed that sampling for a shorter duration (2 h, 4 h, 6 h, and 8 h) a considerable positive artifact remain on the front quartz filter. It is assumed that this underestimation of the positive artifact by the backup quartz filter for short sampling times is due to the fact that it takes considerably longer for condensable organics to reach equilibrium in the vicinity of a quartz filter (Turpin et al., 2000; Mader and Pankow, 2001). It is also important to note that the distribution of the collected aerosol on the quartz fiber filters of the chamber experiment were not homogenous. It could be

seen that the concentration of the sampled aerosols was more dense in the center of the filter and that the concentration decreased from the center outwards. The filter piece which was cut out from the whole filter for analysis was taken from the central region of the filter what also could have led to an overestimation of the nopinone mass sampled with the filters.

The known complication of filter samples described above and the supposedly large positive artefact of the filter samples measured in  $\beta$ -pinene ozonolysis experiment emphasize the importance of aerosol sampling techniques, such as the ACM-GC-MS, which are less susceptible for such artifacts.

## 4.6 SOA Yield and Nopinone Partitioning

In this chapter the measurements of the gas phase and particle phase during the  $\beta$ -pinene ozonolysis experiment were used to calculate and examine important properties of the SOA formation. The maximum SOA yield for the ozonolysis of  $\beta$ -pinene was calculated. Additionally the partitioning of nopinone, the major product in the  $\beta$ -pinene ozonolysis, was determined.

### 4.6.1 SOA Yield of the $\beta$ -pinene ozonolysis

In the following the amount of SOA formed by the oxidation of  $\beta$ -pinene with ozone is presented. The fractional SOA yield for this experiment was calculated using the  $\beta$ -pinene concentration and the total SOA mass produced in the chamber. The SOA mass was calculated using the total volume distribution (see Figure 4.3(a)):

$$M_{SOA} = V_{SOA} * \rho_{SOA} * 10^{-9} \quad (4.1)$$

$$\begin{aligned} M_{SOA} &= \text{SOA total mass concentration} && \left[ \frac{\mu g}{m^3} \right] \\ V_{SOA} &= \text{SOA total volume concentration} && \left[ \frac{nm^3}{cm^3} \right] \\ \rho_{SOA} &= \text{SOA density} && \left[ \frac{g}{cm^3} \right] \end{aligned}$$

The average SOA density of 1.2 g/cm<sup>3</sup> was used for this conversion (chapter 2.8). The fractional SOA yield is defined as the mass of aerosol formed per mass of hydrocarbon reacted (Odum et al., 1996; Kroll and Seinfeld, 2008) and expressed as follows:

$$Y = \frac{\Delta M}{\Delta HC} \quad (4.2)$$

Table 4.4: *Initial conditions of  $\beta$ -pinene ozonolysis experiment and results of the measured aerosol yield.*

$\beta$ -pinene (ini) [ppb]	O <sub>3</sub> (ini) [ppb]	T [°C]	Y [%]	References
600	872	20.5-22	31	this work
85.4	271	19.4	32.1	Hoffmann et al. (1997)
1000	1000	12-17	26.2	Jaoui and Kamens (2003a)
2000	1000	20-22	26.4	Jaoui and Kamens (2003a)
600	500	25	28	Fisseha et al. (2009)

$Y$	= fractional SOA yield	[1]
$\Delta M$	= aerosol mass formed	$[\frac{\mu g}{m^3}]$
$\Delta HC$	= SOA density	$[\frac{\mu g}{m^3}]$

The maximum SOA yield for this experiment was calculated to be  $31 \pm 7.5$  %. The calculated SOA yield is compared to literature values (Table 4.4). Note that in this comparison only studies which does not use OH scavengers are listed. Several studies have to some extent examined the effect of OH scavenger on the aerosol formation from the ozonolysis of terpenes (Keywood et al., 2004; Iinuma et al., 2005). When not using an OH scavenger more organic material is converted due to the additional OH reaction with the organic precursor and its products. Additionally the products formed in an ozonolysis without using an OH scavenger can consist of additional polar groups and are less volatile (Jonsson et al., 2007) which can contribute to an increase in the SOA yield. The maximum SOA yield determined in this work is in good agreement with those reported in the literature for studies with similar experimental condition (see Table 4.4). The reason that the aerosol yield in this work is in the upper range compared to literature values is due to the derived density of  $1.2 \text{ g/cm}^3$  for the SOA used for this calculation instead of  $1 \text{ g/cm}^3$  which is often assumed in other studies.

#### 4.6.2 Nopinone partitioning

The simultaneous measurement of nopinone in the gas phase by the PTR-ToF-MS and particle phase by the ACM-GC-MS system can be used to determining the equilibrium partitioning coefficient of nopinone and comparing the result with calculations done in other studies with the gas-particle partitioning theory based on the Pankow absorption model (Pankow, 1994b). According to the theory the

partitioning of semi-volatile species between the gas phase and the particulate phase can be described by an equilibrium partitioning coefficient (Odum et al., 1996; Donahue et al., 2006; Hallquist et al., 2009):

$$\frac{C_i^p}{C_i^g} = K_{p,i} C_{OA} = \frac{C_{OA}}{C_i^*} \quad (4.3)$$

$K_{p,i}$	= equilibrium partitioning coefficient	$[\frac{m^3}{\mu g}]$
$C_i^p$	= mass concentration of species i per unit volume air in the particulate phase	$[\frac{\mu g}{m^3}]$
$C_i^g$	= mass concentration of species i per unit volume air in the gaseous phase	$[\frac{\mu g}{m^3}]$
$C_{OA}$	= mass concentration of species i per unit volume air of the total absorbing particle phase	$[\frac{\mu g}{m^3}]$
$C_i^*$	= saturation vapor concentration	$[\frac{\mu g}{m^3}]$

$K_p$  can also be derived from theory and is defined as follows (Pankow, 1994b; Kamens et al., 1999; Jenkin, 2004):

$$K_p = \frac{7.501 \cdot 10^{-9} RT}{MW_{om} \zeta p_L^\circ} \quad (4.4)$$

$K_p$	= equilibrium partitioning coefficient	$[\frac{m^3}{\mu g}]$
$R$	= ideal gas constant	$[\frac{J}{K mol}]$
$T$	= temperature	$[K]$
$MW_{om}$	= mean molecular weight of the condensed organic phase	$[\frac{g}{mol}]$
$\zeta$	= activity coefficient for the given species in the condensed organic phase	$[1]$
$p_L^\circ$	= sub-cooled liquid vapor pressure	$[Torr]$

The activity coefficient thermodynamically represents the non ideality of the semi-volatile organic compound which is solved in the layer of the particle. The activity coefficient changes with the composition of the organic layer of the particles. In most studies and models it is assumed that the activity coefficient  $\zeta$  is unity for an oxidized product which partitions into an aerosol which is composed of a mixture of similar compounds (Pankow, 1994b; Kamens et al., 1999). To estimate  $K_p$  also knowledge of the values of  $p_L^\circ$  is necessary. Since information of the vapor pressures are scarce  $p_L^\circ$  is often estimated from boiling point and entropy of

vaporization information using a semi-empirical form of the Clausius-Clapeyron equation (Kamens et al., 1999; Jenkin, 2004):

$$\ln \frac{p_L^\circ}{760} = \frac{-\Delta S_{vap}(T_b)}{R} \left[ 1.8 \left( \frac{T_b}{T} - 1 \right) - 0.8 \left( \ln \frac{T_b}{T} \right) \right] \quad (4.5)$$

$p_L^\circ$	= sub-cooled liquid vapor pressure	[Torr]
$\Delta S_{vap}(T_b)$	= vaporization entropy change at $T_b$	$[\frac{J}{molK}]$
$T_b$	= boiling point	[K]
$T$	= temperature	[K]
$R$	= ideal gas constant	$[\frac{J}{molK}]$

The sub-cooled liquid vapor pressures are also often estimated using group contribution methods (Cordes and Rarey, 2002; Pankow and Asher, 2008). In the group contribution approach the prediction of molecular properties are based on the hypothesis that the value of a property of interest for a specific compound can be estimated from the contribution of structural fragments that comprise this compound.

For the  $\beta$ -pinene ozonolysis experiment the partitioning coefficient for nopinone was determined from the measured values. Values for  $C_i^g$ ,  $C_{OA}$ , and  $C_i^p$  were determined from the measurements with the PTR-ToF-MS, SMPS, and ACM-GC-MS respectively. The gas phase nopinone concentration shown in Figure 4.2 was averaged over each ACM-GC-MS sampling period of 60 minutes. The total SOA mass, that is the total absorbing particle phase, in the chamber was calculated using equation 4.2 and also average over the same time period. The ACM-GC-MS measurement of the total nopinone mass for each sample was converted to concentration values using the following equation:

$$C_n = \frac{M_n \cdot 10^{-6}}{f_{ACM} t_s} \quad (4.6)$$

$C_n$	= nopinone concentration	$[\frac{\mu g}{m^3}]$
$M_n$	= total nopinone mass in the SOA	$[\mu g]$
$f_{ACM}$	= sampling flow of the ACM	$[\frac{cm^3}{s}]$
$t_s$	= sampling time	[s]

#### 4.6. SOA YIELD AND NOPINONE PARTITIONING

Table 4.5: *Upper part: Partitioning coefficients and vapor pressures of nopinone at different time periods in the  $\beta$ -pinene ozonolysis experiment determined from the gas phase and particle phase measurements. Lower part: Partition coefficients and vapor pressures of nopinone determined with two model studies.*

Time after ozone injection [h]	$K_p$ nopinone [ $\frac{m^3}{\mu g}$ ]	$p_L^\circ$ nopinone [Torr]
1.3	$26.8 \cdot 10^{-5} \pm 6.73 \cdot 10^{-5}$	$38.4 \cdot 10^{-3} \pm 0.96 \cdot 10^{-4}$
4.77	$8.65 \cdot 10^{-5} \pm 2.17 \cdot 10^{-5}$	$1.19 \cdot 10^{-3} \pm 2.99 \cdot 10^{-4}$
8.05	$6.79 \cdot 10^{-5} \pm 1.70 \cdot 10^{-5}$	$1.52 \cdot 10^{-3} \pm 3.81 \cdot 10^{-4}$
21.97	$5.72 \cdot 10^{-5} \pm 1.43 \cdot 10^{-5}$	$1.80 \cdot 10^{-3} \pm 4.52 \cdot 10^{-4}$
25.03	$7.04 \cdot 10^{-5} \pm 1.76 \cdot 10^{-5}$	$1.47 \cdot 10^{-3} \pm 3.68 \cdot 10^{-4}$
26.55	$6.39 \cdot 10^{-5} \pm 1.60 \cdot 10^{-5}$	$1.62 \cdot 10^{-3} \pm 4.05 \cdot 10^{-4}$
28.12	$7.16 \cdot 10^{-5} \pm 1.79 \cdot 10^{-5}$	$1.44 \cdot 10^{-3} \pm 3.61 \cdot 10^{-4}$
29.72	$6.66 \cdot 10^{-5} \pm 1.65 \cdot 10^{-5}$	$1.55 \cdot 10^{-3} \pm 3.88 \cdot 10^{-4}$
31.32	$6.58 \cdot 10^{-5} \pm 1.65 \cdot 10^{-5}$	$1.57 \cdot 10^{-3} \pm 3.93 \cdot 10^{-4}$
46.03	$5.68 \cdot 10^{-5} \pm 1.42 \cdot 10^{-5}$	$1.82 \cdot 10^{-3} \pm 4.56 \cdot 10^{-4}$
49.05	$5.93 \cdot 10^{-5} \pm 1.47 \cdot 10^{-5}$	$1.74 \cdot 10^{-3} \pm 4.36 \cdot 10^{-4}$
50.60	$5.89 \cdot 10^{-5} \pm 1.48 \cdot 10^{-5}$	$1.75 \cdot 10^{-3} \pm 4.39 \cdot 10^{-4}$
52.12	$6.02 \cdot 10^{-5} \pm 1.51 \cdot 10^{-5}$	$1.71 \cdot 10^{-3} \pm 4.29 \cdot 10^{-4}$
53.63	$5.50 \cdot 10^{-5} \pm 1.38 \cdot 10^{-5}$	$1.88 \cdot 10^{-3} \pm 4.70 \cdot 10^{-4}$
55.12	$5.45 \cdot 10^{-5} \pm 1.37 \cdot 10^{-5}$	$1.89 \cdot 10^{-3} \pm 4.74 \cdot 10^{-4}$
Reference	$K_p$ nopinone [ $\frac{m^3}{\mu g}$ ]	$p_L^\circ$ nopinone [Torr]
Jenkin (2004)	$2.4 \cdot 10^{-7}$	$6.0 \cdot 10^{-1}$
Chen (2005)	$7.6 \cdot 10^{-4}$	-

The partition coefficient  $K_p$  for nopinone was calculated using equation 4.3. The error for the partitioning coefficient was calculated as follows:

$$\sigma_{K_{p,i}} = \sqrt{\left(\frac{1}{C_{OA}C_i^g}\right)^2 (\sigma_{C_i^p})^2 + \left(-\frac{C_i^p}{C_{OA}^2 C_i^g}\right)^2 (\sigma_{C_{OA}})^2 + \left(-\frac{C_i^p}{C_{OA}(C_i^g)^2}\right)^2 (\sigma_{C_i^g})^2} \quad (4.7)$$

The results for  $K_p$  for each sample are presented in Table 4.5. The calculated partitioning coefficients varied between  $26.8 \cdot 10^{-5} \mu g/m^3$  and  $5.45 \cdot 10^{-5} \mu g/m^3$  during the experiment. It had its maximum at the beginning of the experiment in the first measurement 1.3 hours after the ozone was injected and was considerably lower for the second sample measured 4.7 hours after the reaction was started. Afterwards the partitioning coefficient for nopinone stayed nearly constant between  $7 \cdot 10^{-5} \mu g/m^3$  and  $5 \cdot 10^{-5} \mu g/m^3$ . That the partitioning coefficient measured for the first sample was significantly different from the coefficients measured later in the experiment can be explained due to the changes in the composition in the SOA and the ongoing reaction in the chamber. During the first 5 hours most of

the ozone reacted with the compounds in the chamber so that the composition of the SOA continuously changed during this time period due to the increase of other low- and semi-volatile oxygenated products from the  $\beta$ -pinene ozonolysis. Therefore the conditions for the nopinone to partition into the SOA could have changed which would be reflected by this decrease in the partitioning coefficient. However the time resolution with which  $K_p$  was measured especially at the beginning of the experiment was too low to give any further insight into the time evolution of the partitioning coefficient during the time period of the highest ozone consumption in the chamber.

The values for  $K_p$  were compared to literature values. However the information of the partitioning coefficient of nopinone from direct measurements as conducted in this work are scarce. Therefore the determined values are compared to the results from two model studies (Jenkin, 2004; Chen and Griffin, 2005) presented in the lower part of Table 4.5. Jenkin (2004) used the Master Chemical Mechanism version 3 (MCM v3) to simulate the formation and detailed composition of SOA from the gas phase ozonolysis of  $\alpha$ - and  $\beta$ -pinene. The optimization of the model was done using  $\alpha$ -pinene data sets.  $\beta$ -pinene data sets were used to examine the performance of the mechanism for a wider range of reagent concentrations and experimental conditions. In the calculations for the partitioning coefficient of nopinone Jenkin (2004) used a mean molecular weight of 130 g/mol, an activity coefficient of one, and a temperature of 298 K. The derived  $K_p$  was  $2.4 \cdot 10^{-7} \text{ m}^3/\mu\text{g}$  which is about two orders of magnitudes smaller than the partition coefficient measured in this work.

A possible explanation for the difference might be that the measurements of the nopinone with ACM-GC-MS are too high due to insufficient removal of the gas phase in the vacuum chamber of the ACM and therefore adsorption of nopinone from the gas phase onto the collector during the sampling. However such an artefact can be excluded by the ACM-GC-MS blank measurements performed during the experiment. Since the ACM-GC-MS blank measurements were conducted with a particle filter between the chamber and the ACM inlet the gas phase nevertheless was drawn into the ACM system during the sampling for the blank measurement. The blank measurements were conducted with the same measurement cycle as the sampling of the SOA. If there had been any significant adsorption of nopinone from the gas phase onto the collector during the sampling it would have been seen in the chromatograms of the blank measurement. The chromatograms of the blank measurements are presented in appendix B which show no significant contamination or artefacts.

Chen and Griffin (2005) used the Caltech Atmospheric Chemistry Mechanism (CACM) coupled to an aerosol module (Model to Predict Multi-phase Partition-

ing of Organics (MPMPO)) to simulate the gas-particle partitioning of semi-volatile organic compounds and optimized and tested the model with 15 data sets of photooxidation, ozonolysis, and NO<sub>3</sub>  $\beta$ -pinene experiments. For their calculations of the nopinone partitioning coefficient a mean molecular weight of 180 g/mol, an activity coefficient of one, and a temperature of 308 K were used. The comparison of the determined nopinone partitioning coefficient with values calculated by Chen and Griffin (2005) showed better agreement (see Table 4.5). However the calculated  $K_p$  of Chen and Griffin (2005) is still one order of magnitude higher than the  $K_p$  measured in the experiment in this work. Note that the calculations by Chen and Griffin (2005) were done for a higher temperature compared to the conditions in the aerosol chamber. Therefore the comparison of the partitioning coefficient in this work with the calculated coefficient by Chen and Griffin (2005) has to be regarded with a higher uncertainty. However note that the difference between the two model results regarding the partitioning coefficient of nopinone could not only be explained by the difference in the temperatures and the mean molecular weight chosen for the two simulation.

Also it is important to note that in both model studies it is stated that the partitioning coefficients and/or vapor pressures were adjusted such that the results of the calculations better matched vapor pressure or partitioning coefficient literature values, if such values were available. Also the adjustment was applied to better match the experimental determined values of the studies used for testing the models. Chen and Griffin (2005) adjusted their determined values typically by a factor of 0.001, while the temperature dependence of the vapor pressure was retained. Jenkin (2004) also applied a compound-independent scaling factor to  $K_p$  for all partitioning compounds of approximately 120 in the simulation of the SOA formation.

The partitioning coefficient measured in the aerosol chamber experiment is in between the calculated values of the two model studies which indicates that the result obtained for  $K_p$  is reasonable regarding the still large uncertainties in the prediction of the SOA partitioning.

Additionally the vapor pressure of nopinone was calculated using equation 4.4. For the calculation the previously derived partitioning coefficient  $K_p$  was used. For the mean molecular weight of the condensed organic phase a value of 180 g/mol was adopted from Chen and Griffin (2005) since this model studies reflect the results of this work better. The nopinone partitioned into an aerosol which is composed of products of  $\beta$ -pinene oxidation. Therefore the activity coefficient  $\zeta$  can be assumed to be nearly ideal and is assumed to be unity (Pankow, 1994b; Kamens et al., 1999). The results for the calculated nopinone vapor pressure are presented in Table 4.5. The vapor pressure derived from nopinone were com-



pared to the vapor pressure estimated by Jenkin (2004). The vapor pressure for nopinone determined by Jenkin (2004) differs from the experimentally determined vapor pressure in this work significantly by two orders of magnitude. Unfortunately Chen and Griffin (2005) did not provide any results for the nopinone vapor pressure.

The discrepancies between the model results show that experiments in determining partitioning coefficients such as presented in this work are needed to gain further insight into the particle-gasphase reactions and to provide a wider data base for model studies to rely on. In particular the coupling of the ACM to a PTR-MS would be suitable for these kind of measurements because the particle phase and the gas phase could be measured with the same detector during the experiment. While the ACM is sampling the particle phase the PTR-MS would measure the gas phase simultaneously. Afterwards the PTR-MS would be coupled (see chapter 2.2.2) again with the ACM to measure the content of the evaporated aerosols. This approach would reduce uncertainties in the comparison of the measurements for the gas and particle phase since the measurements would be obtained with the same method. Also possible artifacts from offline measurements of SOA such as gas phase adsorption onto filters could be avoided.

## 4.7 Time evolution of the SOA composition and corresponding ACM marker compounds

In this chapter the AMS data were analyzed to extract factors dominating the time evolution of the organic composition using the so called Positive Matrix Factorization (PMF) analysis. The findings of the PMF analysis were compared to the time series of the fractional abundances of compounds determined by the ACM-GC-MS measurements in chapter 4.4. Also oxygen to carbon ratio (O/C) ratios were determined and compared with the PMF factors and the identified compounds measured with the ACM-GC-MS.

### 4.7.1 Time evolution of PMF factors and O/C ratios

To extract factors dominating the time evolution of the organic composition the Positive Matrix Factorization (PMF) analysis (Paatero and Tapper, 1994; Paatero, 1997) as implemented by Ulbrich et al. (2008) was applied to the AMS data. Details of the PMF analysis are presented in appendix F. In the PMF analysis the number of factors,  $p$ , in the real data set is generally unknown and has

#### 4.7. TIME EVOLUTION OF THE SOA COMPOSITION AND CORRESPONDING ACM MARKER COMPOUNDS

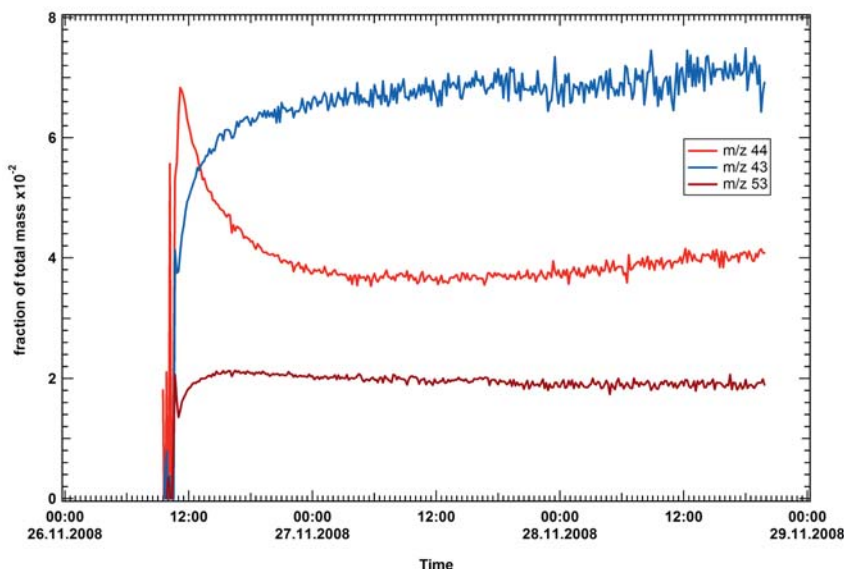


Figure 4.16: *Examples for different AMS  $m/z$  temporal evolution.*

to be estimated. For the estimation of the number of factors for the AMS measurements of the  $\beta$ -pinene experiment trends in different  $m/z$  traces are used. In Figure 4.16 examples for the time evolution of  $m/z$  traces are shown. The time trends of the  $m/z$  traces support the assumption that three factors can be assumed for the PMF analysis. Furthermore the number of factors needed to describe the data set is determined by the requirement of minimal residuals and low correlation in the mass spectral and time dependent behavior of the factors. For example if the number of factors is chosen to large two or more factors might have similar or equal temporal evolutions or the mass spectral profiles are very similar and highly correlated. Therefore several PMF analysis of the AMS data set for the  $\beta$ -pinene ozonolysis experiment were conducted with different values for the number of factors. These analysis were compared regarding correlations between the factors and the minima of the residuals. As indicated with the time evolution of the  $m/z$  traces shown in Figure 4.16 three factors were identified with the PMF analysis. In Figure 4.17 the time series of the three factors derived from the PMF analysis are shown. The factors are normalized to the total organic mass measured with the AMS. As can be seen the three time series of the factors are distinctly different in their temporal behavior. While factor 1 rises steeply in the initial phase of the experiment it reaches its maximum approximately after 1.5 hours after the SOA formation started. Thereafter it decreased steadily. Factor 2 rises not as steep as factor 1 and reaches its maximum after 10.5 hours.

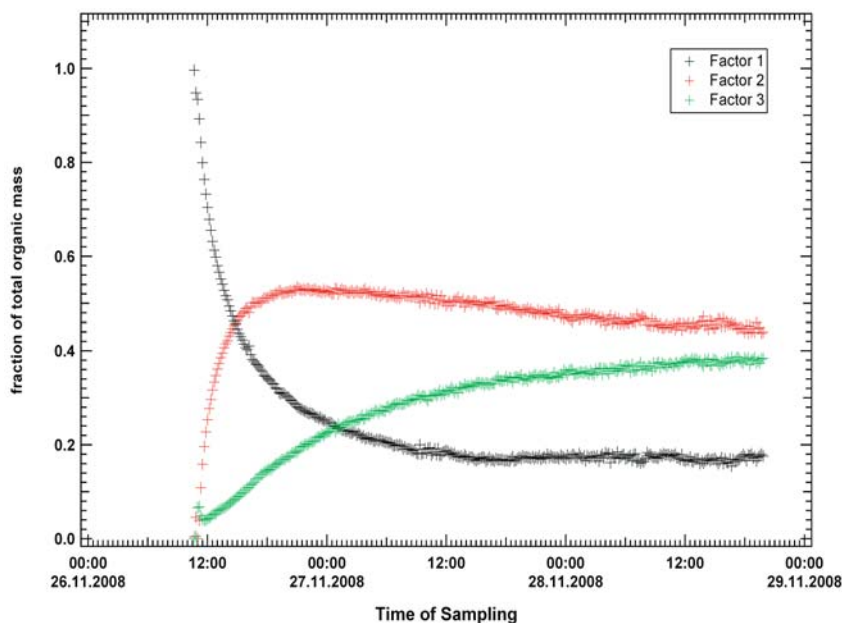


Figure 4.17: *Time dependance of the factors derived from the PMF analysis which dominate the time evolution of the organic composition of the SOA.*

Again factor 2 decreases afterwards steadily. Factor 3 increased even slower and drops only after more than 24 hours. Compared to the two other factors its decrease is significantly lower.

In Figure 4.18 the mass spectra of the individual factors derived for the  $\beta$ -pinene SOA are shown. The main differences in the mass spectra can be seen in the relative contributions of ions at  $m/z$  27 to 29, 41 to 44, and 55. The relative oxygen content in organic aerosol can be estimated using the fraction of the organic signal at  $m/z$  44. The assumption is that the signal of  $m/z$  44 is dominated by  $\text{CO}_2^+$ . Aiken et al. (2008) showed using a high resolution time of flight AMS (HR-ToF-AMS) that 88% of  $m/z$  44 signal is due to  $\text{CO}_2$  in ambient aerosol. Thus it can be considered as a marker for the oxygen to carbon ratio (O/C). For unit mass resolution data such as available from the AMS used in this experiment, the following relation was derived:

$$\text{O/C} = 0.0382 \cdot m/z44 + 0.0794 \quad (4.8)$$

$m/z44$  = contribution of the organic signal at  $m/z$  44 to  
the total organic signal in %

#### 4.7. TIME EVOLUTION OF THE SOA COMPOSITION AND CORRESPONDING ACM MARKER COMPOUNDS

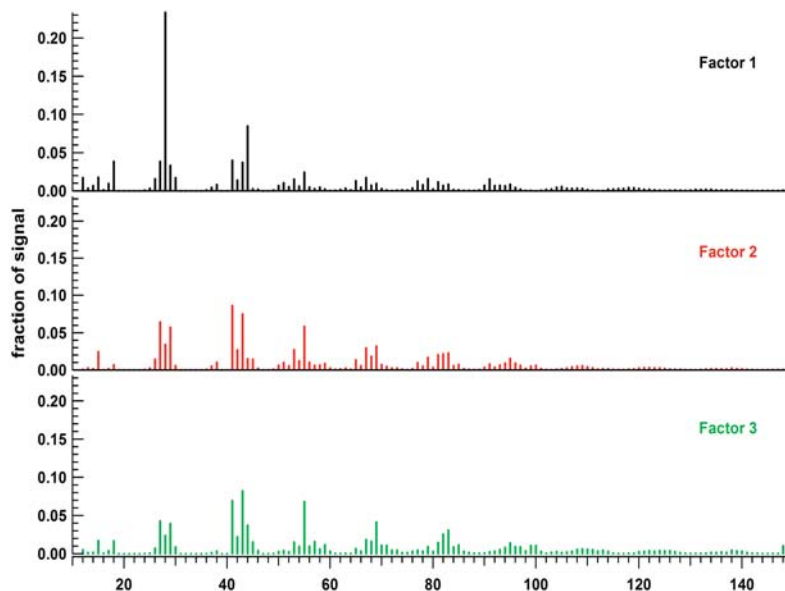


Figure 4.18: Profiles of the factors derived from the PMF analysis.

The O/C ratio of the factors identified in the PMF analysis were determined using equation 4.8 and are presented in the upper part of Table 4.6. The overall O/C ratio can be determined from the weighted contributions of the three factors at each time. Figure 4.19 depicts the PMF factors normalized to the total organic mass (crosses) and the time evolution of the O/C ratio (dark blue line). Because the time evolution of the determined factors are different the O/C ratio also varies

Table 4.6: Upper part: O/C ratios of the PMF factors. Lower part: O/C ratios of the identified components of the ACM-GC-MS measurements.

Factors / Compound Name	Chemical Formula	OC
PMF factor 1	-	0.403
PMF factor 2	-	0.121
PMF factor 3	-	0.286
bicyclo[3,1,1]hept-3-ene-2-one	$C_9H_{12}O$	0.11
nopinone	$C_9H_{14}O$	0.11
myrtanal	$C_{10}H_{16}O$	0.1
myrtenol	$C_{10}H_{16}O$	0.1
1-hydroxynopinone	$C_9H_{14}O_2$	0.22
3-oxonopinone	$C_9H_{12}O_2$	0.22
3,7-dihydroxynopinone	$C_9H_{14}O_3$	0.33

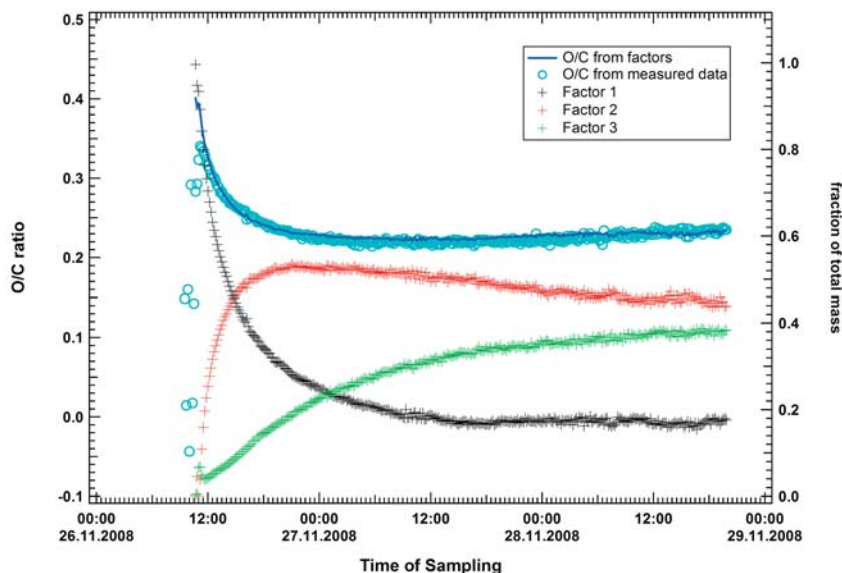


Figure 4.19: *Fraction of total mass and oxygen to carbon ratio of the PMF factors.*

during the experiment. For comparison the O/C ratio was also calculated from the measured AMS data (light blue circles) using equation 4.8. As can be seen both approaches agree very well conveying that the time evolution of  $m/z$  44 is well represented by the sum of the three factors. The O/C ratios determined for the PMF factors will be analyzed in comparison to the O/C ratios of the identified compounds measured by the ACM-GC-MS in the following chapter 4.7.2.

#### 4.7.2 AMS PMF factors and ACM Marker Compounds

The organic components measured and identified with the ACM-GC-MS (chapter 4.3.1) can be correlated with the factors derived from the PMF analysis of the AMS data. In Figures 4.13 and 4.14 it was shown that also for the ACM-GC-MS results the majority of the peaks could be associated with three distinct types of temporal behavior. In Figure 4.20 the time evolution of the derived PMF factors together with the compounds measured with the ACM-GC-MS which were found to best reproduce similar temporal behavior are shown. Note that from here on the ACM-GC-MS groups 1 to 3 will be called ACM factors 1 to 3, respectively, following the notation of the PMF factors. The time series of nopinone, bicyclo[3,1,1]hept-3-ene-2-one and 3,7-dihydroxynopinone match the evolution of PMF factor 1 (Figure 4.20(a)) while the time series of 1-hydroxynopinone corresponds well with factor 3. For the PMF factor 2 only non identified com-

#### 4.7. TIME EVOLUTION OF THE SOA COMPOSITION AND CORRESPONDING ACM MARKER COMPOUNDS

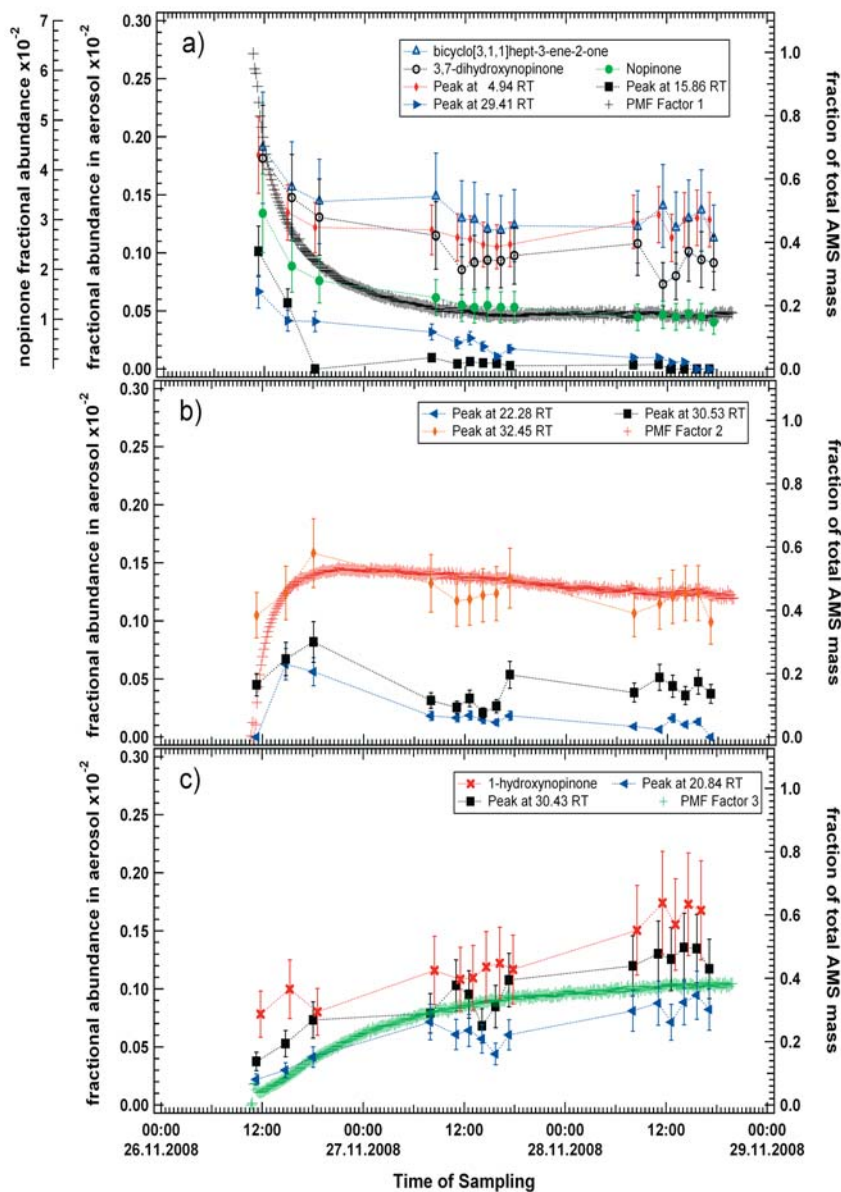


Figure 4.20: Comparison of the temporal evolutions of the PMF factors from AMS data analysis with the temporal evolution of the fractional abundances of the ACM-GC-MS components. Note that following the PMF analysis notation the ACM-GC-MS time series of the fractional abundances will be called ACM factors 1 to 3, respectively. Figure a) shows the comparison of PMF factor 1 to ACM factor 1. Figure b) shows the comparison of PMF factor 2 to ACM factor 2. Figure c) shows the comparison of PMF factor 3 to ACM factor 3.

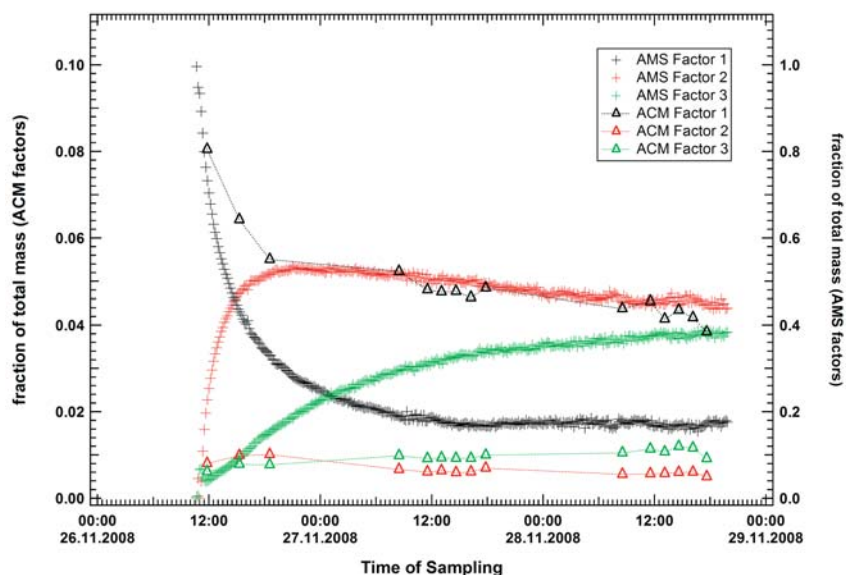


Figure 4.21: Comparison of the PMF factors with the total fractional abundances of the ACM factors.

pounds were found to represent this temporal behavior. In Table 4.6 the O/C ratios of the identified compounds are presented. The ACM-GC-MS compounds have an O/C ratio of 0.11 (nopinone and bicyclo[3,1,1]hept-3-ene-2-one) and 0.33 (3,7-dihydroxynopinone) compared to 0.403 of the PMF factor 1 and 0.22 (1-hydroxynopinone) compared to 0.286 of PMF factor 2. The result of this comparison is ambiguous. While the O/C ratio of 1-hydroxynopinone is within the scope of the O/C ratio of factor 2 the comparison for factor 1 is inconclusive. Thus for the results obtained in this  $\beta$ -pinene ozonolysis experiment no unambiguous marker compounds which can be correlated with the O/C ratios of the different time series of the PMF factors could be identified. However some of the unidentified compounds also correspond well with the time series of the PMF factors. Further improvements of the ACM-GC-MS detection capability and the identification especially of polar compounds would supposedly give more insight if O/C markers can be identified with the ACM-GC-MS. Also this comparison shows that the speciation data further the high time resolution AMS data analysis which would provide further insight into the composition of the SOA.

A comparison of PMF factors and ACM factors are shown in Figure 4.21. For the calculation of the ACM factors all peaks which could be assigned to a specific time evolutions similar to the PMF factors were used. The ACM factors 1, 2, and 3 were determined by adding up the contributions of all identified and unidenti-



fied peaks presented in Figures E.1, E.2, and E.3 in appendix E respectively. The comparison shows that for both, the PMF factors and the ACM factors, factor 1 is the dominant factor. However the drop of the PMF factor 1 is more pronounced than the ACM factor 1. A significant difference can be seen in the contribution of the ACM factor 2 and 3 compared to the corresponding PMF factors. While for example PMF factor 2 contributes up to 50% during the experiment to the mass the ACM factor 2 only contributes 10%. Moreover 12 hours after the reaction was started the contribution of the ACM factor 3 is higher than the contribution of the ACM factor 2 in contrast to the evolution of the corresponding PMF factors. These differences indicate that, although the ACM and AMS sampled the same SOA, the detection capability for different compounds or compound classes is different. As previously discussed for the compound identification and the mass fractional abundances of the identified compounds measured with the ACM-GC-MS (see chapter 4.3.1 and 4.4) this might be due to the specific set up of the GC-MS. Compounds which contributed to increase of the PMF factors 2 and 3 measured by the AMS were not detectable or not significantly good detectable with the ACM-GC-MS. However according to the results of the PMF analysis the O/C ratio decreased during the experiment. Therefore it can not be assumed that it is only due to an increase in the oxidation of the products which are not detectable with the GC-MS. However it might be possible that the higher molecular weight compounds contributed to the PMF factors 2 and 3 which would not be measured by the ACM-GC-MS.

Due to the similar temporal evolution of the ACM factors and the PMF factors it is reasonable to assume that the combination of all compounds representing ACM factor 1 would results in a similar mass spectrum of the PMF factor 1. This assumption should also be true for the ACM factor 2 and 3. However, due to the different measuring technique of the ACM-GC-MS and the AMS the profiles obtained for the ACM factors would not be comparable to the PMF profiles. In the AMS the organic compounds are previously flash evaporated at 600 °C before subjected to 70 eV EI. Therefore the mass spectra measured with the AMS (especially for more complex molecules) can show discrepancies from the mass spectra of molecules which were only ionized with a 70 eV EI ionization source (Allan et al., 2004). Also since the ACM-GC-MS did not measure all compounds or compound classes as discussed previously the mass spectra which would be obtained for the three ACM factors would not include the contribution of these compounds. However, further studies using a HR-TOF-AMS and the ACM equipped with a different column or coupled to different detector such as a PTR-MS would provide further inside into the temporal behavior and contributions to the PMF factors compared to the ACM factors.



## 4.8 Scientific findings of the $\beta$ -pinene ozonolysis experiment

An indoor aerosol chamber experiment was performed investigating the formation of aerosol during the oxidation of  $\beta$ -pinene with elevated ozone concentration. Using a novel aerosol collection technique with subsequent GC-MS analysis several products of the  $\beta$ -pinene ozonolysis could be identified in the aerosol phase. These compounds are listed in the following:

Identified product	Molecular Weight (g mol <sup>-1</sup> )
bicyclo[3,1,1]hept-3-ene-2-one	136
nopinone	138
myrtanal	152
myrtenol	152
1-hydroxynopinone	154
3-oxonopinone	152
3,7-dihydroxynopinone	170

The presence of myrtenol was in previous studies only detected in the gas phase but not in the aerosol phase.

Additionally the temporal evolution of the aerosol composition was analyzed. The relative change in the abundances of all detected compounds in the aerosol could be attributed to three distinct temporal evolutions for the majority of all compounds, the so called ACM factors. These temporal evolution of the organic composition of the aerosols was also found in the analysis of the total organic mass measured with the AMS. With the Positive Matrix Factorization (PMF) analysis the temporal evolution of the total organic mass could also be explained by three distinct, independent PMF mass spectra profiles, the so called PMF factors. The three PMF factors showed similar temporal behaviors as the three ACM factors. This analysis showed for the first time that several marker compounds could be identified and attributed to the statistically derived PMF factors.

The maximum SOA yield of the  $\beta$ -pinene ozonolysis was calculated to  $31 \pm 7.5$  % which is in good agreement with reported elsewhere from experiments under similar conditions.

For nopinone, one of the major oxidation products, the partitioning coefficient was determined. The partitioning coefficient was calculated during the whole  $\beta$ -pinene ozonolysis experiment showing its temporal variability. The nopinone partitioning coefficient ranged from a maximum of  $26.8 \times 10^{-5}$  m<sup>3</sup>μg<sup>-1</sup> to  $5.45 \times 10^{-5}$  m<sup>3</sup>μg<sup>-1</sup> and was on average  $7.75 \times 10^{-5} \pm 1.9 \times 10^{-5}$  m<sup>3</sup>μg<sup>-1</sup>. The mea-

#### 4.8. SCIENTIFIC FINDINGS OF THE $\beta$ -PINENE OZONOLYSIS EXPERIMENT

---

sured partitioning coefficient was found to be between model estimates of  $2.4 \times 10^{-7} \text{ m}^3\mu\text{g}^{-1}$  and  $7.6 \times 10^{-4} \text{ m}^3\mu\text{g}^{-1}$ . The results obtained for the nopinone partitioning coefficient can be used in future modeling efforts to better constrain the contribution of biogenic compounds to SOA production.



## 5. Summary & Outlook

### Summary

Organic matter is a major constituent of atmospheric aerosols, comprising 18-70% of the submicron particle mass. Its chemical composition is complex, and largely not understood. Quantitative knowledge of the composition of organic aerosols is a key to understand its formation and transformation processes.

In the present work a new technique for online compound specific measurements of organic aerosol with a high time resolution was developed. The Aerosol Collection Module (ACM) is a new scientific instrument which samples, collects and transfer atmospheric aerosols to a gas phase detector. Aerosols are efficiently sampled in the 70-500 nm size range by focusing the aerosols in a particle beam which passes a vacuum chamber and impacts onto a cooled collection surface. The organic compounds are then efficiently transferred via thermal desorption into a coupled gas phase detector.

The coupling of the ACM to two types of detectors (GC-MS and PTR-MS) was developed and presented. The ACM coupled to a GC-MS (ACM-GC-MS) was used to determine important instrumental characteristics of the ACM. In a first stage the gas phase transfer efficiency of the ACM valve array and transfer line were determined using a build in diffusion source with octadecane as test compound. Comparison of the ACM diffusion source measurements with the GC-MS calibration measurements showed that no significant losses occur in the ACM valve array and transfer line. The ACM system efficiently transferred the gas phase octadecane with a recovery rate of 100%.

In the second stage of the ACM characterization the particle collection, desorption and transfer efficiency of laboratory generated octadecane test aerosols was determined. The total octadecane mass provided for sampling with the ACM-GC-MS was simultaneously also determined with a Scanning Mobility Particle Sizer (SMPS) which was measuring in parallel to the ACM-GC-MS the same octadecane aerosol flow. The octadecane aerosol was collected, desorbed and

transferred with an efficiency of 100%. The recovery rate of 100% was confirmed for an interval of desorption and valve array temperatures ranging from 150 °C to 270 °C. For both characterization experiments the ACM-GC-MS was linear in response to the measured octadecane mass.

The new sampling and characterization technique of the ACM-GC-MS was also used in its first application in the study of the formation of secondary organic aerosol (SOA) from the ozone oxidation of  $\beta$ -pinene in the Jülich aerosol chamber. During the  $\beta$ -pinene ozonolysis experiment 16 SOA samples over the duration of 58 h were successfully taken and measured with the ACM-GC-MS. Between the collection of the SOA samples blank measurements were taken regularly. The blank measurements were conducted by installing a filter between the ACM-GC-MS and the chamber sampling line. The blanks showed no residuals of the previously collected SOA and also no artifacts such as adsorption of the gas phase onto the collector.

Using the ACM-GC-MS several products of the  $\beta$ -pinene ozonolysis could be identified in the aerosol phase. These compounds were bicyclo[3,1,1]hept-3-ene-2-one, nopinone, myrtanal, myrtenol, 1-hydroxynopinone, 3-oxonopinone, and 3,7-dihydroxynopinone. The presence of myrtenol was detected for the first time also in the aerosol phase.

Comparison of the total nopinone mass between filter samples and the ACM-GC-MS showed in average a significantly higher nopinone mass in the filter measurements. Since no obvious reason for a large underestimation of the total amount of nopinone measured with the ACM-GC-MS could be determined the discrepancy was assumed to be due to the known positive artifact of quartz filter sampling for short durations. This result emphasizes the importance for a artifact free, high time resolution aerosol collection technique.

Using ACM-GC-MS and SMPS measurements the temporal evolution of the aerosol composition was analyzed. The relative change in the abundances of the majority of the detected compounds in the SOA could be attributed to three distinct temporal evolutions. The temporal changes in the constituents of the SOA was described by three ACM factors. Comparable factors, the PMF factors, were also found in the analysis of the total organic mass measured independently with the AMS using the Positive Matrix Factorization (PMF) analysis. These factors follow similar temporal behaviors as the ACM factors. This analysis showed for the first time that several marker compounds could be identified and attributed to the statistically derived PMF factors.

The maximum SOA yield of the aerosol chamber experiment was calculated to  $31 \pm 7.5$  %. This is in good agreement with yields reported in the literature under similar conditions.

---

Using the PTR-ToF-MS gas phase measurements of nopinone and the nopinone concentration in the aerosol derived from the ACM-GC-MS measurements the partitioning coefficient for one of the major compounds of the  $\beta$ -pinene ozonolysis was determined. The partitioning coefficient was calculated for all ACM-GC-MS samples taken which showed its temporal variability during the experiment. The nopinone coefficient ranged from a maximum of  $26.8 \times 10^{-5} \text{ m}^3\mu\text{g}^{-1}$  to  $5.45 \times 10^{-5} \text{ m}^3\mu\text{g}^{-1}$  and was on average  $7.75 \times 10^{-5} \pm 1.9 \times 10^{-5} \text{ m}^3\mu\text{g}^{-1}$ . The measured partitioning coefficient was found to be between model estimates of  $2.4 \times 10^{-7} \text{ m}^3\mu\text{g}^{-1}$  and  $7.6 \times 10^{-4} \text{ m}^3\mu\text{g}^{-1}$ . The experimental determination of partitioning coefficients is important for the modeling efforts to better constrain the contribution of biogenic compounds to SOA production, to understand chemical processes and thereby the impact of SOA on the environment.

## Outlook

The Aerosol Collection Module provides a new sampling technique which opens new windows into the study of organic aerosols. Sampling organic aerosols with a high time resolution and free of artifacts, followed by subsequent online analysis with a gas phase detector appropriate for the scientific purpose will give a deeper insight into the chemistry of organic aerosols and their influence on the environment and human health.

The analytical potential of the ACM can be enhanced by improving the small sample flow of 80 ml/min. The possible technical improvement which should be explored are the use of a critical orifice in the lens system with a larger diameter and the use of a virtual impactor in front of the ACM inlet.

One important advantage of the ACM is that it can be coupled to a variety of different gas phase detectors. The potential of the ACM should be further explored by coupling the ACM to different types of detectors such as PTR-MS, GC-IRMS and a two dimensional GC system. As proposed before, the coupling of the ACM to a PTR-MS would allow measurement of gas phase and aerosol phase with a high time resolution and with the same type of detector. This would give the opportunity of measuring important compound specific properties such as the partitioning coefficient with high accuracy. The coupling of the ACM to a GC-IRMS or a two dimensional GC system with deployment in the field would allow specific studies of individual organic marker compounds in ambient atmospheric aerosols to determine aerosol sources and transformations.



## References

- Aiken, A. C., DeCarlo, P. F., Kroll, J. H., Worsnop, D. R., Huffman, J. A., Docherty, K. S., Ulbrich, I. M., Mohr, C., Kimmel, J. R., Sueper, D., Sun, Y., Zhang, Q., Trimborn, A., Northway, M., Ziemann, P. J., Canagaratna, M. R., Onasch, T. B., Alfarra, M. R., Prevot, A. S. H., Dommen, J., Duplissy, J., Metzger, A., Baltensperger, U., Jimenez, J. L., 2008. O/c and om/oc ratios of primary, secondary, and ambient organic aerosols with high-resolution time-of-flight aerosol mass spectrometry. *Environmental Science & Technology* 42 (12), 4478–4485.
- Allan, J. D., Delia, A. E., Coe, H., Bower, K. N., Alfarra, M. R., Jimenez, J. L., Middlebrook, A. M., Drewnick, F., Onasch, T. B., Canagaratna, M. R., Jayne, J. T., Worsnop, D. R., 2004. A generalised method for the extraction of chemically resolved mass spectra from aerodyne aerosol mass spectrometer data. *Journal of Aerosol Science* 35 (7), 909–922.
- Atkinson, R., 1997. Gas-phase tropospheric chemistry of volatile organic compounds: 1. alkanes and alkenes. *Journal of Physical and Chemical Reference Data* 26 (2), 215–290.
- Atkinson, R., Arey, J., 2003. Gas-phase tropospheric chemistry of biogenic volatile organic compounds: a review. *Atmospheric Environment* 37, S197–S219.
- Baltensperger, U., Kalberer, M., Dommen, J., Paulsen, D., Alfarra, M. R., Coe, H., Fisseha, R., Gascho, A., Gysel, M., Nyeki, S., Sax, M., Steinbacher, M., Prevot, A. S. H., Sjogren, S., Weingartner, E., Zenobi, R., 2005. Secondary organic aerosols from anthropogenic and biogenic precursors. *Faraday Discussions* 130, 265–278.
- Calogirou, A., Jensen, N. R., Nielsen, C. J., Kotzias, D., Hjorth, J., 1999. Gas-phase reactions of nopinone, 3-isopropenyl-6-oxo-heptanal, and 5-methyl-5-vinyltetrahydrofuran-2-ol with oh, no<sub>3</sub>, and ozone. *Environmental Science & Technology* 33 (3), 453–460.
- Chen, J., Griffin, R. J., 2005. Modeling secondary organic aerosol formation from oxidation of [alpha]-pinene, [beta]-pinene, and d-limonene. *Atmospheric Environment* 39 (40), 7731–7744.
- Cordes, W., Rarey, J., 2002. A new method for the estimation of the normal boiling point of non-electrolyte organic compounds. *Fluid Phase Equilibria* 201 (2), 409–433.



## REFERENCES

---

- de Gouw, J., Warneke, C., 2007. Measurements of volatile organic compounds in the earth's atmosphere using proton-transfer-reaction mass spectrometry. *Mass Spectrometry Reviews* 26 (2), 223–257.
- DeCarlo, P. F., Slowik, J. G., Worsnop, D. R., Davidovits, P., Jimenez, J. L., 2004. Particle morphology and density characterization by combined mobility and aerodynamic diameter measurements. part 1: Theory. *Aerosol Science & Technology* 38 (12), 1185–1205.
- Docherty, K. S., Ziemann, P. J., 2001. On-line, inlet-based trimethylsilyl derivatization for gas chromatography of mono- and dicarboxylic acids. *Journal of Chromatography A* 921 (2), 265–275, tY - JOUR.
- Donahue, N. M., Robinson, A. L., Stanier, C. O., Pandis, S. N., 2006. Coupled partitioning, dilution, and chemical aging of semivolatile organics. *Environmental Science & Technology* 40 (8), 2635–2643.
- Finlayson-Pitts, B. J., Pitts, J. N., 2000. *Chemistry of the upper and lower atmosphere*. Academic Press.
- Fisseha, R., Spahn, H., Wegener, R., Hohaus, T., Brasse, G., Wissel, H., Tillmann, R., Wahner, A., Koppmann, R., Kiendler-Scharr, A., 2009. Stable carbon isotope composition of secondary organic aerosol from beta-pinene oxidation. *J. Geophys. Res.* 114.
- Forster, P., Ramaswamy, V., Artaxo, P., Berntsen, T., Betts, R., Fahey, D., Haywood, J., Lean, J., Lowe, D., Myhre, G., Nganga, J., Prinn, R., Raga, G., Schulz, M., Van Dorland, R., 2007. Changes in atmospheric constituents and in radiative forcing. in: *Climate change 2007: The physical science basis. contribution of working group i to the fourth assessment report of the inter-governmental panel on climate change*, [Solomon, S., D. Qin, M. Manning, Z. Chen, M. Marquis, K.B. Averyt, M. Tignor and H.L. Miller (eds.)]. Cambridge University Press, Cambridge, United Kingdom and New York, NY, USA.
- Gao, S., Keywood, M., Ng, N. L., Surratt, J., Varutbangkul, V., Bahreini, R., Flagan, R. C., Seinfeld, J. H., 2004. Low-molecular-weight and oligomeric components in secondary organic aerosol from the ozonolysis of cycloalkenes and alpha-pinene. *The Journal of Physical Chemistry A* 108 (46), 10147–10164.
- Goldstein, A. H., Daube, B. C., Munger, J. W., Wofsy, S. C., 1995. Automated in-situ monitoring of atmospheric nonmethane hydrocarbon concentrations and gradients. *Journal of Atmospheric Chemistry* 21 (1), 43–59.
- Goldstein, A. H., Galbally, I. E., 2007. Known and unexplored organic constituents in the earth's atmosphere. *Environmental Science & Technology* 41 (5), 1514–1521.
- Grosjean, D., Williams, E. L., Grosjean, E., Andino, J. M., Seinfeld, J. H., 1993. Atmospheric oxidation of biogenic hydrocarbons - reaction of ozone with beta-pinene, d-limonene and trans-caryophyllene. *Environmental Science & Technology* 27 (13), 2754–2758.

- Guenther, A., Hewitt, C. N., Erickson, D., Fall, R., Geron, C., Graedel, T., Harley, P., Klinger, L., Lerdau, M., McKay, W. A., Pierce, T., Scholes, B., Steinbrecher, R., Tallamraju, R., Taylor, J., Zimmerman, P., 1995. A global model of natural volatile organic compound emissions. *J. Geophys. Res.* 100.
- Hakola, H., Arey, J., Aschmann, S. M., Atkinson, R., 1994. Product formation from the gas-phase reactions of OH radicals and O<sub>3</sub> with a series of monoterpenes. *Journal of Atmospheric Chemistry* 18 (1), 75–102.
- Hallquist, M., Wenger, J. C., Baltensperger, U., Rudich, Y., Simpson, D., Claeys, M., Dommen, J., Donahue, N. M., George, C., Goldstein, A. H., Hamilton, J. F., Herrmann, H., Hoffmann, T., Iinuma, Y., Jang, M., Jenkin, M. E., Jimenez, J. L., Kiendler-Scharr, A., Maenhaut, W., McFiggans, G., Mentel, T. F., Monod, A., Prvt, A. S. H., Seinfeld, J. H., Surratt, J. D., Szmigielski, R., Wildt, J., 2009. The formation, properties and impact of secondary organic aerosol: current and emerging issues. *Atmos. Chem. Phys.* J1 - ACP 9 (14), 5155–5235.
- Hamilton, J. F., Webb, P. J., Lewis, A. C., Hopkins, J. R., Smith, S., Davy, P., 2004. Partially oxidised organic components in urban aerosol using gcxgc-tof/ms. *Atmos. Chem. Phys.* J1 - ACP 4 (5), 1279–1290, tY - JOUR.
- Heald, C. L., Jacob, D. J., Park, R. J., Russell, L. M., Huebert, B. J., Seinfeld, J. H., Liao, H., Weber, R. J., 2005. A large organic aerosol source in the free troposphere missing from current models. *Geophys. Res. Lett.* 32.
- Hoffmann, T., Odum, J. R., Bowman, F., Collins, D., Klockow, D., Flagan, R. C., Seinfeld, J. H., 1997. Formation of organic aerosols from the oxidation of biogenic hydrocarbons. *Journal of Atmospheric Chemistry* 26, 189–222.
- Iannone, R., Koppmann, R., Rudolph, J., 2007. A technique for atmospheric measurements of stable carbon isotope ratios of isoprene, methacrolein, and methyl vinyl ketone. *Journal of Atmospheric Chemistry* 58 (3), 181–202.
- Iinuma, Y., Boge, O., Miao, Y., Sierau, B., Gnauk, T., Herrmann, H., 2005. Laboratory studies on secondary organic aerosol formation from terpenes. *Faraday Discussions* 130, 279–294.
- Jaoui, M., Kamens, R. M., 2003a. Gaseous and particulate oxidation products analysis of a mixture of alpha-pinene plus beta-pinene/o-3/air in the absence of light and alpha-pinene plus beta-pinene/NOx/air in the presence of natural sunlight. *Journal of Atmospheric Chemistry* 44 (3), 259–297.
- Jaoui, M., Kamens, R. M., 2003b. Mass balance of gaseous and particulate products from beta-pinene/o-3/air in the absence of light and beta-pinene/NOx/air in the presence of natural sunlight. *Journal of Atmospheric Chemistry* 45 (2), 101–141.
- Jayne, J. T., Leard, D. C., Zhang, X. F., Davidovits, P., Smith, K. A., Kolb, C. E., Worsnop, D. R., 2000. Development of an aerosol mass spectrometer for size and composition analysis of submicron particles. *Aerosol Science and Technology* 33 (1-2), 49–70.

## REFERENCES

---

- Jenkin, M. E., 2004. Modelling the formation and composition of secondary organic aerosol from alpha- and beta-pinene ozonolysis using mcm v3. *Atmospheric Chemistry and Physics* 4, 1741–1757.
- Jimenez, J. L., Jayne, J. T., Shi, Q., Kolb, C. E., Worsnop, D. R., Yourshaw, I., Seinfeld, J. H., Flagan, R. C., Zhang, X., Smith, K. A., Morris, J. W., Davidovits, P., 2003. Ambient aerosol sampling using the aerodyne aerosol mass spectrometer. *J. Geophys. Res.* 108.
- Jonsson, A. M., Hallquist, M., Saathoff, H., 2007. Volatility of secondary organic aerosols from the ozone initiated oxidation of [alpha]-pinene and limonene. *Journal of Aerosol Science* 38 (8), 843–852.
- Jorgensen, A. D., Picel, K. C., Stamoudis, V. C., 1990. Prediction of gas chromatography flame ionization detector response factors from molecular structures. *Analytical Chemistry* 62 (7), 685.
- Kallio, M., Jussila, M., Rissanen, T., Anttila, P., Hartonen, K., Reissell, A., Vreuls, R., Adahchour, M., Hyotylainen, T., 2006. Comprehensive two-dimensional gas chromatography coupled to time-of-flight mass spectrometry in the identification of organic compounds in atmospheric aerosols from coniferous forest. *Journal of Chromatography A* 1125 (2), 234–243.
- Kamens, R., Jang, M., Chien, C.-J., Leach, K., 1999. Aerosol formation from the reaction of a-pinene and ozone using a gas-phase kinetics-aerosol partitioning model. *Environmental Science & Technology* 33 (9), 1430–1438.
- Kanakidou, M., Seinfeld, J. H., Pandis, S. N., Barnes, I., Dentener, F. J., Facchini, M. C., Dingenen, R. v., Ervens, B., Nenes, A., Nielsen, C. J., Swietlicki, E., Putaud, J. P., Balkanski, Y., Fuzzi, S., Horth, J., Moortgat, G. K., Winterhalter, R., Myhre, C. E. L., Tsigaridis, K., Vignati, E., Stephanou, E. G., Wilson, J., 2005. Organic aerosol and global climate modelling: a review. *Atmospheric Chemistry and Physics* 5, 1053–1123.
- Kesselmeier, J., Staudt, M., 1999. Biogenic volatile organic compounds (voc): An overview on emission, physiology and ecology. *Journal of Atmospheric Chemistry* 33, 23–88.
- Keywood, M. D., Kroll, J. H., Varutbangkul, V., Bahreini, R., Flagan, R. C., Seinfeld, J. H., 2004. Secondary organic aerosol formation from cyclohexene ozonolysis: Effect of oh scavenger and the role of radical chemistry. *Environmental Science & Technology* 38 (12), 3343–3350.
- Kirchstetter, T. W., Corrigan, C. E., Novakov, T., 2001. Laboratory and field investigation of the adsorption of gaseous organic compounds onto quartz filters. *Atmospheric Environment* 35 (9), 1663–1671.
- Komenda, M., Parusel, E., Wedel, A., Koppmann, R., 2001. Measurements of biogenic voc emissions: sampling, analysis and calibration. *Atmospheric Environment* 35 (12), 2069–2080.

- Kovats, E., 1958. Gas chromatographic characterization of organic compounds. i. retention indexes of aliphatic halides, alcohols, aldehydes, and ketones. *Helv. Chim. Acta.* 41, 1915–1932.
- Kowalski, R., Wolski, T., 2005. The chemical composition of essential oils of *silphium perfoliatum* l. *Flavour and Fragrance Journal* 20 (3), 306–310.
- Kroll, J. H., Seinfeld, J. H., 2008. Chemistry of secondary organic aerosol: Formation and evolution of low-volatility organics in the atmosphere. *Atmospheric Environment* 42 (16), 3593–3624.
- Kulmala, M., Vehkamäki, H., Petäjä, T., Dal Maso, M., Lauri, A., Kerminen, V. M., Birmili, W., McMurry, P. H., 2004. Formation and growth rates of ultrafine atmospheric particles: a review of observations. *Journal of Aerosol Science* 35 (2), 143–176.
- Lamanna, M. S., Goldstein, A. H., 1999. In situ measurements of c2-c10 volatile organic compounds above a sierra nevada ponderosa pine plantation. *J. Geophys. Res.* 104.
- Larsen, B. R., Di Bella, D., Glasius, M., Winterhalter, R., Jensen, N. R., Hjorth, J., 2001. Gas-phase oxidation of monoterpenes: Gaseous and particulate products. *Journal of Atmospheric Chemistry* 38 (3), 231–276.
- Lee, A., Goldstein, A. H., Keywood, M. D., Gao, S., Varutbangkul, V., Bahreini, R., Ng, N. L., Flagan, R. C., Seinfeld, J. H., 2006. Gas-phase products and secondary aerosol yields from the ozonolysis of ten different terpenes. *Journal of Geophysical Research* 111, D07302.
- Li, J., 2002. Comparison of the capability of peak functions in describing real chromatographic peaks. *Journal of Chromatography A* 952 (1-2), 63–70.
- Lindinger, W., Hansel, A., Jordan, A., 1998. On-line monitoring of volatile organic compounds at pptv levels by means of proton-transfer-reaction mass spectrometry (ptr-ms) - medical applications, food control and environmental research. *International Journal of Mass Spectrometry* 173 (3), 191–241.
- Liu, P., Ziemann, P. J., Kittelson, D. B., McMurry, P. H., 1995a. Generating particle beams of controlled dimensions and divergence .1. theory of particle motion in aerodynamic lenses and nozzle expansions. *Aerosol Science and Technology* 22 (3), 293–313.
- Liu, P., Ziemann, P. J., Kittelson, D. B., McMurry, P. H., 1995b. Generating particle beams of controlled dimensions and divergence .2. experimental evaluation of particle motion in aerodynamic lenses and nozzle expansions. *Aerosol Science and Technology* 22 (3), 314–324.
- Liu, P. S. K., Deng, R., Smith, K. A., Williams, L. R., Jayne, J. T., Canagaratna, M. R., Moore, K., Onasch, T. B., Worsnop, D. R., Deshler, T., 2007. Transmission efficiency of an aerodynamic focusing lens system: Comparison of model calculations and laboratory measurements for the aerodyne aerosol mass spectrometer. *Aerosol Science and Technology* 41 (8), 721–733.

## REFERENCES

---

- Ma, Y., Marston, G., 2008. Multifunctional acid formation from the gas-phase ozonolysis of beta-pinene. *Physical Chemistry Chemical Physics* 10 (40), 6115–6126.
- Mader, B. T., Pankow, J. F., 2001. Gas-solid partitioning of semivolatile organic compounds (socs) to air filters. 3. an analysis of gas adsorption artifacts in measurements of atmospheric socs and organic carbon (oc) when using teflon membrane filters and quartz fiber filters. *Environmental Science & Technology* 35 (17), 3422–3432.
- McMurry, P. H., 2000. A review of atmospheric aerosol measurements. *Atmospheric Environment* 34, 1959–1999.
- Mentel, T., Wahner, A., 1996. A large reaction chamber for nighttime atmospheric chemistry: Design and characteristics of the reaction chamber. *Berichte des Forschungszentrums Jülich GmbH* 3196.
- Müller, L., Reinnig, M.-C., Warnke, J., Hoffmann, T., 2008. Unambiguous identification of esters as oligomers in secondary organic aerosol formed from cyclohexene and cyclohexene/alpha-pinene ozonolysis. *Atmos. Chem. Phys.* J1 - ACP 8 (5), 1423–1433.
- Odum, J. R., Hoffmann, T., Bowman, F., Collins, D., Flagan, R. C., Seinfeld, J. H., 1996. Gas/particle partitioning and secondary organic aerosol yields. *Environmental Science & Technology* 30 (8), 2580–2585.
- Orlando, J. J., Nozire, B., Tyndall, G. S., Orzechowska, G. E., Paulson, S. E., Rudich, Y., 2000. Product studies of the oh- and ozone-initiated oxidation of some monoterpenes. *J. Geophys. Res.* 105.
- Paatero, P., 1997. Least squares formulation of robust non-negative factor analysis. *Chemometrics and Intelligent Laboratory Systems* 37 (1), 23–35.
- Paatero, P., Tapper, U., 1994. Positive matrix factorization - a nonnegative factor model with optimal utilization of error-estimates of data values. *Environmetrics* 5 (2), 111–126.
- Pankow, J. F., 1994a. An absorption model of gas/particle partitioning of organic compounds in the atmosphere. *Atmospheric Environment* 28 (2), 185–188.
- Pankow, J. F., 1994b. An absorption-model of the gas aerosol partitioning involved in the formation of secondary organic aerosol. *Atmospheric Environment* 28 (2), 189–193.
- Pankow, J. F., Asher, W. E., 2008. Simpol.1: a simple group contribution method for predicting vapor pressures and enthalpies of vaporization of multifunctional organic compounds. *Atmos. Chem. Phys.* J1 - ACP 8 (10), 2773–2796.
- Papandreou, V., Magiatis, P., Chinou, I., Kalpoutzakis, E., Skaltsounis, A. L., Tsarbopoulos, A., 2002. Volatiles with antimicrobial activity from the roots of greek paeonia taxa. *Journal of Ethnopharmacology* 81 (1), 101–104.

- Penner, J. E., Andreae, M. O., Annegarn, H., Barrie, L., Feichter, J., Hegg, D., Jayaraman, A., Leaitch, R., Murphy, D., Nganga, J., Pitari, G., 2001. Aerosols, their direct and indirect effects. In: Houghton, J. T., Ding, Y., Griggs, D. J., Noguer, M., van der Linden, P. J., Dai, X., Maskell, K., Johnson, C. A. (Eds.), Intergovernmental Panel on Climate Change: Climate Change 2001 - The Scientific Basis. Contribution of Working Group I to the Third Assessment Report of the Intergovernmental Panel on Climate Change. Cambridge University Press, pp. 289–348.
- Pope, C. A., 2007. Mortality effects of longer term exposures to fine particulate air pollution: Review of recent epidemiological evidence. *Inhalation Toxicology* 19, 33–38.
- Pöschl, U., 2005. Atmospheric aerosols: Composition, transformation, climate and health effects. *Angewandte Chemie International Edition* 44 (46), 7520–7540.
- Rogge, W. F., Mazurek, M. A., Hildemann, L. M., Cass, G. R., Simoneit, B. R. T., 1993. Quantification of urban organic aerosols at a molecular-level - identification, abundance and seasonal-variation. *Atmospheric Environment Part a-General Topics* 27 (8), 1309–1330.
- Rudich, Y., Donahue, N. M., Mentel, T. F., 2007. Aging of organic aerosol: Bridging the gap between laboratory and field studies. *Annual Review of Physical Chemistry* 58 (1).
- Seinfeld, J. H., Pandis, S. N., 1998. *Atmospheric Chemistry and Physics: From Air Pollution to Climate Change*. Wiley-Interscience.
- Seinfeld, J. H., Pankow, J. F., 2003. Organic atmospheric particulate material. *Annual Review of Physical Chemistry* 54 (1), 121–140.
- Subramanian, R., Khlystov, A. Y., Cabada, J. C., Robinson, A. L., 2004. Positive and negative artifacts in particulate organic carbon measurements with denuded and undenuded sampler configurations. *Aerosol Science & Technology* 38, 27–48.
- Tani, A., Hayward, S., Hansel, A., Hewitt, C. N., 2004. Effect of water vapour pressure on monoterpene measurements using proton transfer reaction-mass spectrometry (ptr-ms). *International Journal of Mass Spectrometry Proton Transfer Reaction Mass Spectrometry* 239 (2-3), 161–169.
- Turpin, B. J., Huntzicker, J. J., Hering, S. V., 1994. Investigation of organic aerosol sampling artifacts in the los angeles basin. *Atmospheric Environment* 28 (19), 3061–3071.
- Turpin, B. J., Saxena, P., Andrews, E., 2000. Measuring and simulating particulate organics in the atmosphere: problems and prospects. *Atmospheric Environment* 34 (18), 2983–3013.

## REFERENCES

---

- Ulbrich, I. M., Canagaratna, M. R., Zhang, Q., Worsnop, D. R., Jimenez, J. L., 2008. Interpretation of organic components from positive matrix factorization of aerosol mass spectrometric data. *Atmos. Chem. Phys. Discuss.* J1 - ACPD 8 (2), 6729–6791.
- van den Dool, H. ., Kratz, P. D., 1963. A generalization of the retention index system including linear temperature programmed gas-liquid partition chromatography. *J. Chromatogr.* 11, 463–471.
- Volkamer, R., Jimenez, J. L., San Martini, F., Dzepina, K., Zhang, Q., Salcedo, D., Molina, L. T., Worsnop, D. R., Molina, M. J., 2006. Secondary organic aerosol formation from anthropogenic air pollution: Rapid and higher than expected. *Geophys. Res. Lett.* 33.
- Wang, Y., Finn, C., Qian, M. C., 2005. Impact of growing environment on chickasaw blackberry (*rubus l.*) aroma evaluated by gas chromatography olfactometry dilution analysis. *Journal of Agricultural and Food Chemistry* 53 (9), 3563–3571.
- Whitby, K. T., Sverdrup, G. M., 1980. California aerosols: Their physical and chemical characteristics. *Adv. Environ. Sci. Technol.* 8, 477–525.
- Williams, B., Goldstein, A., Kreisberg, N., Hering, S., 2006. An in-situ instrument for speciated organic composition of atmospheric aerosols: Thermal desorption aerosol gc/ms-fid (tag). *Aerosol Science and Technology* 40 (8), 627–638(12).
- Winterhalter, R., Neeb, P., Grossmann, D., Kolloff, A., Horie, O., Moortgat, G., 2000. Products and mechanism of the gas phase reaction of ozone with beta-pinene. *Journal of Atmospheric Chemistry* 35, 165–197(33).
- Wisthaler, A., Jensen, N., Winterhalter, R., Lindinger, W., Hjorth, J., 2001. Measurements of acetone and other gas phase product yields from the oh-initiated oxidation of terpenes by proton-transfer-reaction mass spectrometry (ptr-ms). *Atmospheric Environment* 35, 6181–6191(11).
- Yokouchi, Y., Ambe, Y., 1985. Aerosols formed from the chemical reaction of monoterpenes and ozone. *Atmospheric Environment* 19 (8), 1271–1276.
- Yu, J., III, D. R. C., Griffin, R. J., Flagan, R. C., Seinfeld, J. H., 1999. Gas-phase ozone oxidation of monoterpenes: Gaseous and particulate products. *Journal of Atmospheric Chemistry* 34, 207258.
- Zhang, Q., Jimenez, J. L., Canagaratna, M. R., Allan, J. D., Coe, H., Ulbrich, I., Alfarra, M. R., Takami, A., Middlebrook, A. M., Sun, Y. L., Dzepina, K., Dunlea, E., Docherty, K., DeCarlo, P. F., Salcedo, D., Onasch, T., Jayne, J. T., Miyoshi, T., Shimono, A., Hatakeyama, S., Takegawa, N., Kondo, Y., Schneider, J., Drewnick, F., Borrmann, S., Weimer, S., Demerjian, K., Williams, P., Bower, K., Bahreini, R., Cottrell, L., Griffin, R. J., Rautiainen, J., Sun, J. Y., Zhang, Y. M., Worsnop, D. R., 2007. Ubiquity and dominance of oxygenated species in organic aerosols in anthropogenically-influenced northern hemisphere midlatitudes. *Geophysical Research Letters* 34 (13).

## A. Fit Coefficients for the Characterization Measurements

In the following the results of the fit coefficients for the calibration curves of the GC-MS characterization (in chapter 3.1), for the results of the octadecane diffusion source measurements (in chapter 3.2) are listed.



APPENDIX A. FIT COEFFICIENTS FOR THE CHARACTERIZATION MEASUREMENTS

---

Table A.1: *Upper part: Fit coefficients of the calibration curves of the direct injection into the GC-MS. Lower part: Fit coefficients of the octadecane diffusion source measurements.*

Coefficients	Coefficient Values $\pm$ one standard deviation
Acetone calibration (Figure 3.4(a))	
Linear Fit	
Intercept	$1310.5 \pm 4660$
Slope	$254.26 \pm 53.90$
R <sup>2</sup>	0.92904
Linear Fit through the origin	
Slope	$262.79 \pm 19.20$
R <sup>2</sup>	0.95409
Nopinone calibration (Figure 3.4(b))	
Linear Fit	
Intercept	$-4353.7 \pm 1.05 \times 10^4$
Slope	$629.29 \pm 116.00$
R <sup>2</sup>	0.95541
Linear Fit through the origin	
Slope	$538.46 \pm 48.80$
R <sup>2</sup>	0.95460
Octadecane calibration (Figure 3.4(c))	
Linear Fit	
Intercept	$-5116.8 \pm 9.76 \times 10^3$
Slope	$438.75 \pm 34.90$
R <sup>2</sup>	0.95194
Linear Fit through the origin	
Slope	$374.18 \pm 34.90$
R <sup>2</sup>	0.98157
Octadecane DS results (Figure 3.8)	
Linear Fit	
Intercept	$-1909.6 \pm 2030$
Slope	$378.48 \pm 13.80$
R <sup>2</sup>	0.84492
Linear Fit through the origin	
Slope	$359.69 \pm 7.12$
R <sup>2</sup>	0.98401

## B. ACM-GC-MS Chromatograms of the aerosol chamber experiment

In the following the FID Chromatograms of the all samples (S1 to S16) and blank measurements (B1 to B7) measured with ACM-GC-MS during the  $\beta$ -pinene ozonolysis experiment are presented (for further details see chapter 4.2.3). Note that the chromatograms are presented in the chronological order of the course of the experiment (see also Table 4.1).

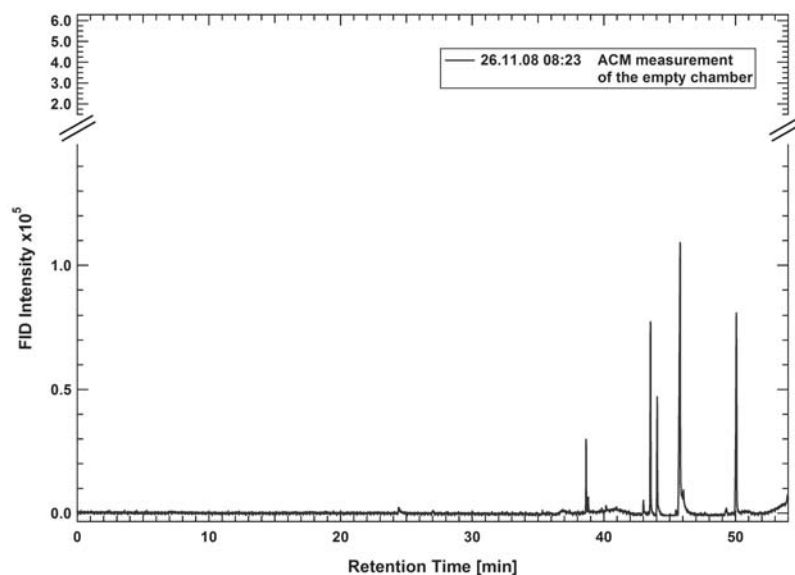


Figure B.1: ACM-GC-MS FID Chromatogram of sample S1.

APPENDIX B. ACM-GC-MS CHROMATOGRAMS OF THE AEROSOL  
CHAMBER EXPERIMENT

---

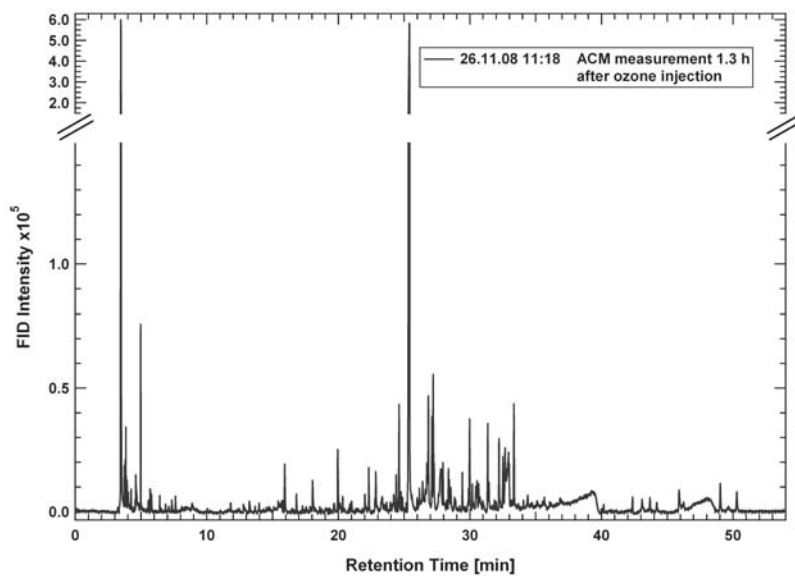


Figure B.2: ACM-GC-MS FID Chromatogram of sample S2.

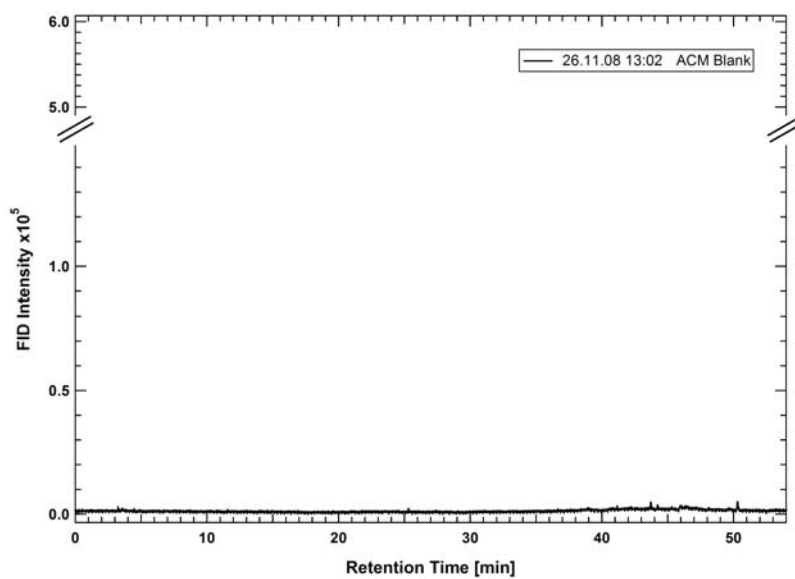


Figure B.3: ACM-GC-MS FID Chromatogram of blank B1.

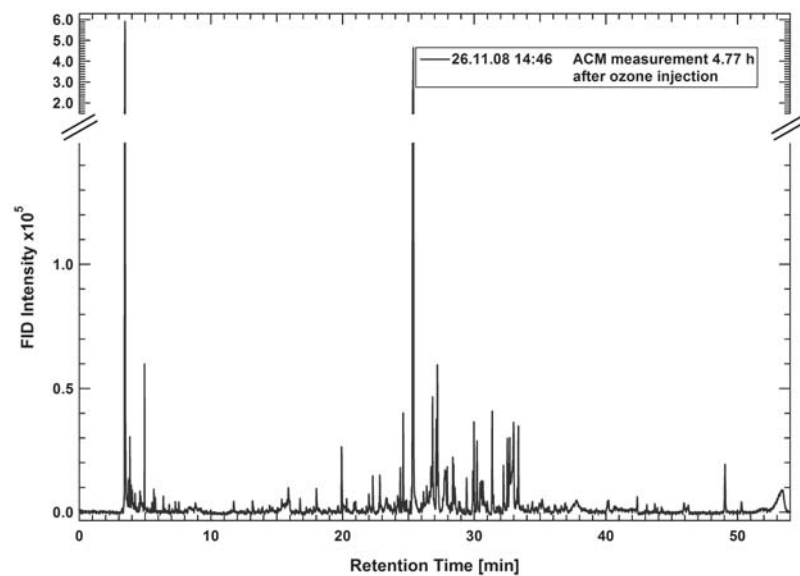


Figure B.4: *ACM-GC-MS FID Chromatogram of sample S3.*

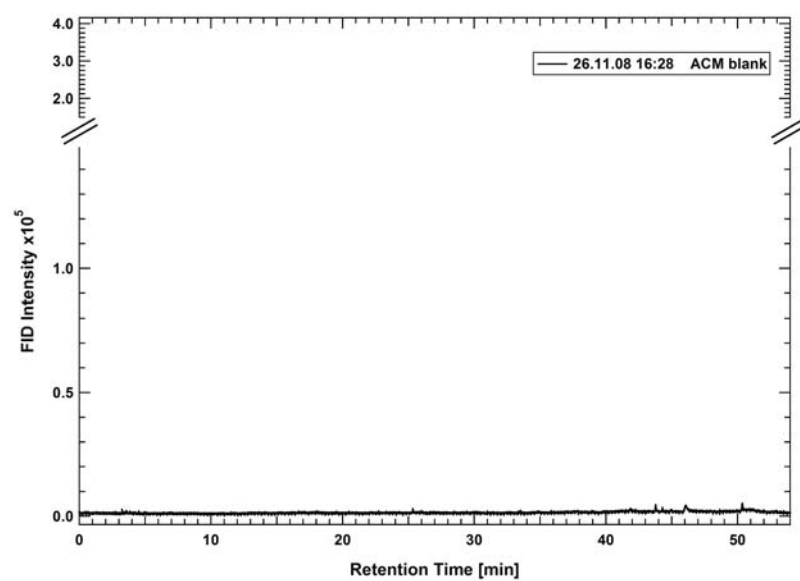


Figure B.5: *ACM-GC-MS FID Chromatogram of blank B2.*

APPENDIX B. ACM-GC-MS CHROMATOGRAMS OF THE AEROSOL  
CHAMBER EXPERIMENT

---

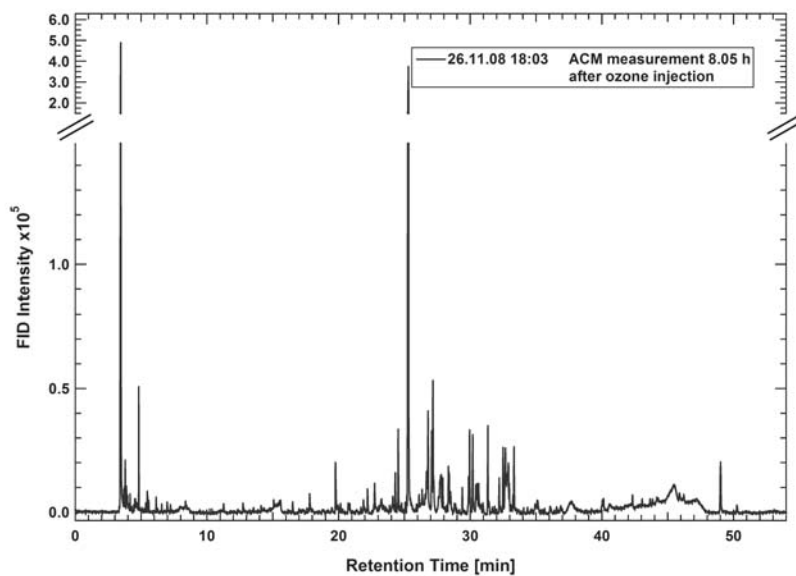


Figure B.6: ACM-GC-MS FID Chromatogram of sample *S4*.

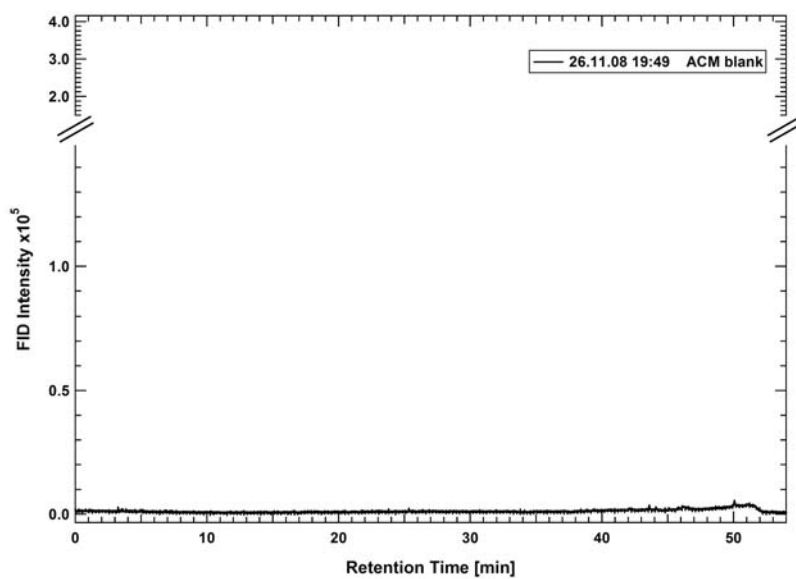


Figure B.7: ACM-GC-MS FID Chromatogram of blank *B3*.

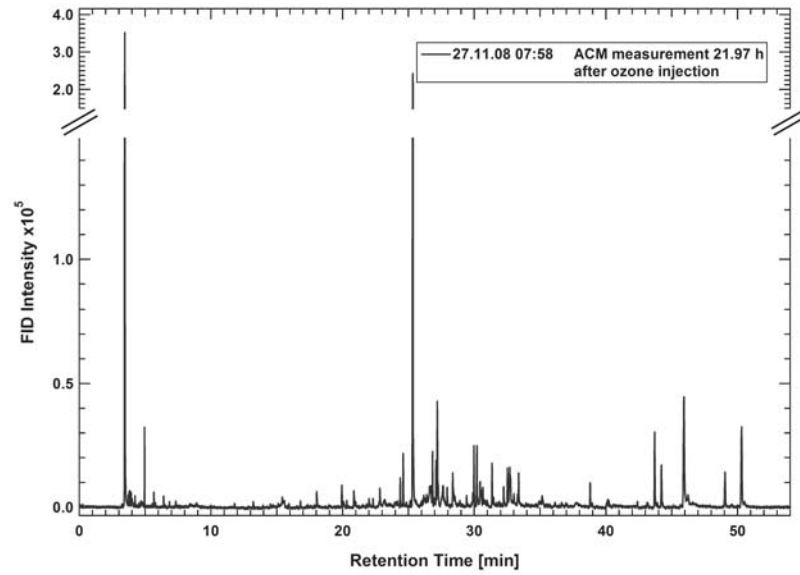


Figure B.8: *ACM-GC-MS FID Chromatogram of sample S5.*

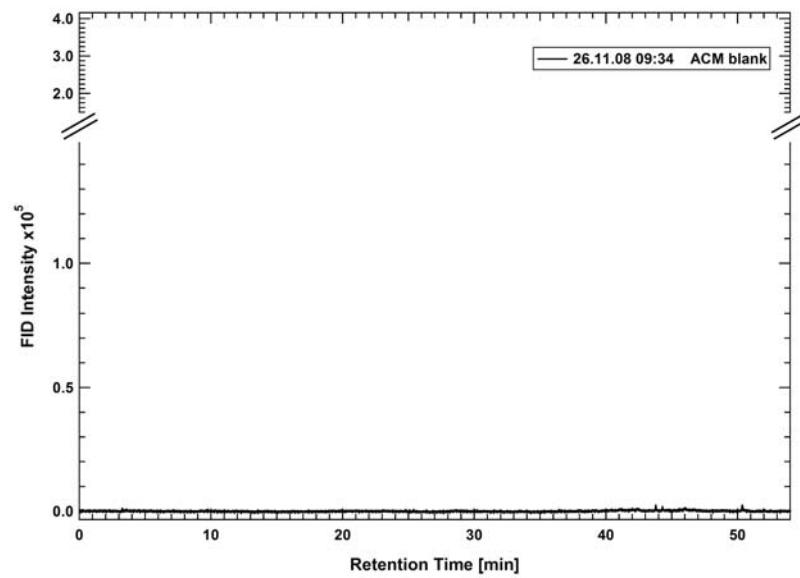


Figure B.9: *ACM-GC-MS FID Chromatogram of blank B4.*

APPENDIX B. ACM-GC-MS CHROMATOGRAMS OF THE AEROSOL  
CHAMBER EXPERIMENT

---

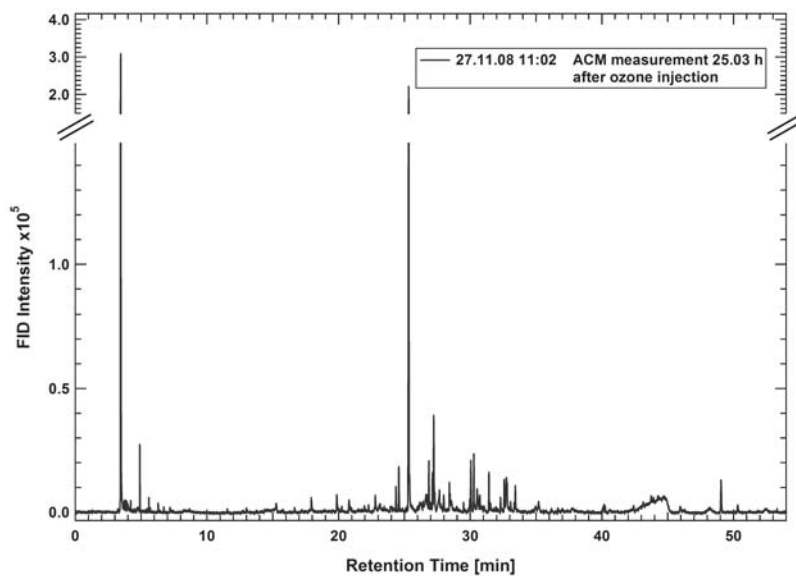


Figure B.10: *ACM-GC-MS FID Chromatogram of sample S6.*

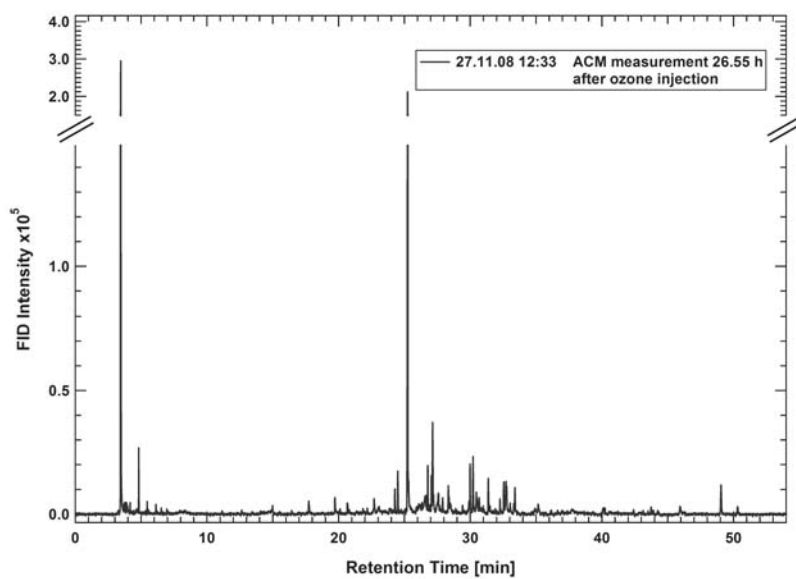


Figure B.11: *ACM-GC-MS FID Chromatogram of sample S7.*

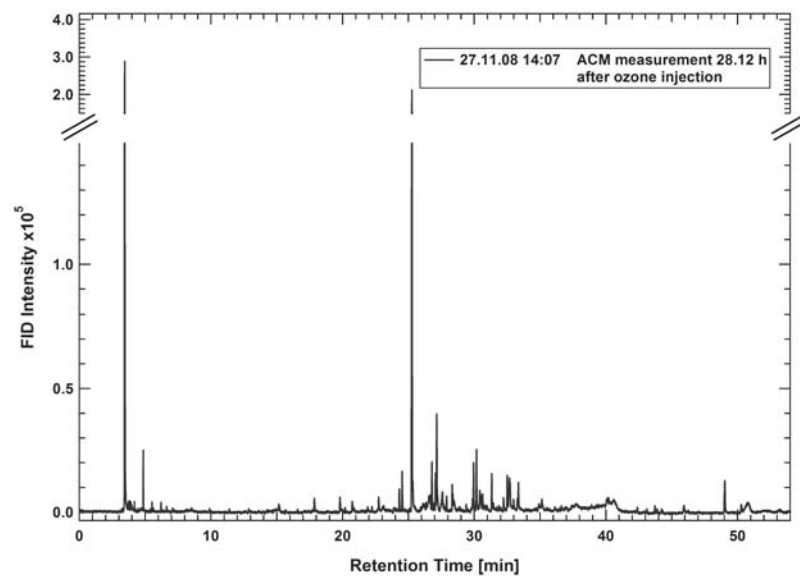


Figure B.12: *ACM-GC-MS FID Chromatogram of sample S8.*

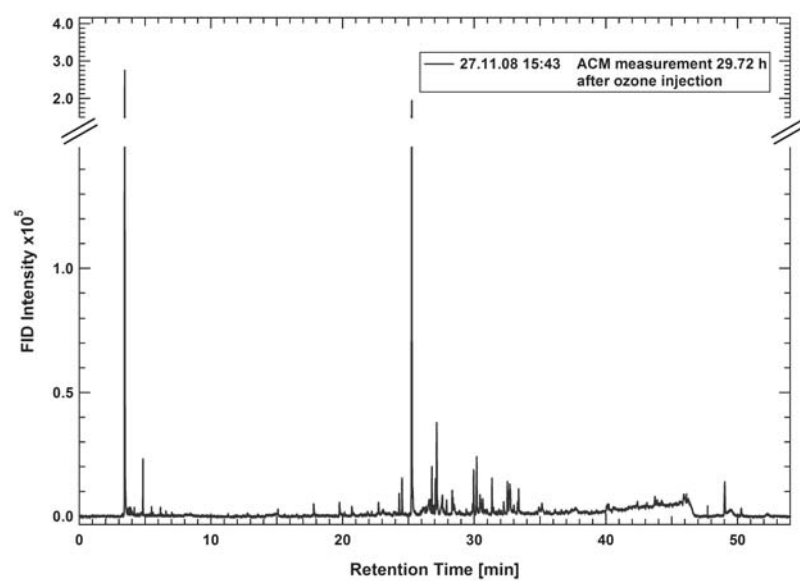


Figure B.13: *ACM-GC-MS FID Chromatogram of sample S9.*



APPENDIX B. ACM-GC-MS CHROMATOGRAMS OF THE AEROSOL  
CHAMBER EXPERIMENT

---

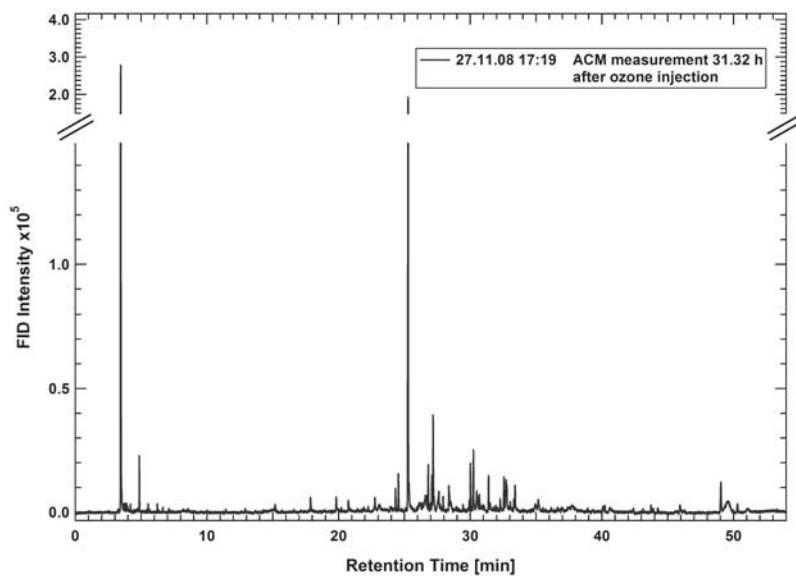


Figure B.14: ACM-GC-MS FID Chromatogram of sample S10.

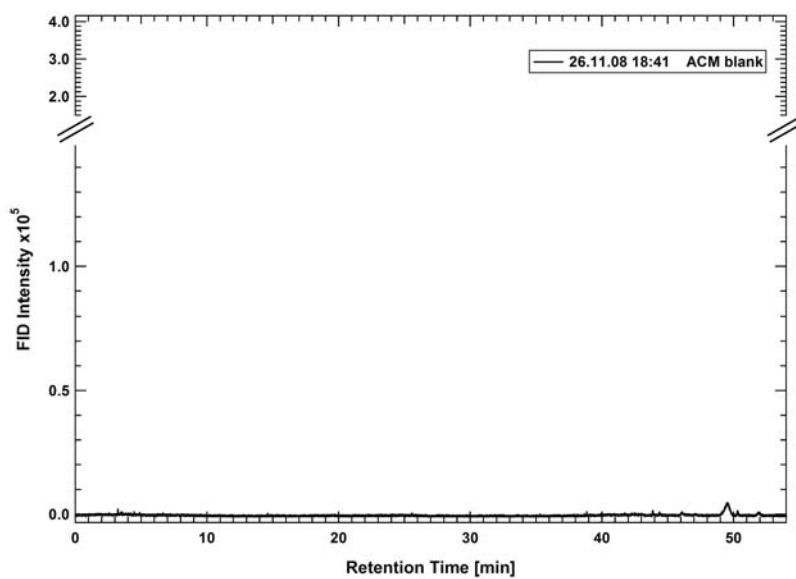


Figure B.15: ACM-GC-MS FID Chromatogram of blank B5.

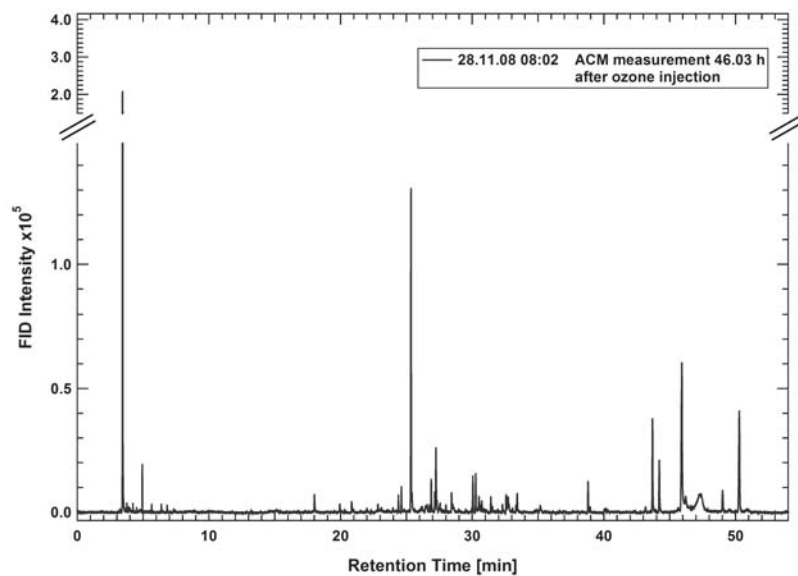


Figure B.16: *ACM-GC-MS FID Chromatogram of sample S11.*

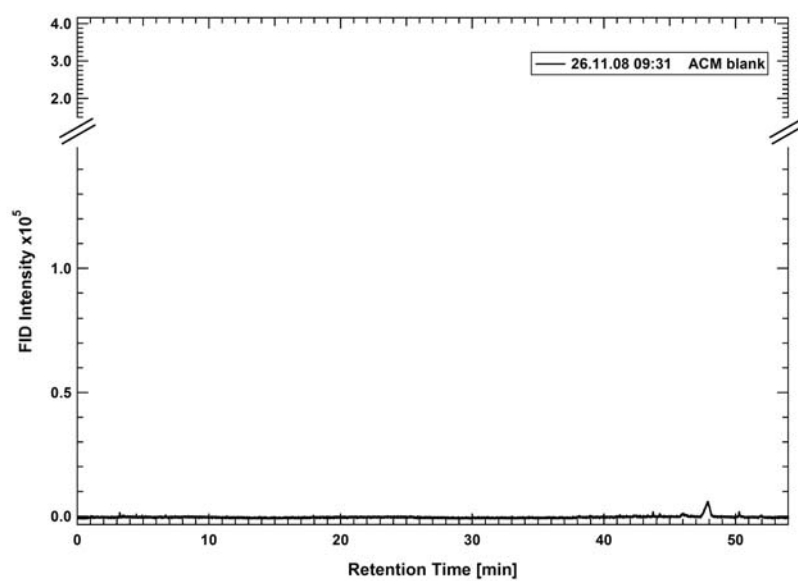


Figure B.17: *ACM-GC-MS FID Chromatogram of blank B6.*

APPENDIX B. ACM-GC-MS CHROMATOGRAMS OF THE AEROSOL  
CHAMBER EXPERIMENT

---

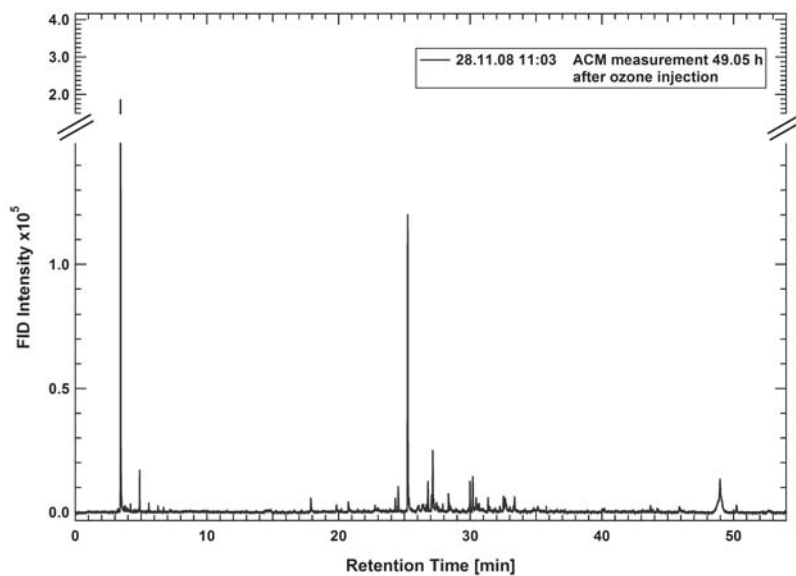


Figure B.18: ACM-GC-MS FID Chromatogram of sample S12.

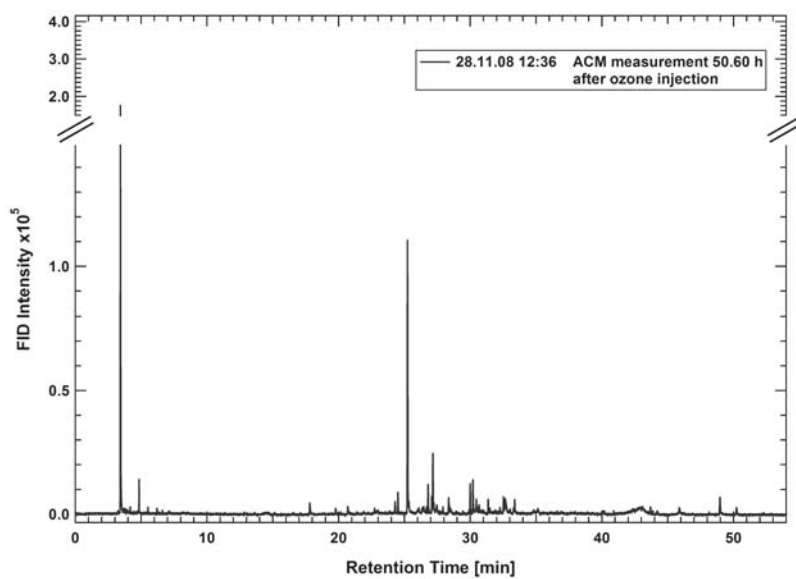


Figure B.19: ACM-GC-MS FID Chromatogram of sample S13.

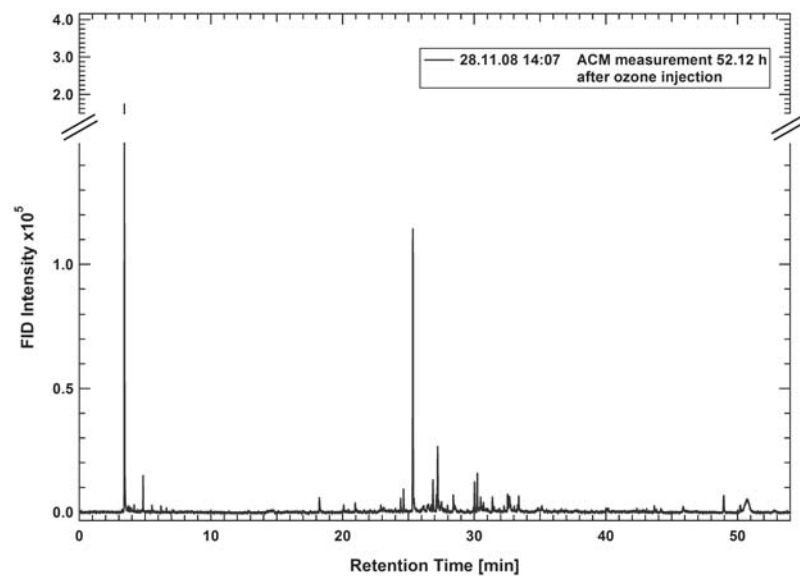


Figure B.20: ACM-GC-MS FID Chromatogram of sample S14.

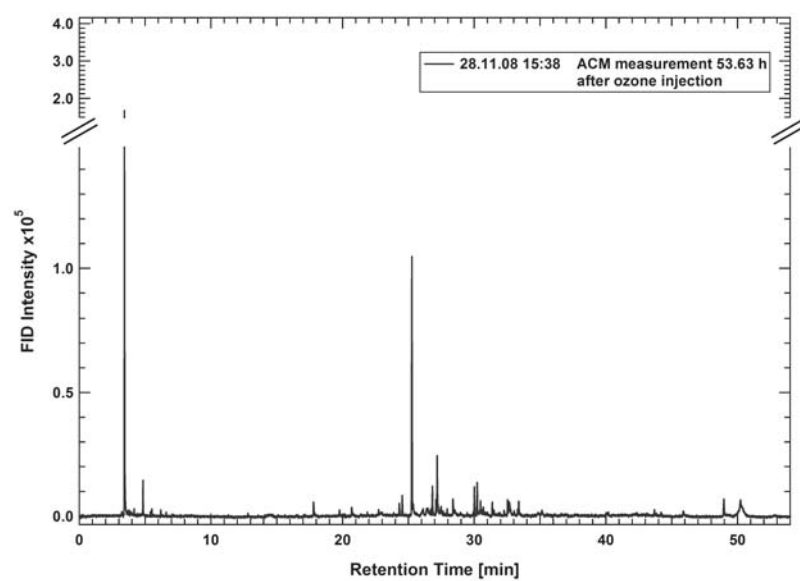


Figure B.21: ACM-GC-MS FID Chromatogram of sample S15.

APPENDIX B. ACM-GC-MS CHROMATOGRAMS OF THE AEROSOL  
CHAMBER EXPERIMENT

---

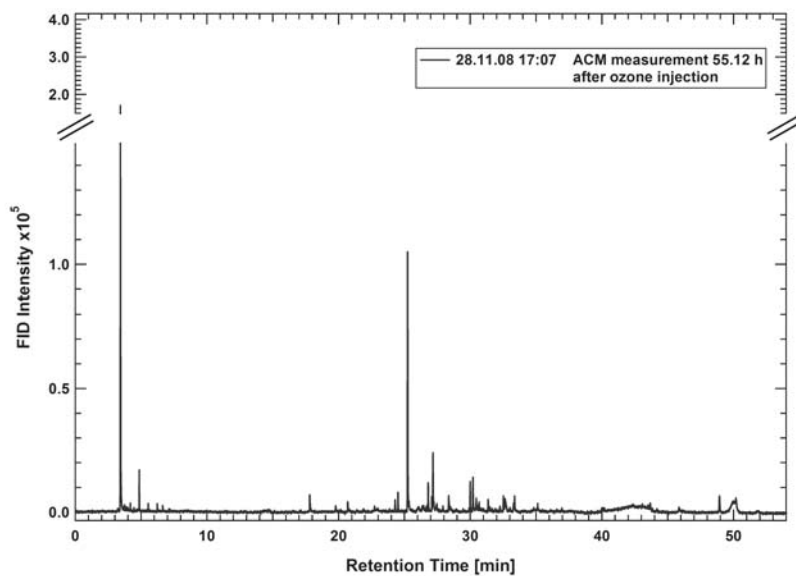


Figure B.22: ACM-GC-MS FID Chromatogram of sample S16.

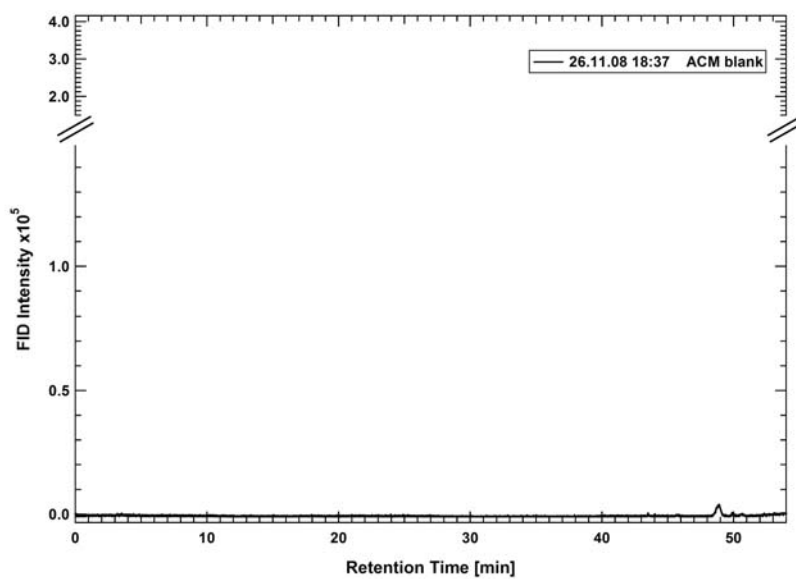


Figure B.23: ACM-GC-MS FID Chromatogram of blank B7.

## C. Mass Spectra of the identified $\beta$ -pinene ozonolysis products

In the following the EI mass spectra (70eV) of the identified compounds in the SOA sampled during the  $\beta$ -pinene ozonolysis experiment with the ACM-GC-MS are presented (see chapter 4.3.1). Details of the identified compounds are also listed in Table 4.2.

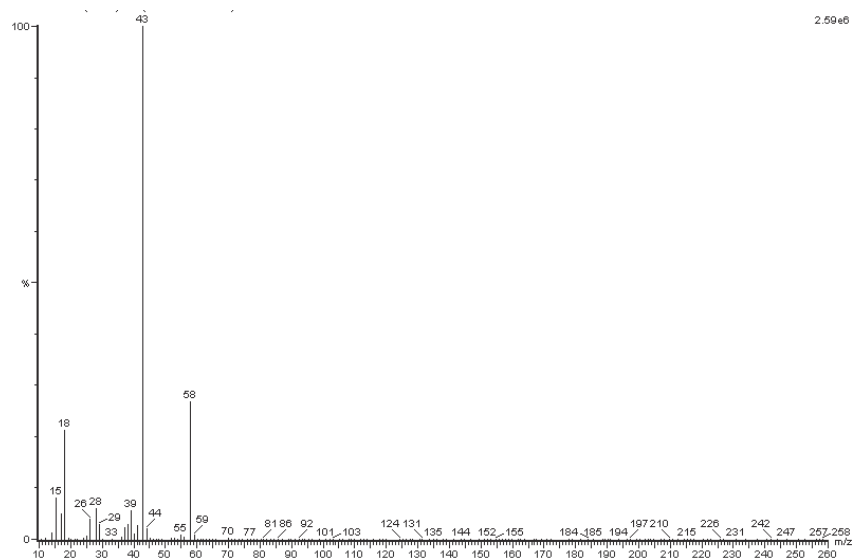


Figure C.1: *Mass spectrum of acetone.*

## APPENDIX C. MASS SPECTRA OF THE IDENTIFIED $\beta$ -PINENE OZONOLYSIS PRODUCTS

---

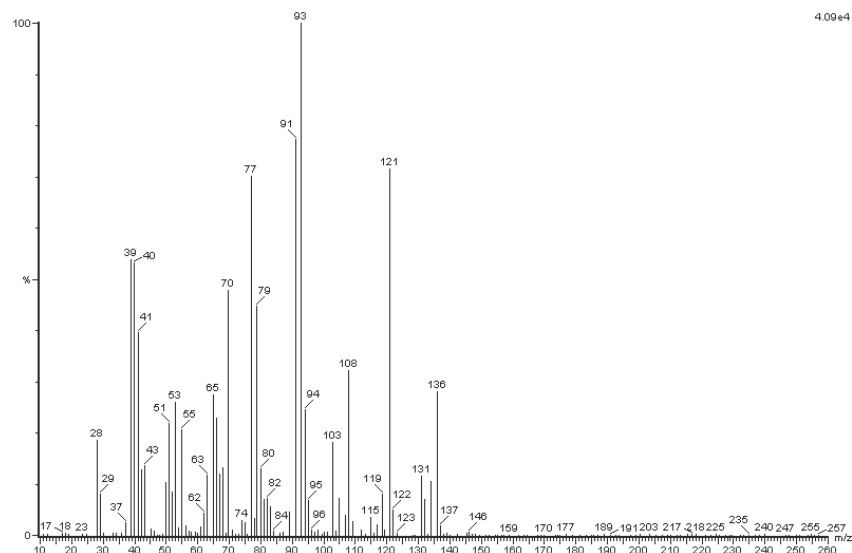


Figure C.2: Mass spectrum of bicyclo[3,1,1]hept-3-ene-2-one.

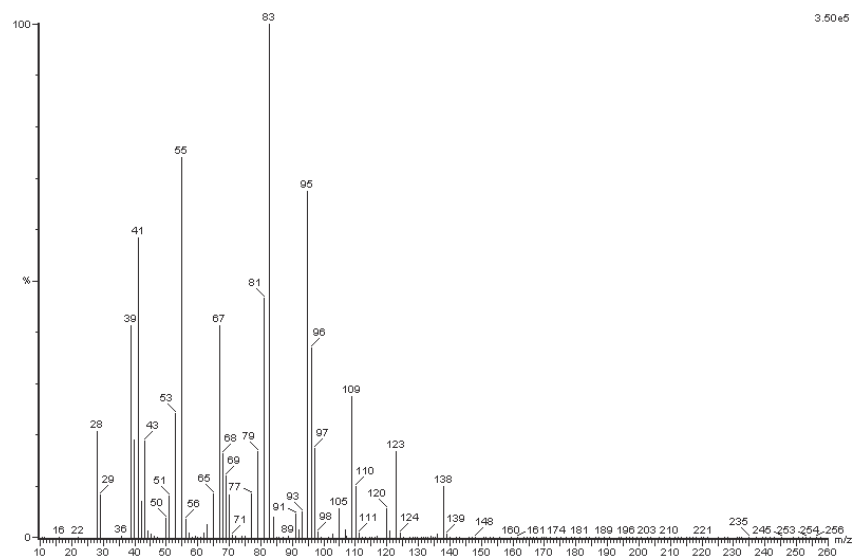


Figure C.3: Mass spectrum of nopinone.

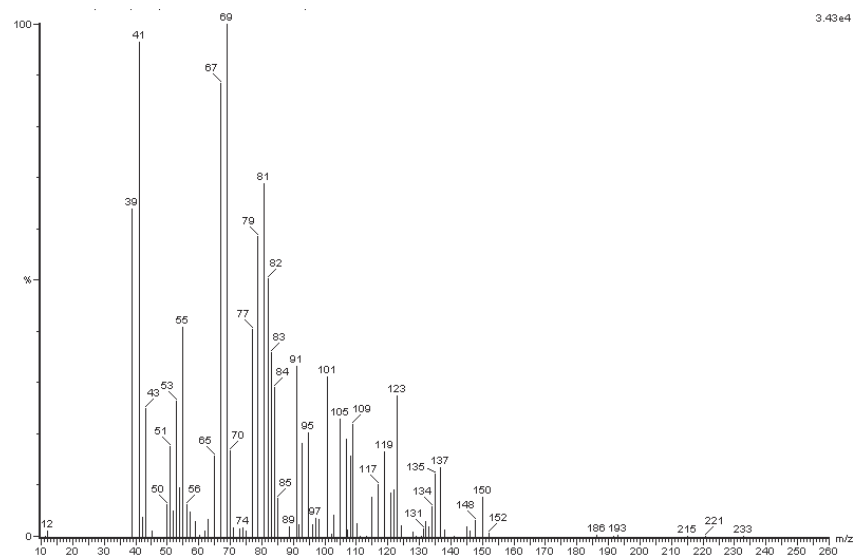


Figure C.4: *Mass spectrum of myrtanal.*

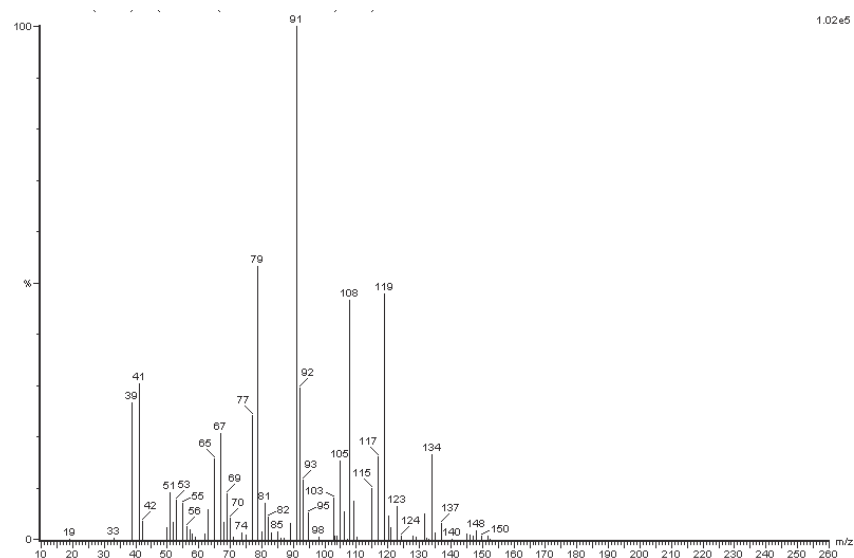


Figure C.5: *Mass spectrum of myrtenol.*



## APPENDIX C. MASS SPECTRA OF THE IDENTIFIED $\beta$ -PINENE OZONOLYSIS PRODUCTS

---

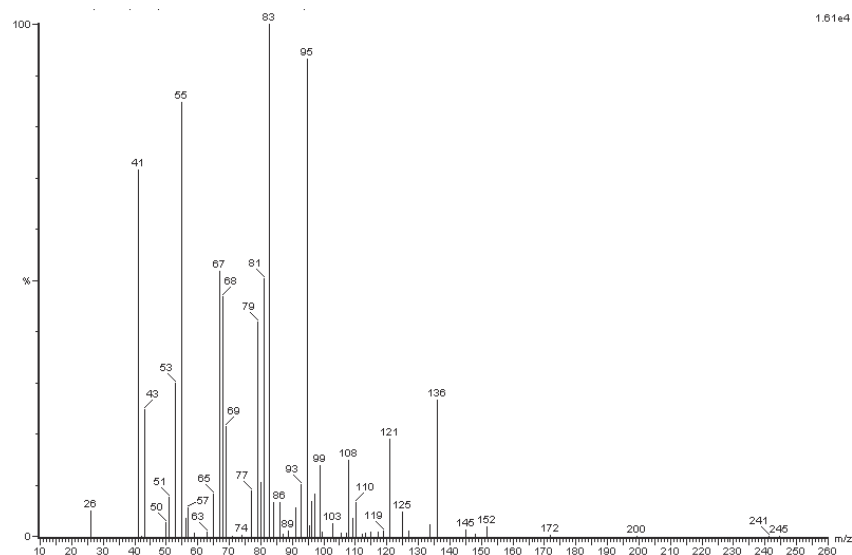


Figure C.6: Mass spectrum of 1-hydroxipinone.

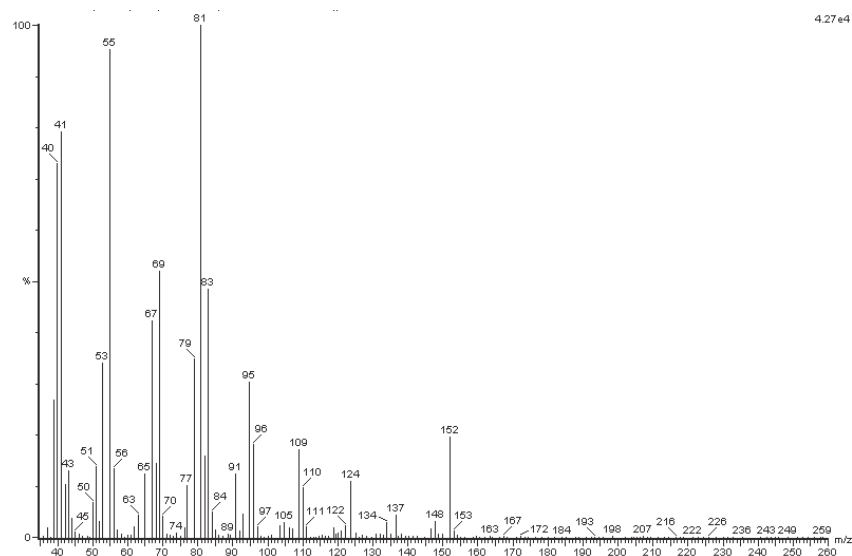


Figure C.7: Mass spectrum of 3-oxopinone.

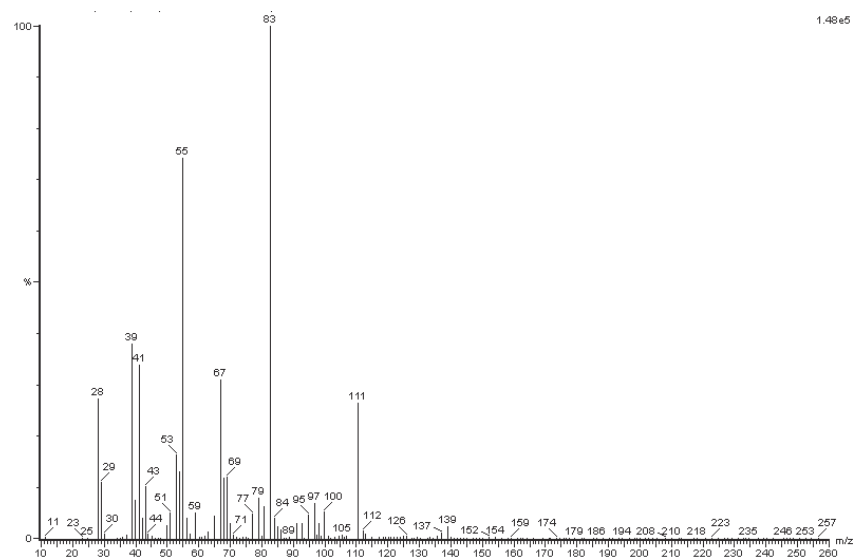


Figure C.8: *Mass spectrum of 3,7-dihydroxynopinone.*

APPENDIX C. MASS SPECTRA OF THE IDENTIFIED  $\beta$ -PINENE  
OZONOLYSIS PRODUCTS

---

## D. Retention Index Method for GC-MS Peak Identification

In general the retention index (also known as the Kovats index (Kovats, 1958)) of a sample component is a number, obtained by logarithmic interpolation, relating the adjusted retention time to the adjusted retention times of two standards eluted before and after the peak of the sample component. In the Kovats index used in gas chromatography alkanes serve as the standards and logarithmic interpolation is used. The Kovats index is always measured under isothermal conditions. However the analysis of the SOA samples were done using a temperature-programmed GC analysis. In the case of temperature-programmed gas chromatography a similar value can be calculated using direct numbers instead of their logarithm. This value is often called the linear retention index (van den Dool and Kratz, 1963) which is calculated as follows:

$$I^T = 100 \left( \frac{t_i^T - t_n^T}{t_{n+1}^T - t_n^T} + n \right) \quad (\text{D.1})$$

$I^T$	= linear retention index	[1]
$t_i^T$	= retention time measured for the sample compound under the condition of temperature programming	[min]
$t_n^T$	= retention time of the alkane eluting before the sample component	[min]
$t_{n+1}^T$	= adjusted retention time of the alkane eluting after the sample component	[min]
$n$	= number of carbon atoms	[1]

The linear retention index of the peaks can be compared to literature values if the gas chromatographic conditions are equal or very similar.

APPENDIX D. RETENTION INDEX METHOD FOR GC-MS PEAK  
IDENTIFICATION

---

## E. Temporal evolution of the mass fractional abundances of all unidentified SOA compounds

In the following the mass fractional abundances of all unidentified compounds group together according to their specific temporal evolution is shown. These graphs represent the complete overview of Figure 4.14(a) to (c) in chapter 4.4.2. In Figure E.1, E.2, and E.3 are the ACM groups 1, 2, and 3, respectively. In Figure E.4 are all unidentified compounds shown which could not be confidently assigned to one of the three groups.

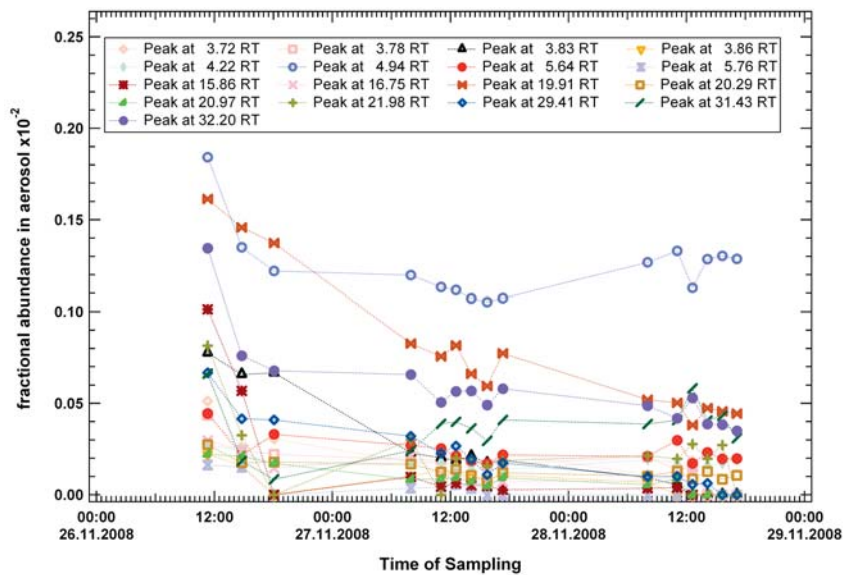


Figure E.1: *Unidentified compounds in the SOA assigned to group 1.*

APPENDIX E. TEMPORAL EVOLUTION OF THE MASS FRACTIONAL ABUNDANCES OF ALL UNIDENTIFIED SOA COMPOUNDS

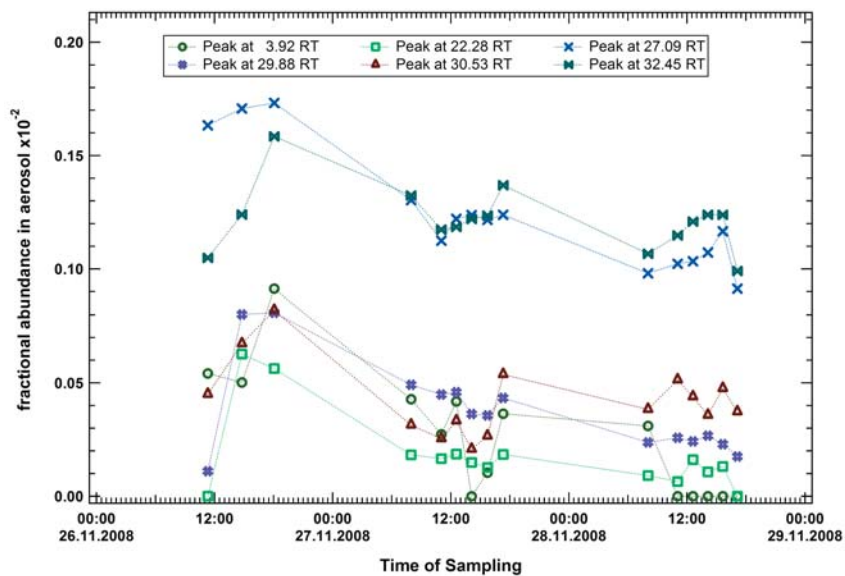


Figure E.2: Unidentified compounds in the SOA assigned to group 2.

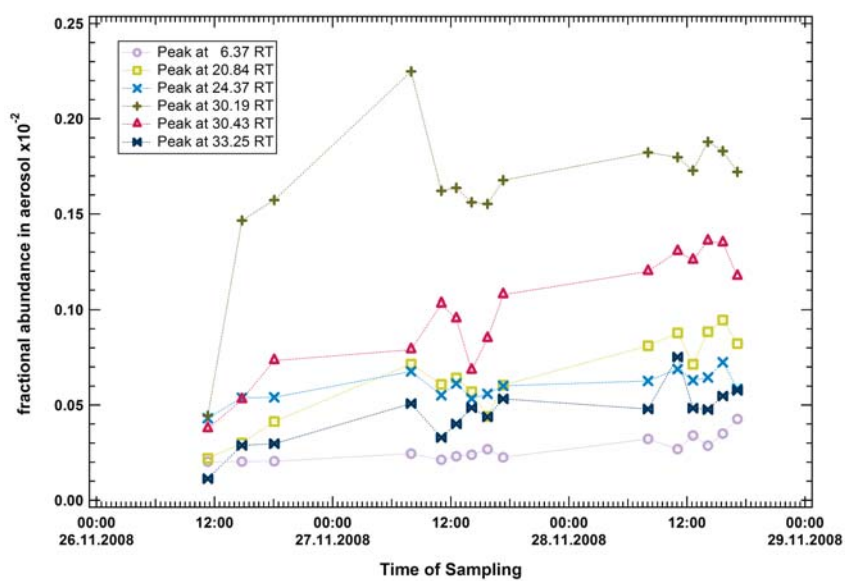


Figure E.3: Unidentified compounds in the SOA assigned to group 3.

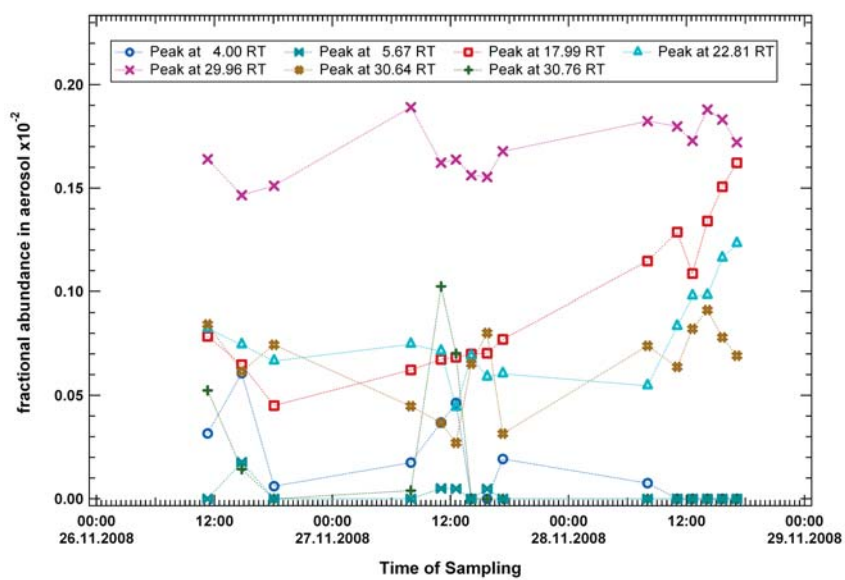


Figure E.4: *Unidentified compounds in the SOA which could not be clearly assigned to group 1, 2 or 3.*



APPENDIX E. TEMPORAL EVOLUTION OF THE MASS FRACTIONAL  
ABUNDANCES OF ALL UNIDENTIFIED SOA COMPOUNDS

---

## F. Positive Matrix Factorization (PMF) Analysis

The positive matrix factorization (PMF) analysis is a variant of factor analysis. Factor analysis in general is a statistical method used to describe the variability among observed variables in terms of fewer unobserved variables called factors. In the PMF analysis data is grouped by similarity between variables, for example variables that are highly correlated are grouped. The factors indicate the best associations among the variables.

In the PMF analysis it is assumed that the matrix of the measured dataset  $X_{ij}$  conforms to a mass balance equation which can be expressed as:

$$X_{ij} = G_{ip}F_{pj} + E_{ij} \quad (\text{F.1})$$

$X_{ij}$  = measured data elements to be fit

$G_{ip}$  = score matrix

$F_{pj}$  = loading matrix

$E_{ij}$  = residual matrix

$i$  = row index of the matrices

$j$  = column index of the matrices

$p$  = number of factors in the solution

In this equation the matrix  $X_{ij}$  is decomposed into the product of two smaller matrices  $G_{ip}$  and  $F_{pj}$ , the factor matrices which have to be determined. The matrix  $G_{ip}$  is also called the score matrix and contains a number of constant source profiles while  $F_{pj}$  is called the loading matrix and consists of the contributions of varying concentrations to each profile over the time of the dataset.  $E_{ip}$  is the matrix of residuals, the unexplained part of the matrix  $X_{ij}$ :

$$E_{ij} = X_{ij} - G_{ip}F_{pj} \quad (\text{F.2})$$

## APPENDIX F. POSITIVE MATRIX FACTORIZATION (PMF) ANALYSIS

---

In case of AMS measurements the matrix  $X_{ij}$  are the actually measured mass spectra during the experiment. The rows of the  $X_{ij}$  matrix are the averaged mass spectra of the SOA measured at each averaging time period during the experiment. The columns of  $X_{ij}$  are the time series of each m/z measured. The columns of the matrix  $G_{ip}$  contains the factor time series and the rows of  $F_{pj}$  matrix consist of the factor profiles, the mass spectra of each factor. The elements of the  $F_{pj}$  and  $G_{ip}$  are iteratively fit to the measured data. The objective of PMF fitting procedure is to minimize the sum of weighted residuals, that is minimizing an object function  $Q$  defined as

$$Q(E) = \sum_{i=1}^m \sum_{j=1}^n \left( \frac{E_{ij}}{\sigma_{ij}} \right)^2 \quad (\text{F.3})$$

where  $\sigma_{ij}$  is an estimate of the uncertainty (standard deviations) in the  $i$ th variable measured in the  $j$ th sample thus the PMF weights data points by their actual analytical uncertainties.  $Q(E)$  is minimized with respect to  $F_{pj}$  and  $G_{ip}$  with the constraint that each of the elements of  $F_{pj}$  and  $G_{ip}$  has to be non-negative, thus reflecting positive contributions of each factors and positive signals in each m/z. In the PMF analysis no a priori information of the values of the  $F_{pj}$  and  $G_{ip}$  matrices are needed. However the number of factors,  $p$ , in the real data set is unknown and has to be estimated. For the estimation of the number of factors the number of factors needed to describe the data set is determined by the requirement of minimal residuals and low correlation in the mass spectral and time dependent behavior of the factors. For example if the number of factors is chosen to large two or more factors might have similar or equal temporal evolutions or the mass spectral profiles are very similar and highly correlated. Therefore several PMF analysis of the same data set are conducted with different values for the number of factors. These analysis will be compared regarding correlations between the factors and the minima of the residuals to determine the best estimate.

# Abbreviations

ACM	Aerosol Collection Module
AMS	Aerosol Mass Spectrometer
CFM	Cryofocusing Module
CPC	Condensation Particle Counter
DMA	Differential Mobility Analyzer
EC	Electrostatic Classifier
EI	Electron Impact
FID	Flame Ionization Detector
FZJ	Forschungszentrum Jülich
GC	Gas Chromatograph
GC-IRMS	Gas Chromatograph - Isotope Ratio Mass Spectrometer
HEPA	High Efficiency Particulate Airfilter
HR-ToF-AMS	High Resolution Time of Flight AMS
MS	Mass Spectrometer
NIST	National Institute of Standards and Technology
O/C	Oxygen to Carbon ratio
OA	Organic Aerosols
PMF	Positive Matrix Factorization
ppb	Parts Per Billion
ppm	Parts Per Million
PSL	Polystyrene Latex Particles
PTR-MS	Proton Transfer Reaction Mass Spectrometer
PTR-ToF-MS	Proton Transfer Reaction Time of Flight Mass Spectrometer
RH	Relative Humidity
RI	Retention Index
SMPS	Scanning Mobility Particle Sizer
SOA	Secondary Organic Aerosols
VOC	Volatile Organic Compounds

---

# Danksagung

Zum Abschluss möchte ich mich bei allen Bedanken, die diese Promotion ermöglicht und mich in Taten, Worten und Gedanken unterstützt haben.

Ich möchte mich bei Herrn Prof. R. Koppmann ganz herzlich für die übernahme des Referats und für alle konstruktiven Anregungen bedanken.

Herrn Prof. A. Wahner möchte ich für die übernahme des Koreferates und danken für die Möglichkeit am Forschungszentrum Jülich spannenden Themen nachgehen zu dürfen.

Mein besonderer Dank gilt meiner Betreuerin Frau Dr. Astrid Kiendler-Scharr für die fruchtbaren Diskussionen, zahlreichen Anregungen und die tatkräftige Unterstützung, die entscheidend zum Gelingen dieser Arbeit beigetragen haben.

Im Weiteren möchte ich mich aufrichtig bei folgenden Personen bedanken:

Bei der gesamten Hetero-Gruppe für das ausgezeichnete Klima und jeglicher Unterstützung während dieser Zeit. Ins besondere bei PD Dr. Thomas Mentel für seinen wertvollen und tiefen Einblicke in die Chemie, Dr. Ralf Tillmann für die Hilfe in allen experimentellen Fragen und Notlagen, Klaus Peter Müller für seine Einblicke in die Gas Chromatographie und Amewu Mensa für die gegenseitige Unterstützung und ein sehr gutes Büroklima.

Dr. Iulia Gensch, Werner Laumer, Stefanie Andres und Beatrix Kammer für die Unterstützung bei den Filtermessungen.

Dr. Robert Wegner und Holger Spahn für die Hilfe in allen GC-MS-Fragen.

Helga London und Michael Decker für die wunderbare IT-Unterstützung und den Plausch zwischendurch.

---

Brigitte Berger für die Hilfe und Sorgfalt bei allen Formalitäten die zu erledigen waren.

Dr. John Jayne und Dr. Dagmar Trimborn für die Hilfe bei allen Fragen rund um den ACM und für die gute Zusammenarbeit.

Meinen Fahrgemeinschaftskollegen Dr. Cornelia Richter und Dr. Olaf Stein für ihre Unterstützung und den vielen sehr angenehmen Autostunden mit Gesprächen in denen alle Themen, vom fachlichen bis zum kulinarischen, ihren Platz hatten.

Mein ganz besonderer Dank gehört meinen Eltern, ohne die all das, was ich bis hierhin erreicht habe, nicht möglich gewesen wäre und meiner Schwester Andrea mit ihrem Mann Markus, die mich immer tatkräftig unterstützt haben.

Nicht zuletzt möchte ich Aneta dafür danken, dass Sie in dieser Zeit immer für mich da war und mich unermüdlich unterstützt hat. Danke dass es Dich gibt, denn ohne Dich wäre alles nicht möglich gewesen.

1. **Einsatz von multispektralen Satellitenbilddaten in der Wasserhaushalts- und Stoffstrommodellierung – dargestellt am Beispiel des Rureinzugsgebietes**  
von C. Montzka (2008), XX, 238 Seiten  
ISBN: 978-3-89336-508-1
2. **Ozone Production in the Atmosphere Simulation Chamber SAPHIR**  
by C. A. Richter (2008), XIV, 147 pages  
ISBN: 978-3-89336-513-5
3. **Entwicklung neuer Schutz- und Kontaktierungsschichten für Hochtemperatur-Brennstoffzellen**  
von T. Kiefer (2008), 138 Seiten  
ISBN: 978-3-89336-514-2
4. **Optimierung der Reflektivität keramischer Wärmedämmschichten aus Yttrium-teilstabilisiertem Zirkoniumdioxid für den Einsatz auf metallischen Komponenten in Gasturbinen**  
von A. Stuke (2008), X, 201 Seiten  
ISBN: 978-3-89336-515-9
5. **Lichtstreuende Oberflächen, Schichten und Schichtsysteme zur Verbesserung der Lichteinkopplung in Silizium-Dünnschichtsolarzellen**  
von M. Berginski (2008), XV, 171 Seiten  
ISBN: 978-3-89336-516-6
6. **Politiksznarien für den Klimaschutz IV – Szenarien bis 2030**  
hrsg.von P. Markewitz, F. Chr. Matthes (2008), 376 Seiten  
ISBN 978-3-89336-518-0
7. **Untersuchungen zum Verschmutzungsverhalten rheinischer Braunkohlen in Kohledampferzeugern**  
von A. Schlüter (2008), 164 Seiten  
ISBN 978-3-89336-524-1
8. **Inorganic Microporous Membranes for Gas Separation in Fossil Fuel Power Plants**  
by G. van der Donk (2008), VI, 120 pages  
ISBN: 978-3-89336-525-8
9. **Sinterung von Zirkoniumdioxid-Elektrolyten im Mehrlagenverbund der oxidkeramischen Brennstoffzelle (SOFC)**  
von R. Mücke (2008), VI, 165 Seiten  
ISBN: 978-3-89336-529-6
10. **Safety Considerations on Liquid Hydrogen**  
by K. Verfondern (2008), VIII, 167 pages  
ISBN: 978-3-89336-530-2



11. **Kerosinreformierung für Luftfahrtanwendungen**  
von R. C. Samsun (2008), VII, 218 Seiten  
ISBN: 978-3-89336-531-9
12. **Der 4. Deutsche Wasserstoff Congress 2008 – Tagungsband**  
hrsg. von D. Stolten, B. Emonts, Th. Grube (2008), 269 Seiten  
ISBN: 978-3-89336-533-3
13. **Organic matter in Late Devonian sediments as an indicator for environmental changes**  
by M. Kloppisch (2008), XII, 188 pages  
ISBN: 978-3-89336-534-0
14. **Entschwefelung von Mitteldestillaten für die Anwendung in mobilen Brennstoffzellen-Systemen**  
von J. Latz (2008), XII, 215 Seiten  
ISBN: 978-3-89336-535-7
15. **RED-IMPACT**  
**Impact of Partitioning, Transmutation and Waste Reduction Technologies on the Final Nuclear Waste Disposal**  
**SYNTHESIS REPORT**  
ed. by W. von Lensa, R. Nabbi, M. Rossbach (2008), 178 pages  
ISBN 978-3-89336-538-8
16. **Ferritic Steel Interconnectors and their Interactions with Ni Base Anodes in Solid Oxide Fuel Cells (SOFC)**  
by J. H. Froitzheim (2008), 169 pages  
ISBN: 978-3-89336-540-1
17. **Integrated Modelling of Nutrients in Selected River Basins of Turkey**  
Results of a bilateral German-Turkish Research Project  
project coord. M. Karpuzcu, F. Wendland (2008), XVI, 183 pages  
ISBN: 978-3-89336-541-8
18. **Isotopengeochemische Studien zur klimatischen Ausprägung der Jüngerer Dryas in terrestrischen Archiven Eurasiens**  
von J. Parplies (2008), XI, 155 Seiten, Anh.  
ISBN: 978-3-89336-542-5
19. **Untersuchungen zur Klimavariabilität auf dem Tibetischen Plateau - Ein Beitrag auf der Basis stabiler Kohlenstoff- und Sauerstoffisotope in Jahrringen von Bäumen waldgrenznaher Standorte**  
von J. Griessinger (2008), XIII, 172 Seiten  
ISBN: 978-3-89336-544-9

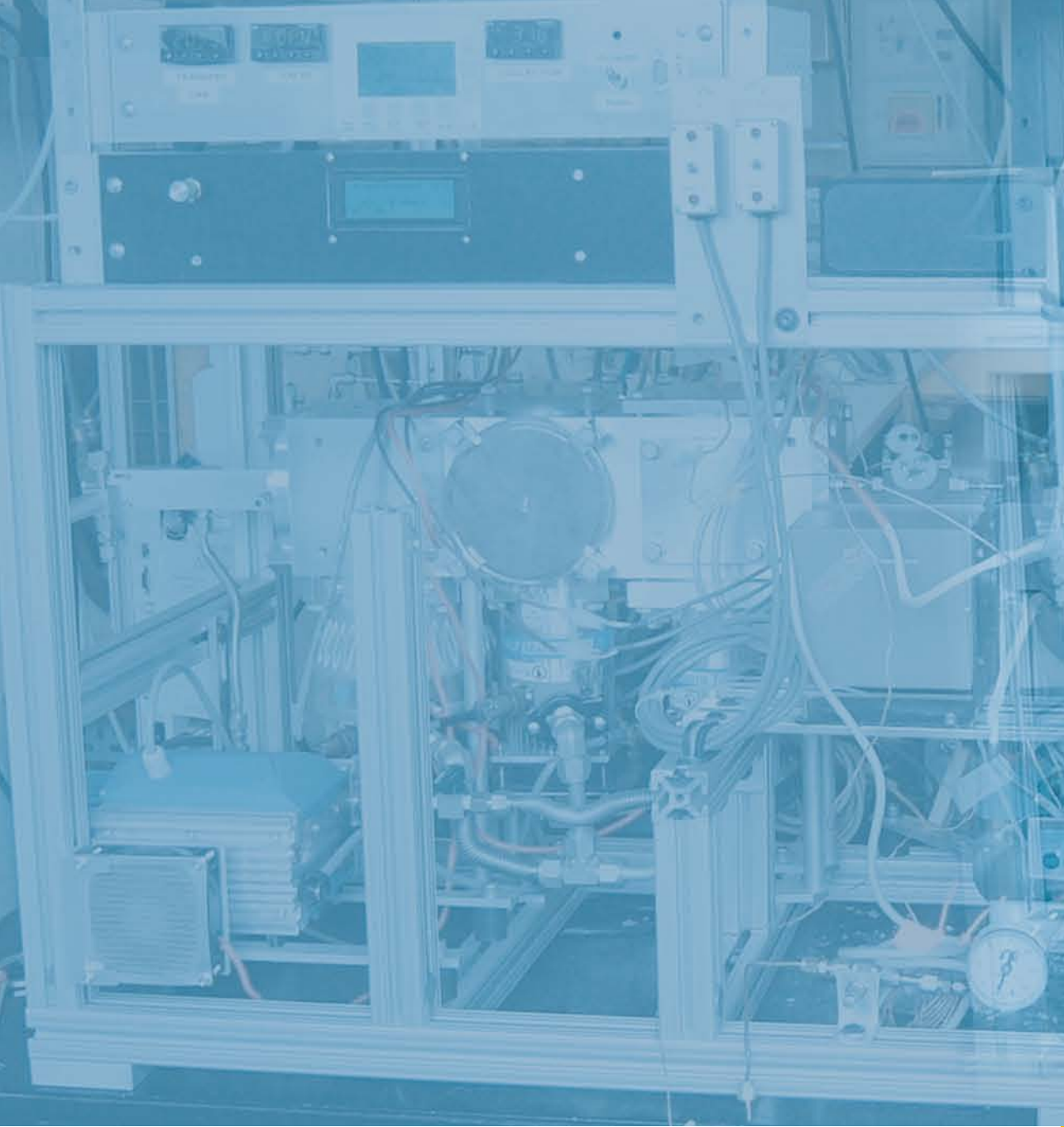
20. **Neutron-Irradiation + Helium Hardening & Embrittlement Modeling of 9%Cr-Steels in an Engineering Perspective (HELENA)**  
by R. Chaouadi (2008), VIII, 139 pages  
ISBN: 978-3-89336-545-6
21. **Messung und Bewertung von Verkehrsemissionen**  
von D. Klemp, B. Mittermaier (2009), ca. 230 Seiten  
ISBN: 978-3-89336-546-3
22. **Verbundvorhaben APAWAGS (AOEV und Wassergenerierung) – Teilprojekt: Brennstoffreformierung – Schlussbericht**  
von R. Peters, R. C. Samsun, J. Pasel, Z. Porš, D. Stolten (2008), VI, 106 Seiten  
ISBN: 978-3-89336-547-0
23. **FREEVAL**  
Evaluation of a Fire Radiative Power Product derived from Meteosat 8/9 and Identification of Operational User Needs  
Final Report  
project coord. M. Schultz, M. Wooster (2008), 139 pages  
ISBN: 978-3-89336-549-4
24. **Untersuchungen zum Alkaliverhalten unter Oxycoal-Bedingungen**  
von C. Weber (2008), VII, 143, XII Seiten  
ISBN: 978-3-89336-551-7
25. **Grundlegende Untersuchungen zur Freisetzung von Spurstoffen, Heißgaschemie, Korrosionsbeständigkeit keramischer Werkstoffe und Alkalirückhaltung in der Druckkohlenstaubfeuerung**  
von M. Müller (2008), 207 Seiten  
ISBN: 978-3-89336-552-4
26. **Analytik von ozoninduzierten phenolischen Sekundärmetaboliten in *Nicotiana tabacum* L. cv Bel W3 mittels LC-MS**  
von I. Koch (2008), III, V, 153 Seiten  
ISBN 978-3-89336-553-1
27. **IEF-3 Report 2009. Grundlagenforschung für die Anwendung**  
(2009), ca. 230 Seiten  
ISBN: 978-3-89336-554-8
28. **Influence of Composition and Processing in the Oxidation Behavior of MCrAlY-Coatings for TBC Applications**  
by J. Toscano (2009), 168 pages  
ISBN: 978-3-89336-556-2
29. **Modellgestützte Analyse signifikanter Phosphorbelastungen in hessischen Oberflächengewässern aus diffusen und punktuellen Quellen**  
von B. Tetzlaff (2009), 149 Seiten  
ISBN: 978-3-89336-557-9

30. **Nickelreaktivlot / Oxidkeramik – Fügungen als elektrisch isolierende Dichtungskonzepte für Hochtemperatur-Brennstoffzellen-Stacks**  
von S. Zügner (2009), 136 Seiten  
ISBN: 978-3-89336-558-6
31. **Langzeitbeobachtung der Dosisbelastung der Bevölkerung in radioaktiv kontaminierten Gebieten Weißrusslands – Korma-Studie**  
von H. Dederichs, J. Pillath, B. Heuel-Fabianek, P. Hill, R. Lennartz (2009),  
Getr. Pag.  
ISBN: 978-3-89336-532-3
32. **Herstellung von Hochtemperatur-Brennstoffzellen über physikalische Gasphasenabscheidung**  
von N. Jordán Escalona (2009), 148 Seiten  
ISBN: 978-3-89336-532-3
33. **Real-time Digital Control of Plasma Position and Shape on the TEXTOR Tokamak**  
by M. Mitri (2009), IV, 128 Seiten  
ISBN: 978-3-89336-567-8
34. **Freisetzung und Einbindung von Alkalimetallverbindungen in kohle-befeuerten Kombikraftwerken**  
von M. Müller (2009), 155 Seiten  
ISBN: 978-3-89336-568-5
35. **Kosten von Brennstoffzellensystemen auf Massenbasis in Abhängigkeit von der Absatzmenge**  
von J. Werhahn (2009), 242 Seiten  
ISBN: 978-3-89336-569-2
36. **Einfluss von Reoxidationszyklen auf die Betriebsfestigkeit von anodengestützten Festoxid-Brennstoffzellen**  
von M. Ettler (2009), 138 Seiten  
ISBN: 978-3-89336-570-8
37. **Großflächige Plasmaabscheidung von mikrokristallinem Silizium für mikromorphe Dünnschichtsolarmodule**  
von T. Kilper (2009), XVII, 154 Seiten  
ISBN: 978-3-89336-572-2
38. **Generalized detailed balance theory of solar cells**  
von T. Kirchartz (2009), IV, 198 Seiten  
ISBN: 978-3-89336-573-9
39. **The Influence of the Dynamic Ergodic Divertor on the Radial Electric Field at the Tokamak TEXTOR**  
von J. W. Coenen (2009), xii, 122, XXVI Seiten  
ISBN: 978-3-89336-574-6

40. **Sicherheitstechnik im Wandel Nuklearer Systeme**  
von K. Nünighoff (2009), viii, 215 Seiten  
ISBN: 978-3-89336-578-4
41. **Pulvermetallurgie hochporöser NiTi-Legierungen für Implantat- und Dämpfungsanwendungen**  
von M. Köhl (2009), XVII, 199 Seiten  
ISBN: 978-3-89336-580-7
42. **Einfluss der Bondcoatzusammensetzung und Herstellungsparameter auf die Lebensdauer von Wärmedämmschichten bei zyklischer Temperaturbelastung**  
von M. Subanovic (2009), 188, VI Seiten  
ISBN: 978-3-89336-582-1
43. **Oxygen Permeation and Thermo-Chemical Stability of Oxygen Permeation Membrane Materials for the Oxyfuel Process**  
by A. J. Ellett (2009), 176 Seiten  
ISBN: 978-3-89336-581-4
44. **Korrosion von polykristallinem Aluminiumoxid (PCA) durch Metalljodidschmelzen sowie deren Benetzungseigenschaften**  
von S. C. Fischer (2009), 148 Seiten  
ISBN: 978-3-89336-584-5
45. **IEF-3 Report 2009. Basic Research for Applications**  
(2009), 217 Seiten  
ISBN: 978-3-89336-585-2
46. **Verbundvorhaben ELBASYS (Elektrische Basissysteme in einem CFK-Rumpf) - Teilprojekt: Brennstoffzellenabgase zur Tankinertisierung - Schlussbericht**  
von R. Peters, J. Latz, J. Pasel, R. C. Samsun, D. Stolten  
(2009), xi, 202 Seiten  
ISBN: 978-3-89336-587-6
47. **Aging of <sup>14</sup>C-labeled Atrazine Residues in Soil: Location, Characterization and Biological Accessibility**  
by N. D. Jablonowski (2009), IX, 104 Seiten  
ISBN: 978-3-89336-588-3
48. **Entwicklung eines energetischen Sanierungsmodells für den europäischen Wohngebäudesektor unter dem Aspekt der Erstellung von Szenarien für Energie- und CO<sub>2</sub> - Einsparpotenziale bis 2030**  
von P. Hansen (2009), XXII, 281 Seiten  
ISBN: 978-3-89336-590-6

49. **Reduktion der Chromfreisetzung aus metallischen Interkonnektoren für Hochtemperaturbrennstoffzellen durch Schutzschichtsysteme**  
von R. Trebbels (2009), iii, 135 Seiten  
ISBN: 978-3-89336-591-3
50. **Bruchmechanische Untersuchung von Metall / Keramik-Verbundsystemen für die Anwendung in der Hochtemperaturbrennstoffzelle**  
von B. Kuhn (2009), 118 Seiten  
ISBN: 978-3-89336-592-0
51. **Wasserstoff-Emissionen und ihre Auswirkungen auf den arktischen Ozonverlust**  
**Risikoanalyse einer globalen Wasserstoffwirtschaft**  
von T. Feck (2009), 180 Seiten  
ISBN: 978-3-89336-593-7
52. **Development of a new Online Method for Compound Specific Measurements of Organic Aerosols**  
by T. Hohaus (2009), 156 Seiten  
ISBN: 978-3-89336-596-8





**Energie & Umwelt / Energy & Environment**  
**Band / Volume 52**  
**ISBN 978-3-89336-596-8**